# Experimental Wireless Communications

**Florian Kaltenberger**

February 19, 2014

# Foreword

This document is written as support for my French "Habilitation à diriger des récherches" (HdR) degree. Unlike a Ph.D. thesis, a HdR thesis does not aim at providing a detailed description of a particular research problematic, but rather describes the various facets of responsibilities that I experienced as researcher and assistant professor since obtaining my Ph.D.

My post-doctoral career started at Eurecom in September 2007, after having completed my Ph.D. entitled "Low-Complexity Real-Time Signal Processing for Wireless Communications" at the Vienna University of Technology in July 2007. I deliberately choose to do my post-doc at Eurecom because of their experimental platform OpenAir-Interface, which allowed me to work on practical aspects of wireless communication systems. This means working on aspects that are sometimes overlooked (or not found interesting) by other researchers or collecting and analyzing data from experiments to prove a concept or a point. Working with this platform is an unique experience, since one has to deal with many practical problems. And sometimes these problems lead to very interesting research avenues. Furthermore the platform is ideal for teaching, giving students hand-on experience and showing them the problems of real implementations.

This document is composed in two parts. The first part describes the highlights of my research work I have been conducting after my Ph.D. The bulk of the text is based on existing publications, but I have also added an introductory chapter summarizing all the works and putting them in context to each other, and a conclusions chapter elaborating on the lessons learnt and giving directions for future work. The second part contains an extended CV, which includes teaching and supervising activities, project management and acquisition, as well as a full list of my post-Ph.D. publications.

# Acknowledgments

No researcher is an island and the work presented in this thesis would not have been possible without my fellow co-workers, colleagues, and students. First of all I would like to thank my mentor Raymond Knopp, under whose supervision I carried out my post-doc at Eurecom and who introduced me into the world of experimental research and more particularly into the OpenAirInterface platform. Thanks to him and also Christian Bonnet, who was head of the department at the time, I was able to follow my career at Eurecom, which was a truly wonderful experience. Regarding my research work I would like to thank in particular Rizwan Ghaffar, Maxime Guillaud, Marios Kountouris, Imran Latif, and Sebastian Wagner, who have significantly contributed to the research work that I am presenting in this thesis. Moreover, I would like to thank all my co-workers, co-authors, PhD and master students that have helped me in carrying out my research work. Last but definitely not least I would like to thank my wife Gillian, for always supporting my dreams and bearing my craziness and geekiness.

# Contents

# Part I

# Research Summary

# Chapter 1

# Introduction

<div align="right">

Truth is what works

Heinz Zemanek
</div>

Experiments are an integral part of wireless communications. An experiment is a procedure carried out with the goal of verifying, refuting, or establishing the validity of a hypothesis[1]. One of the very first experiments that defined this field was carried out by Heinrich Hertz in 1887, proving the fact that electromagnetic waves can travel over free space. Another more recent example is the concept of spatial multiplexing using multiple antennas. The concept was first proposed by Foschini in 1996 [1] but it was only proven by experiments some years later by Golden et al. in 1999 [2]. More generally speaking, experiments can also be used to collect data in order to analyze a specific phenomenon not yet very well understood. For example, channel sounding is used to collect measurements in order to analyze the nature of the wireless propagation channel.

Experimentation is a very time consuming and expensive undertaking. This is true today more than ever, since wireless communications systems have become very complex and comprise many different fields, such as electrical engineering, computer science, information and communication theory, signal processing, etc. The development of today's wireless communication systems happens mainly in big industrial companies that bring together experts from those different fields and that provide the necessary infrastructure for this development. An academic research center or university on the other hand does not have such a team or infrastructure and thus researchers often need to work with simplified models and assumptions when developing or testing a new algorithm. However, this process is very dangerous as often these assumptions are never met.

One way to bridge the gap between visionary academic research and industrial research are testbeds. Wireless testbeds are usually highly flexible and easily reconfigurable but at the same time provide a framework that forces the researcher to be realistic. One of those testbeds is the EURECOM OpenAirInterface testbed, a wireless

---

[1]`http://en.wikipedia.org/wiki/Experiment`
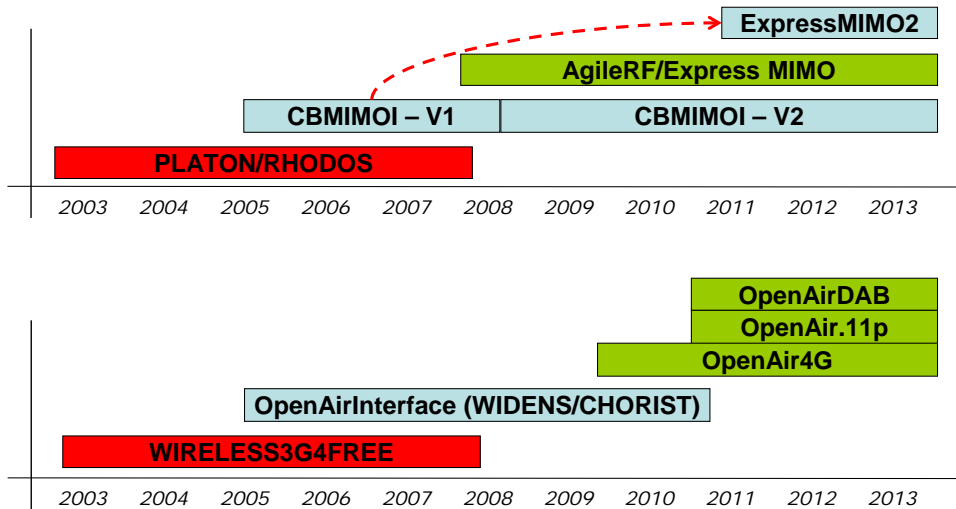
Figure 1.1: OpenAirInterface hardware (top) and software (bottom) roadmaps. The activity started around 2003 with the first generation hardware and software. Wireless3G4Free was a TD-SCDMA software defined radio (SDR) with an IPv6 interconnect running on the PLATON/RHODOS boards. The term OpenAirInterface was coined in the second generation and was a SDR using an in-house MIMO-OFDMA TDD waveform (WiMAX 2004 like) but was targeted to mesh networks. It was running on the CBMIMO1 hardware, which was used for a very long time due to its simple and effective design. OpenAir4G, the open-source implementation of the LTE standard stared around 2009. In the beginning it was running on the CBMIMO1 hardware, later on the ExpressMIMO and today on the ExpressMIMO2 platform. In parallel also implementation of DAB and 802.11p were started.

technology platform comprising (*i*) a radio transceiver card combining radio front-end and analogue/digital converters and (*ii*) an open-source software defined radio that runs in real-time on common x86 Linux machines.

Eurecom started its experimental activity around 2003 and since then both hardware and software changed quite significantly (see Figure 1.1). Some of the main concepts have not changed however. Firstly, the interface between the radio acquisition card and the PC has always been based on PCI (or PCI express), which allows the card direct memory access to the PC, which is of utmost importance to guarantee real-time performance from a latency point of view. Secondly, the modem has always been implemented entirely in software using C programming language and relying on single-instruction multiple-data (SIMD) extensions of general purpose CPUs. This allows an easy manipulation and a real-time performance form an execution time point of view.

Today, OpenAirInterface is focused on the 3GPP long-term evolution (LTE) and

provides the following components:

- User equipment (UE) software radio comprising all levels of the protocol stack, from the physical layer to the networking layer for both the user-plane and control-plane.

- Evolved Node B (eNB) software radio comprising all levels of the protocol stack, from the physical layer to the networking layer for both the user-plane and control-plane.

- eNB application responsible for controlling the software modem and to interface with the EPC.

- Evolved Packet Core (EPC), featuring Mobility Management Entity (MME), home subscriber server (HSS), serving gateway (SGW) and packet data network gateway (PGW).

This thesis gives some examples of how the OpenAirInterface testbed can be used to do experimental research. It also presents the evolution of the different hardware modules from the CBMIMO1 card (Chapters 2 and 3) over the ExpressMIMO1 card (Chapter 4) to the most recent ExpressMIMO2 card (Chapter 5). The following section gives a summary of the thesis highlighting my key contributions to the field of experimental wireless communications.

## 1.1 Synopsis and Contributions

### 1.1.1 Design and implementation of a single-frequency mesh network

Compared to a cellular network, in a wireless mesh network connectivity between nodes in the network is not provided through a fixed backhaul network between access points or base stations but rather through relays connecting the access points wirelessly. Wireless mesh networks are thus very attractive for applications where no fixed infrastructure is available such as disaster recovery operations.

Chapter 2 presents some results of the project CHORIST, in which we developed a rapidly deployable broadband mesh network for disaster recovery operations. The network is made up of clusterheads (CHs), assuming the role of access points or base stations, and mesh routers (MRs), which serve as relays between two CHs. In order to support high bandwidth applications like video streaming, a frequency reuse of one between neighboring CHs is required. In such a setup the challenges are ($i$) how to synchronize multiple CHs over-the-air, and ($ii$) how to design a receiver architecture that allows a mesh relay node to communicate with up to two cluster heads on the same frequency.

The first problem has been solved using a distributed synchronization algorithm that is inspired by the synchronization of fireflies in nature. A synchronization signal from a master CH is first used by MRs to synchronize themselves and then rebroadcast to let further CHs synchronize to the network. This system was also implemented in OpenAirInterface and worked reasonably well for small network sizes.

Once the CHs are synchronized, the system can be seen as a distributed multiple-input multiple-output (MIMO) system where the two spatially multiplexed streams originate from two neighboring CHs. The main challenge in this setting is the design of an efficient receiver that can decode the two spatially multiplexed streams. The first receiver architectures that we investigated was a linear preprocessor based on the minimum mean squared error (MMSE) criterion. The MMSE receiver requires a matrix inversion, which is not a trivial task on a fixed point system. Especially in a frequency selective channel the dynamic range of the received signals on each subcarrier of the OFDM system is very high leading to a numerically unstable system. The second receiver architecture was a successive interference cancellation receiver using reduced complexity max-log MAP detector. It exploits the fact that the interference is not Gaussian but comes from a finite constellation. This receiver is more numerically robust than the MMSE receiver as it does not require any inversion operations and thus has a better performance. Both receiver architectures have been implemented on the OpenAirInterface and were tested and evaluated under real conditions.

For this work we used the CBMIMO1 cards and the OpenAirMesh software of the OpenAirInterface platform. More details about this work can be found in Chapter 2, which is based on the publication [3]:

- Florian Kaltenberger, Rizwan Ghaffar, Raymond Knopp, Hicham Anouar, and Christian Bonnet. Design and implementation of a single-frequency mesh network using OpenAirInterface. *EURASIP Journal on Communications and Networking*, 2010, 2010. Article ID 719523, 16 pages, doi:10.1155/2010/719523.

### 1.1.2 Multi-user MIMO

In a multi-user MIMO system a base station with multiple antennas communicates with multiple users simultaneously on the same time-frequency resources, employing some space-time coding. The users can have multiple antennas too, but this is not a requirement. The difference to a single-user MIMO system is that the users cannot cooperate, and thus all the space-time coding has to be done at the base station. This in turn requires channel state information at the transmitter (CSIT), which is hard to obtain.

In Chapter 3 we study different aspects of multi-user MIMO systems based on real channel measurements. The measurements have been conducted with the CBMIMO1 boards using the Eurecom MIMO OpenAir Sounder (EMOS), which is also part of the OpenAirInterface platform. Firstly, we compare the sum rate of different MU-MIMO precoding schemes in various channel conditions assuming full CSIT. However, full CSIT is hard to obtain, especially in a frequency division duplex (FDD) system, where the channel state information has to be fed back to the base station using a low-rate feedback channel. In particular we study codebook based feedback, where a codebook of precoding matrices is know to both the base station and the user and the user just feeds back the index of the codebook entry that corresponds the most to the measured channel. As is can be expected the performance of such a system strongly depends on

the chosen codebook, which is why secondly we study the performance of several possible codebook-based precoding schemes using the channel measurements. The results show, for example, that having a large user separation as well as codebooks adapted to the second order statistics of the channel gives a sum rate close to the theoretical limit. A small user separation due to bad scheduling or a poorly adapted codebook on the other hand can impair the gain brought by MU-MIMO. Moreover, a larger codebook (requiring a higher feedback rate) leads to better CSIT and thus better performance however, it is not trivial to trade-off the feedback rate with the rate at the downlink channel. Therefore we thirdly relate the required feedback rate with the achievable rate on the downlink channel and show this trade-off for the different measurements.

To the best of our knowledge, these are the first measurement results giving evidence of how MU-MIMO precoding schemes depend on the precoding scheme, channel characteristics, user separation, and codebook. More details about this work can be found in In Chapter 3, which is based on the publication [4]:

- F. Kaltenberger, M. Kountouris, D. Gesbert, and R. Knopp. On the trade-off between feedback and capacity in measured MU-MIMO channels. *IEEE Trans. Wireless Commun.*, 8(9):4866–4875, September 2009.

### 1.1.3 Exploiting Channel Reciprocity

As we have seen in the previous section, channel state information at the transmitter (CSIT) can greatly improve the capacity of a wireless MIMO communication system. In a FDD system, CSIT can only be acquired by using a feedback channel. In a time division duplex (TDD) system on the other hand, CSIT can be obtained by exploiting the reciprocity of the wireless channel. However, while the physical wireless channel is known to be reciprocal the radio frequency (RF) chains of the receiver and the transmitter are in general not. This problem can be solved by either absolute calibration or relative calibration. Absolute calibration is done using specialized equipment (anechoic cambers and high-precision measurement tools) while relative calibration can be done without any additional equipment. Relative calibration is thus not only more attractive from an economic point of view, but also because it enable easy re-calibration should parameters change due to the climate or other external factors.

The relative calibration problem can be formulated as a non-linear total least squares problem[2] for the calibration coefficients. Depending on the antenna configuration (SISO, MISO, SIMO, or MIMO), and the bandwidth (narrowband vs wideband) different solutions to this problem exist. Our main interest is to validate some of these algorithms using real measurement data collected with OpenAirInterface. To solve the least squares problem we assumed that the calibration matrices are diagonal, which requires that there is neither mutual coupling nor cross-talk between the RF chains. This is a rather strong assumption, but it greatly simplifies the solution of the problem (we will discuss the

---

[2]In a *total* least square problem, observational errors on both dependent and independent variables are taken into account

validity of this assumption later) to a system of linear total least squares problem which can be solved using a classical algorithms.

The first result showed a very poor performance of the algorithm. It was found out that this is due to the frequency offsets present in the measurements. In fact already very small frequency offsets in the order of a few Hertz can strongly impair the performance of the estimation algorithm. To overcome this problem, two different solutions have been proposed. In a first approach [5] we simply estimate the frequency offsets and then compensate them before applying the estimation algorithm. This results in an improved performance, but still far from optimum. In a second approach [6] the frequency offsets were incorporated in the data model and the estimation algorithm. This leads to significantly improved results, which were also validated using measurements.

More details about this work can be found in chapter 4, which is based on the following publications [6],[7]:

- Florian Kaltenberger, Haiyong Jiang, Maxime Guillaud, and Raymond Knopp. Relative channel reciprocity calibration in MIMO/TDD systems. In *Proc. ICT Future Network and Mobile Summit*, Florence, Italy, June 2010.

- Maxime Guillaud and Florian Kaltenberger. Towards practical channel reciprocity exploitation: Relative calibration in the presence of frequency offset. In *WCNC 2013, IEEE Wireless Communications and Networking Conference*, Shanghai, CHINA, April 2013.

### 1.1.4 Interference-aware receiver design for MU-MIMO

Chapter 5 continues with the study of MU-MIMO channels, but this time in the context of LTE. In LTE rel 8, MU-MIMO was introduced through transmission mode 5. However, the precoding scheme used for MU-MIMO in LTE is based on very low resolution codebooks (4 codewords for 2 transmit antennas and 16 codewords for 4 transmit antennas). It is thus far from optimal and results in a significant amount of residual MU interference especially if the channel state information at the basestation is outdated or in small cells with a limited number of users available.

To tackle the MU interference, an interference-aware (IA) receiver design similar to the one that was used in Chapter 2 is employed. Unlike the interference-unaware (IU) receiver, the IA receiver exploits information about the modulation order of the interfering data stream in the decoding process, resulting in a significant performance gain while maintaining a moderate complexity. We study two different cases: (*i*) a network-assisted interference aware (NA-IA) receiver that knows the modulation order of the interfering stream through some additional signaling and (*ii*) an IA receiver that assumes the same modulation order of the interfering stream as its own stream (this heuristic was obtained from simulation results).

We evaluate the performance of all three receivers in terms of throughput through real-time measurements carried out with the ExpressMIMO2 boards and the OpenAir4G LTE software modem, which are part of the OpenAirInterface development platform.

The measurement results show that the IA receiver achieves significantly higher data rates compared to the IU receiver if the user has multiple receive antennas. The gain depends on the scenario, where the least gains were observed in a line-of-sight (LOS) channel. However, for both single and receiver antennas, the measurements revealed that the NA-IA receiver significantly outperforms the IA receiver for higher order modulations, 64QAM. This result suggests that the signaling of the interfering modulation order can greatly improve performance in case 64QAM is applied. For lower order modulations the simplified IA receiver without knowledge of the interfering modulation order performs equally well as the NA-IA.

Although the measurements have been done using an LTE rel 8 framework, they have a strong relevance for future releases, where the inclusion of a Network-Assisted Interference Cancellation and Suppression (NAICS) is discussed [8].

More details about this work can be found in Chapter 5 which is based on the publication [9]:

- Sebastian Wagner and Florian Kaltenberger. Interference-aware receiver design for MU-MIMO in LTE: Real-time performance measurements. *Intel Technology Journal (special issue on 4G communications)*, 2014.

### 1.1.5 Physical Layer Abstraction for LTE systems

Chapter 6 finally deals with topic that is not necessary related to experiments on the hardware platform but more to experiments with the system level simulator of OpenAir-Interface. PHY abstraction is an extremely valuable low complexity tool for efficient and realistic large scale system evaluations. Together with my PhD student Imran Latif, we developed a PHY abstraction methodology for the special case of MU-MIMO in LTE [10]. We further developed a novel semi-analytical PHY abstraction approach towards incorporating the incremental-redundancy hybrid automatic repeat request (IR HARQ) for a wide variety of resource block assignments in LTE [11]. This method reduces the storage requirements for PHY abstraction by bringing down the number of required reference curves to only three from hundreds. These methods were also integrated in the OpenAirInterface system level simulator and we have shown in [12] that we achieve the same throughput results when compared to the full PHY implementation while reducing the computational complexity by a factor of 30.

More details on this work can be found in Chapter 6, which is based on the article [13]:

- Florian Kaltenberger, Imran Latif, and Raymond Knopp. On scalability, robustness and accuracy of physical layer abstraction for large-scale system-level evaluations of LTE networks. In *in Proc. Asilomar Conference on Signals, Systems, and Computers*, Pacific Grove, CA, November 2013. invited.

### 1.1.6 Conclusions

Final conclusions, lessons learnt from OpenAirInterface and future directions are given in Chapter 7

# Chapter 2

# Design and implementation of a single-frequency mesh network using OpenAirInterface

In this chapter we focus on mesh networks and show how to implement a single-frequency mesh network with OpenAirInterface. The key ingredients to enable such a network are a dual-stream MIMO receiver structure and a distributed network synchronization algorithm. We show how to implement these two algorithms in real-time on the OpenAirInterface platform. Further we provide results from field trials and compare them to the simulation results.

## 2.1   Introduction

The design and implementation of next generation wireless networks is a very challenging task. To ensure optimal performance it is necessary to carry out performance evaluations and field trials in parallel to standard development. Easily reconfigurable testbeds are a convenient way to investigate new ideas and to tackle many problems at an early development stage.

Novel ideas for wireless networks are usually first studied using computer simulations based on some kind of model of the network, the hardware and the radio channel. These models usually make assumptions in order to simplify or isolate the problem at hand. However, it might turn out that the assumptions are not fulfilled in a real environment. An easily reconfigurable experimental platform allows to study novel algorithms under realistic conditions. Comparing simulation results with results from lab tests and field trials reveals if initial assumptions were correct or if they need to be refined.

This paper presents the Eurecom testbed OpenAirInterface, which is an experimental real-time, open-source hardware and software platform for future wireless networks. OpenAirInterface can be seen as a mock standard for realistic experimentation purposes which retains the salient features of a real radio system, without all the required mech-

anisms one would find in a standard used in deployment of commercial networks. Its aim is to study techniques such as multi-cell cooperative techniques, distributed synchronization, interference coordination and cancellation.

OpenAirInterface features an open-source software modem written in C comprising physical and link layer functionalities for cellular and mesh network topologies. This software modem can be used either for extensive computer simulations using different channel models or it can be used for real-time operation. In the latter case, it is run under the control of the real-time application interface (RTAI) which is an extension of the Linux operating system.

The use of an open-source software modem has several advantages. Firstly, the same code can be initially debugged and tuned in simulation before using it in the real-time modem (where debugging and performance analysis is much harder). Secondly, the system is very flexible and parameters like frame structure, pilot placement, etc., can be changed rather easily. Thirdly, researchers can implement new ideas rather fast, without having to use very sophisticated hardware description languages (HDL). Last but not least since all code is open-source, other researchers can use easily adjust the modem to their needs and collaboration is fostered.

Other highlights of the OpenAirInterface platform are its usage as measurement platform or as an emulation platform which allow to study different aspects of a wireless network in isolation. In the emulation mode, the physical layer is abstracted and emulated over the ethernet. This approach allows to test and investigate MAC and link-level algorithms without using the radio interface [14]. The OpenAirInterface can also be used to perform channel measurements which can be used for channel characterization and capacity analysis [4].

Apart from a general overview of OpenAirInterface, in this paper we present OpenAirMesh—a specification of wireless mesh network and its implementation on the OpenAirInterface platform. OpenAirMesh exemplifies two major challenges in future wireless networks. The first challenge is interference which is caused by a very tight frequency reuse in order to increase the network throughput. Interference is especially strong for users at the cell edge severely limiting user's throughput. We propose a low-complexity dual-stream MIMO receiver that is able to cancel out interference from a neighboring cell and show its implementation and performance on the OpenAirInterface. This example also highlights the insight that OpenAirInterface provides for developing multi-cell algorithms. More concretely it was found out that frequency offsets and receive correlation have a very strong influence on the receiver performance and can thus not be neglected in the simulations.

Another big challenge in future wireless networks is synchronization between nodes, especially indoors where a reference timing signal such as the one provided by the global positioning system (GPS) cannot be used. Synchronization is needed for example for the dual-stream MIMO receiver and to enable the collaboration between base-stations both on the media access (MAC) and the physical (PHY) layer. The distributed synchronization algorithm proposed in this paper can be interpreted as a form of firefly synchronization [15].

**Related Work**   Many people have recognized the advantages of testbeds for wireless networks. However, many of them focus on a particular layer, such as the physical layer, the link layer or the network layer. A good overview of testbeds that focus on the physical layer and especially MIMO communications is given in [16, 17].

Most of the testbeds that provide both physical and link layer functionalities (like OpenAirInterface) are either based on the Universal Software Radio Peripheral (USRP) from Ettus Research [18] together with the GNU software radio [19] or the wireless open-access research platform (WARP) from Rice University [20]. For example, the Hydra testbed of the University of Texas in Austin [21] is based on the GNU radio platform while the WAPRnet testbed [22] is based on WARP platform. The WiTestLab from the Polytechnic Institute of NYU [23] has been experimenting with both platforms. Another testbed example it the Cognitive Radio Testbed from Berkley [24], which uses the Berkeley Emulation Engine 2 (BEE2) [25] as an implementation platform.

Compared to the OpenAirInterface platform, the GNU radio project does not provide a full reference design, but only building blocks. Further, a MAC layer implementation is missing in the current distribution. Also the USRP hardware has its limitations, mainly due to the connection to the PC over USB or Ethernet, which severely limits the achievable system throughput. Like the OpenAirInterface, WARP is also a full software defined radio (SDR), but physical layer algorithms have to be developed either directly in VHDL or using the Xilinx System Generator toolchain for Matlab. Compared to the use of C language in OpenAirInterface, the use of VHDL is more cumbersome and time consuming. Also, the Xilinx System Generator is not openly available. The BEE2 platform is a very flexible hardware platform, which has been designed for a multitude of applications. However, no software modem exists for this platform.

Last but not least we mention here the two testbeds developed within the EASY-C project[1] that were set up in Berlin [26] and in Dresden [27] (both Germany). The project is a cooperation between German universities, research centers and industry and focuses on LTE-Advanced technologies. However, both testbeds use proprietary hardware and software and are not openly accessible.

**Organization**   Section 2.2 gives an overview of the OpenAirInterface experimental platform. Section 2.3 presents the network, the link layer and the physical layer architecture of OpenAirMesh—a mesh network built using the OpenAirInterface. Section 2.4 describes the two building blocks for the implementation of OpenAirMesh: a novel low-complexity dual-stream receiver architecture and the distributed synchronization algorithm. Finally we show results from computer simulations as well as real experiments in Section 2.5. We conclude the paper in Section 2.6.

**Notation**   Let $\mathbb{C}$ denote the set of complex numbers. Scalars are denoted by $x$. Column vectors and matrices are denoted by $\mathbf{a}$ and $\mathbf{A}$ and their elements are denoted by $a_i$ and $A_{i,j}$ respectively. Transpose and Hermitian transpose are denoted by $\cdot^T$ and $\cdot^H$. $\mathbf{I}_M$ is the identity matrix of size $M$ and $\mathbf{0}_M$ is an $M$-dimensional vector of zeros. The

---

[1] http://www.easy-c.de

| FPGA Components | Xilinx Virtex 2 3000 |
|---|---|
| Data Converters | 2x AD9832 (dual 14-bit 128 Msps D/A, dual 12-bit 64 Msps A/D) |
| MIMO Capability | 2x2 |
| RF TX Chipset | 2x Maxim MAX2395 (1900-1920 MHz) Zero-IF |
| RF RX Chipset | 2x Maxim MAX2393 (1900-1920 MHz) Zero-IF |
| TX Power | 21 dBm per antenna |
| RX Noise Figure | 6-7 dB at highest gain setting |
| Bus Interface | 32-bit PCI (CardBus) |
| Configuration | Flash EEPROM, Xilinx JTAG port (FPGA and EEPROM) |

Table 2.1: Hardware characteristics of the CardBus MIMO 1 card.

| FPGA Components | Virtex 5 LX330, Virtex 5 LX110T |
|---|---|
| Data Converters | 4x AD9832 (dual 14-bit 128 Msps D/A, dual 12-bit 64 Msps A/D) |
| MIMO Capability | 4x4 Quadrature, 8x8 low-IF |
| Memory | 128 Mbytes/133 MHz DDR (LX110T), 1-2 Gbytes DDR2 (LX330) |
| Bus Interface | PCIExpress 8-way |
| Configuration | 512 Mbytes Compact Flash (SystemACE), JTAG |

Table 2.2: Hardware characteristics of the Express MIMO card.

Euclidean ($\ell_2$) norm of a vector $\mathbf{a}$ is denoted by $\|\mathbf{a}\|$ and the Frobenius norm of a matrix $\mathbf{A}$ is denoted by $\|\mathbf{A}\|_F$. $\mathbb{E}$ denotes expectation, and $\mathcal{CN}(\mathbf{m}, \mathbf{C})$ denotes a multivariate proper complex normal distribution with mean vector $\mathbf{m}$ and covariance matrix $\mathbf{C}$.

## 2.2 OpenAirInterface Overview

The OpenAirInterface platform consists of both hardware and the software components. Additionally it comprises different simulation tools as well as collaborative web tools. The hardware components are described in subsection 2.2.1. In subsection 2.2.2 we describe the basic organization of the OpenAirInterface software components (which are available under the GNU GPL from the OpenAirInterface website[2]).

### 2.2.1 Hardware Components

In OpenAirInterface there are two different hardware modules available: CardBus MIMO 1 (CBMIMO1) and it successor Express MIMO. All current activities (including the experiments described in this paper) are based on CBMIMO1. In the following we will describe the main characteristics of the two boards.

---

[2]http://www.openairinterface.org
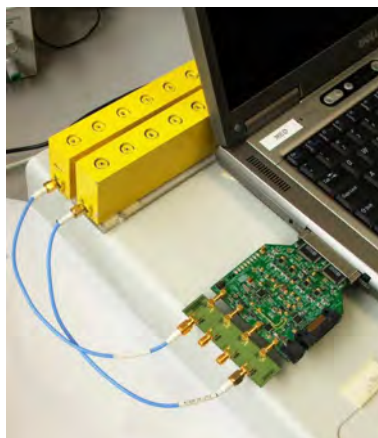
Figure 2.1: The CBMIMO1 board.

The CBMIMO1 board (cf. Figure 2.1) comprises two time-division duplex (TDD) radio frequency (RF) chains operating at 1.900-1.920 GHz with 5 MHz channels and 21dBM transmit power per antenna for an orthogonal frequency division modulated (OFDM) waveform[3]. The cards house a medium-scale field programmable gate array (FPGA) (Xilinx X2CV3000) which makes use of the open-source LEON3 embedded processor from Gaisler research [28]. In the current version, the FPGA implements the interfaces with the Peripheral Component Interconnect (PCI) bus, with the RF frontend as well as with the A/D and D/A converters. The card can be connected to a host PC (in our lab we use Dell Precision M2300 laptops) using a CardBus PCI interface. See Table 2.1 for an overview of the card's components.

Express MIMO is a baseband processing board, which provides significantly more processing power and bandwidth than CBMIMO1 and will be used for future applications. It comprises two FPGAs: one Xilinx XC5VLX330 for real-time embedded signal processing applications [29] and one Xilinx XC5VLX110T for control. The card uses an eight-way PCI express interface to communicate with the host PC. The card employs four high-speed A/D and D/A converters from Analog Devices (AD9832) allowing to drive four RF chains using quadrature modulation or eight RF chains in low intermediate frequency (IF) for bandwidths of up to 20MHz. See Table 2.2 for an overview of the card's components. A RF board for Express MIMO called Agile RF is also available. It offers significantly more RF functionality in terms of tuning range and channel bandwidth than CBMIMO1. The tuning range per RF chain is 180MHz-8GHz with 20MHz channels.

### 2.2.2 Software Components

The software components are organized into four areas (folders), which correspond more or less to the different layers of the Open Systems Interconnection (OSI) reference model.

---

[3]EURECOM has a frequency allocation for experimentation around its premises in Sophia Antipolis.

The areas also correspond to the directory structure on the OpenAirInterface Subversion (SVN) server.

**openair0: Wireless Embedded System Design**  This folder mainly contains descriptions of the CBMIMO1 and Express MIMO hardware and the firmware for the corresponding FPGAs.

**openair1: Baseband signal processing**  This folder contains the code for the physical layer software modem along with RTAI/Linux device drivers and user-space tools to control the hardware. It also contains simulation environments and channel models to test the code without the hardware or to do performance simulations. Further, openair1 provides also the functionality for the Eurecom MIMO OpenAir Sounder (EMOS) to perform MIMO channel measurements over multiple users [4].

**openair2: Medium-Access Protocols**  This folder contains the layer 2 protocol stack development for PCs along with Linux networking device drivers for Internet Protocol (IP) and Multiprotocol Label Switching (MPLS) interconnection. This pertains to both cellular and mesh network topologies. The folder also contains an abstraction of the PHY layer, providing an efficient emulation platform for layer 2 and higher algorithms.

**openair3: Wireless Networking**  This contains the layer 3 protocol stack development for both all-IP cellular and IP/MPLS mesh networks.

## 2.3  OpenAirMesh Specification

In this section we present the specification of OpenAirMesh, a mesh network built using the OpenAirInterface [14]. We start off by describing the network topology in Subsection 2.3.1. In Subsection 2.3.2 we describe the layer 2 and finally in Subsection 2.3.3 the physical layer. A more detailed specification can be found in [30].

### 2.3.1  Network Topology

In OpenAirMesh, the network is organized in clusters, where nodes can either take the role of a cluster-heads (CHs) or a mesh router (MR). CHs are typically the best-connected nodes in a particular geographical area and manage radio resources within the cluster. MRs are used to relay information between CHs. An example of a mesh architecture with 5 nodes is shown in Figure 2.2.

**Cluster Head**

The primary role of the CH is to manage radio resources in their cluster, much as a base-station would do in a cellular network. The cluster is defined as the set of nodes which are characterized by one-hop connectivity with the CH. The system is designed
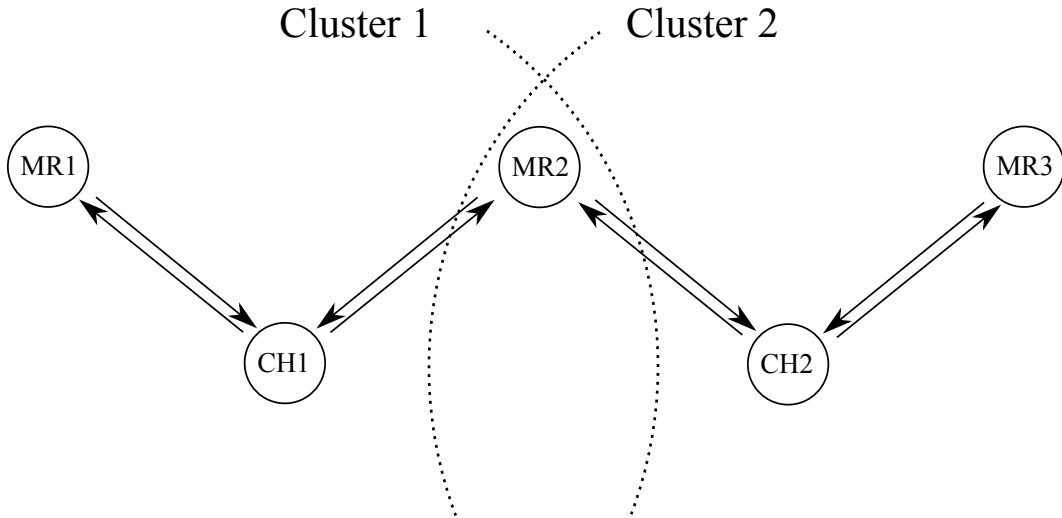
Figure 2.2: The mesh network topology is organized in clusters. Each cluster is controlled by a cluster head (CH). Other nodes in the network are called mesh routers (MR) since they can be used to relay information between CHs.

as a TDD system, where CHs and MRs transmit in alternating transmission time intervals. Thus—due to the half duplex constraint—direct CH $\leftrightarrow$ CH communication is not supported. The downlink (CH $\rightarrow$ MR) signaling channels allow for the CH to schedule transmission of labels (in the form of time and frequency mappings on the radio resource) each of which carry different types of traffic throughout the mesh network according to pre-defined quality-of-service (QoS) descriptors. The Uplink (UL) signaling channels (MR $\rightarrow$ CH) are used for relaying bandwidth requirement indicators and channel quality measurements from nodes within the cluster. These feed the scheduling algorithms residing in the CH and allow for proper resource allocation satisfying QoS negotiations carried out using Layer 3 (L3) signaling. The latter are beyond the scope of the description in this paper.

**Mesh Router**

The primary role of an MR is to interpret the scheduling information from the CH on the downlink (DL) signaling channels in order to route the traffic corresponding to the scheduled labels on the allocated physical resources. MRs can also be connected to more than one cluster at the same time. Since all CHs transmit on the same time-frequency ressources, MRs must be able to cancel interference. See Section 2.4.1 for details.

### 2.3.2 Layer 2 Protocol Stack

The OpenAirMesh Layer 2 protocol stack is depicted in Figure 2.3 and comprises:

- A IP/MPLS networking device (non-access stratum (NAS) driver) responsible for

21
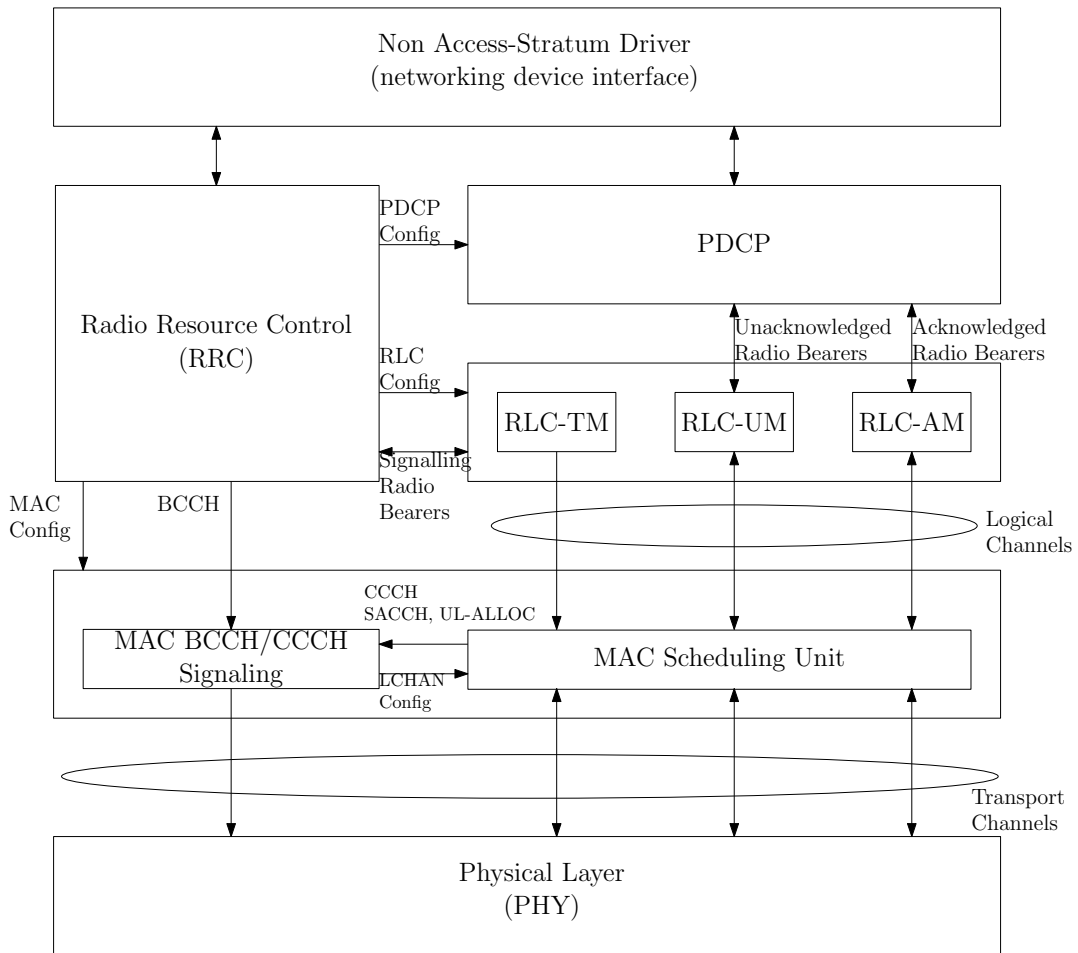
Figure 2.3: OpenAirMesh CH Layer 2 Protocol Stack.

provision of IP/MPLS layer services to Layer 2 and vice-versa

- A Radio resource control (RRC) entity responsible for MAC layer signaling for configuration of logical channels and retrieval of measurement information.

- A Radio Link Control (RLC) entity which is responsible for hybrid automatic repeat request (HARQ) protocols and IP packet segmentation

- A convergence protocol (PDCP) responsible for IP interface and related functions (header compression, ciphering, etc.)

- A scheduling and multiplexing unit to control the media access (MAC).

The information flow is organized into different traffic queues:

- Radio bearers are the user-plane traffic queues at the PDCP-RLC interface

- Signaling radio bearers are the control-plane traffic queues at the RRC-RLC interface

- Logical channels are the traffic queues at the RLC-MAC interface (both control and user-plane data, see Table 2.3)

- Transport channels are the traffic queues at the MAC-PHY interface which are mapped to physical channels by PHY (see Table 2.4)

The MAC layer scheduling and multiplexing entity is responsible for scheduling control plane and user plane traffic (logical channels) on the physical OFDMA resources (transport channels). It is important to note that although dedicated resources are configured at the input of the MAC layer, the physical resources allocated in the scheduling entities (with exception of the CHBCH) are dynamically allocated every CH transmission time interval (TTI) and thus all physical resources are shared. The BCCH is multiplexed in the scheduling entity responsible for generation of the CH-BCH transport channel along with MAC-layer signaling. MAC signaling concerns both allocations of CH-SACH in the current frame and MR-SACH in the next frame (uplink, downlink and direct link map of PHY resources). The CCCH (uplink) is used exclusively during the attachment phase of the MR with a particular cluster and corresponds to the only random-access resources allocated by the CH in the frame.

The DCCHs are multiplexed along with user-plane traffic DTCHs on the available CH-SACH resources. Based on measurement and feedback information, SACH scheduling (see Figure 2.4) aims to respect the negotiated QoS of each logical channel, while maximizing the aggregate spectral efficiency of the data streams. Different wideband scheduling policies taking into account both queuing measures from RLC and channel quality feedback can be accommodated (see for instance [31]). Channel quality information is signaled between corresponding MAC-layers based quantized wideband channel estimates received from PHY.

23

| Broadcast Control Channel | BCCH | Low bit-rate control channel used by a CH for broadcasting basic information to nodes in the cluster. |
|---|---|---|
| Common Control Channel | CCCH | Low bit-rate control channel used both during the attachment or association phase of a new node. |
| Dedicated Control Channel | DCCH | Access-layer signaling information (RLC return channels, RF measurement reporting, traffic measurement reporting, power control, etc.) to the corresponding node. |
| Dedicated Traffic Channel | DTCH | Variable bit-rate traffic channel with negotiated QoS parameters used by the mesh network to transport data traffic corresponding to a particular flow. |

Table 2.3: Logical channels.

| CH Broadcast Channel | CH-BCH | Broadcast control channel which houses MAC-layer signaling for CH and MR physical resource scheduling as well as layer 2 radio-resource control (RRC) signaling for topology and QoS management. |
|---|---|---|
| CH Scheduled-Access Channel | CH-SACH | Data channel (for both control and user-plane logical channels) used by CH to communicate with a node in its cluster. |
| MR Broadcast Channel | MR-BCH | Broadcast resource used by MR to extend the coverage of a cluster during topological discovery. |
| MR Scheduled-Access Channel | MR-SACH | Data channel (for both control and user-plane logical channels) used by MR to communicate with a CH. |
| Random-Access Channel | RACH | Signaling channel used by a MR during the association phase with the CH. |

Table 2.4: Transport and physical channels. Each of the transport channels is mapped to a corresponding physical channel of the same name.

| Physical CH Synchronization Channel | CHSCH | Pilot resource reserved to a CH which is responsible for delivering synchronization information to nodes in the cluster. |
|---|---|---|
| Physical Synchronization Channel | MRSCH | Pilot resource used by a MR to allow the CH to estimate the channel of an MR. |

Table 2.5: Additional physical channels.
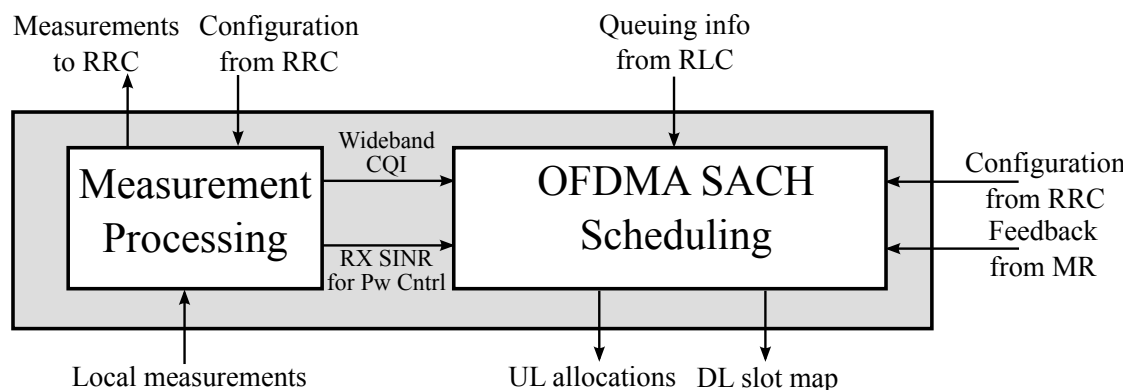
Figure 2.4: Overview of the MAC Scheduler.

| Symbol (DFT/IDFT) size | 256 samples |
|---|---|
| Prefix length | 64 samples |
| Useful carriers | 160 |
| Number of subbands (chunks) | 16 |
| Data carriers per subband | 8 |
| Pilots per subband | 2 |
| OFDM symbols/frame | 64 |

Table 2.6: OFDMA Parameters in OpenAirMesh.

### 2.3.3 Physical Layer

The physical layer of the platform uses orthogonal frequency division multiple access (OFDMA) together with multiple-input multiple-output (MIMO) techniques and is similar to that of fourth generation wireless networks such as WiMAX or LTE. The parameters for OpenAirMesh are given in Table 2.6.

The MIMO-OFDMA system provides the means for transmitting several multiple-bitrate streams (multiplexed over sub-carriers and antennas) in parallel. Moreover, PHY signaling strategies are included to provide the means for exploiting channel state feedback at the transmitters in order to allow for advanced PHY allocation of OFDMA resources via the MAC.

In addition to the physical channels of Table 2.4, there are two synchronization channels (see Table 2.5) which are used for parameter estimation. In the following we describe the framing and channel multiplexing as well as the coding and modulation scheme.

### Framing and Channel Multiplexing

The physical resources are organized in frames of OFDM symbols. One frame consists of 64 OFDM symbols and is divided equally in a CH transmission time interval (TTI) and a MR TTI (see Figure 2.5). The first four symbols of the CH TTI are reserved for pilot symbols. Each CH transmits one common pilot symbol (CHSCH$_0$) at position 0 and
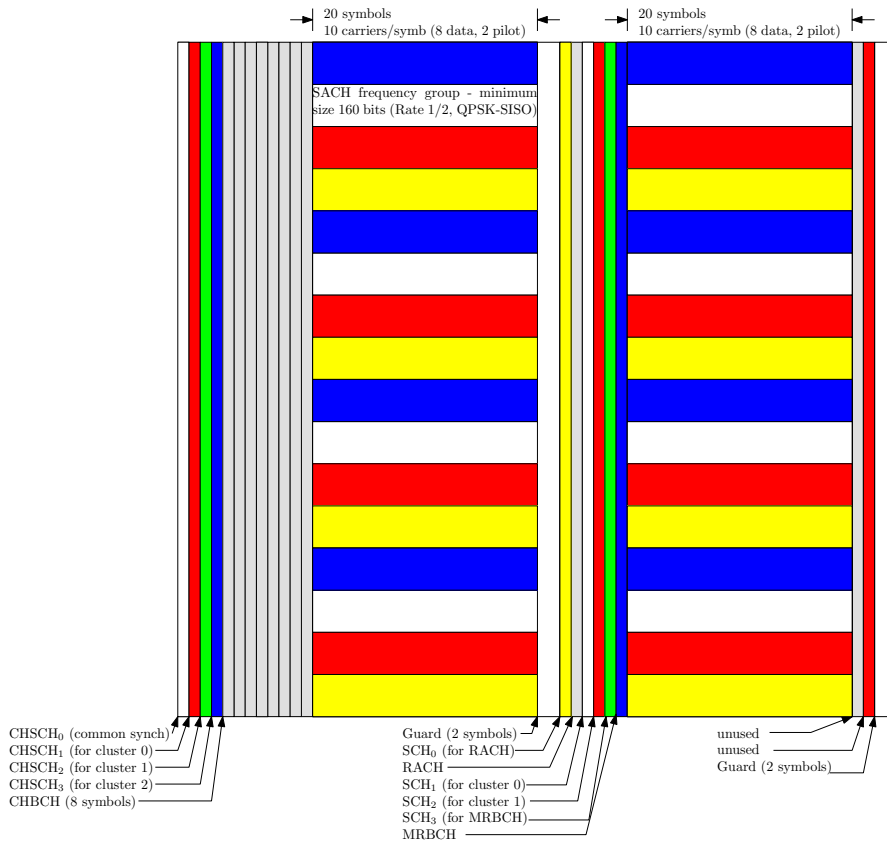
Figure 2.5: OpenAirMesh frame structure.
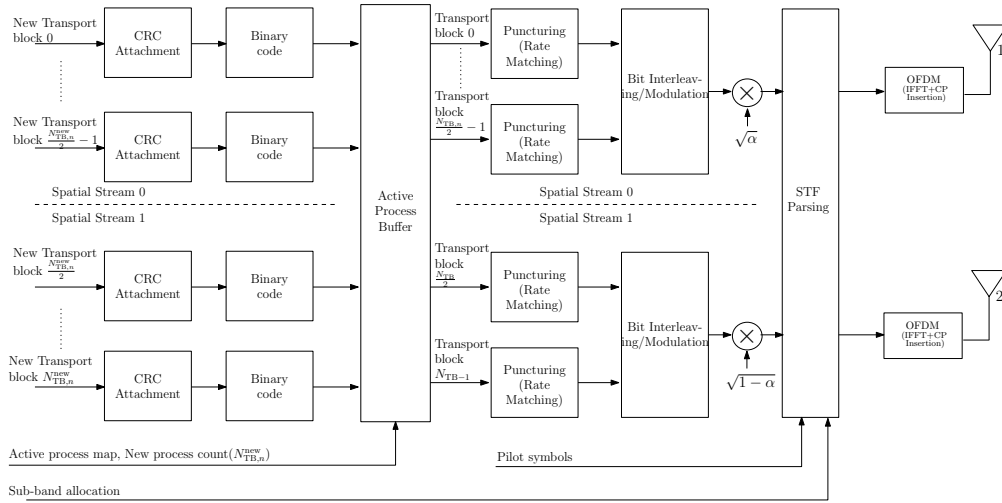
Figure 2.6: OpenAirMesh Coded Modulation and HARQ.

one dedicated pilot symbol ($CHSCH_i$) at position $i \in \{1, 2, 3\}$. This way we can ensure orthogonality between the pilots of different CH received at one MR. The pilot symbols are followed by the broadcast channel (CH-BCH), which contains 128 data subcarriers and 32 pilot subcarriers. The remaining 20 OFDM symbols of the CH TTI frame are divided into 16 ressource blocks (RB), which constitute the multiplexed scheduled access channels (CH-SACH). Each RB contains 8 subcarriers for data and 2 pilot subcarriers (one for each CH), which are used for frequency offset compensation.

The MR TTI contains the random access channel (MR-RACH) with an associated pilot symbol ($SCH_0$). The next two symbols are reserved for pilots. Each MR transmits a pilot symbol $SCH_i$, $i \in \{1, 2\}$ corresponding to the cluster it belongs to. This way we can ensure orthogonality between the pilots of different CHs. The pilot symbols are followed by the uplink broadcast channel (MR-BCH) with an associated pilot symbol (MRSCH). The rest of the uplink frame contains the multiplexed scheduled access channels (MR-SACH). The end of the CH and MR TTIs are protected by a guard interval of two symbols. All pilots are designed for MIMO and/or multi-user channel estimation at the corresponding end.

### Coding and Modulation

OpenAirMesh makes use of punctured binary codes (64-state rate 1/2 convolutional or 8-state rate 1/3 3GPP/LTE Turbo code). Puncturing can use either 3GPP rate matching or random puncturing in order to fine tune the coding rate to adapt to configurable transport block sizes delivered to PHY by the MAC. The overall coding sub-system is shown in Figure 2.6. New transport blocks arriving from the MAC layer (based on multi-user scheduling) are coded using a CRC extension and the chosen binary code. These are then fed to the active transport block buffer along with those that are to be

retransmitted. Each transmitted block is punctured and then passed to a bit-interleaver and modulation mapper (BICM). OpenAirMesh supports QPSK, 16-QAM and 64-QAM modulation. The transmitted transport blocks can be split into two spatial streams in the case of point-to-point MIMO transmission.

The modulated symbols are then multiplied by an adjustable amplitude and passed to the space-time-frequency (STF) parser. The STF parser multiplexes the pilot symbols and the data symbols into OFDM symbols, taking into account the sub-band allocation from the scheduler. In the case of one available spatial stream the STF parser also performs fast antenna cycling, i.e., every subcarrier is transmitted from a different antenna. This way each stream can access all the degrees of freedom of the channel. In the case of two spatial streams the STF parser guarantees that both streams use different antennas in the same time/frequency dimension. This is a form of superposition coding since the two streams are combined additively in the air through the use of multiple transmit antennas. Last but not least the symbols are transformed to the time domain using an IFFT and a cyclic prefix is appended.

This design allows to use the same transmitter and receiver structure both for point-to-point MIMO as well as distributed MIMO transmission. In the latter case one spatial stream is used at each source and the second stream originates in another part of the network, either in the same cluster or an adjacent cluster. A particular user can decode both streams or simply select the one it requires. In Section 2.4.1 we derive a low-complexity successive interference cancellation (SIC) receiver for this design.

## 2.4 Implementation of OpenAirMesh

In this section we show how OpenAirMesh as specified in Section 2.3 can be implemented as a single-frequency network. The solution makes use of a distributed network synchronization procedure and a dual-stream MIMO interference cancellation receiver. In this section we describe these novel solutions and their implementation on OpenAirInterface. We present results from simulations and field trials in Section 2.5.

The implementation is based on the CBMIMO1 hardware (cf. Section 2.2.1) and is thus restricted to two antennas. Therefore we can process up to two spatial streams coming from two different CHs. The extension of the receiver structure to more antennas can be found in [32].

### 2.4.1 Dual-stream MIMO Receiver Architecture

In this section, after the general overview of the receiver structure in Subsection 2.4.1, we describe two different dual-stream multi-antenna demodulators, namely a linear minimum mean squared error (MMSE) receiver (see Subsection 2.4.1) and an approximate maximum likelihood receiver (see Subsection 2.4.1) [33–35]. The derivations are based on the signal model presented in Subsection 2.4.1.
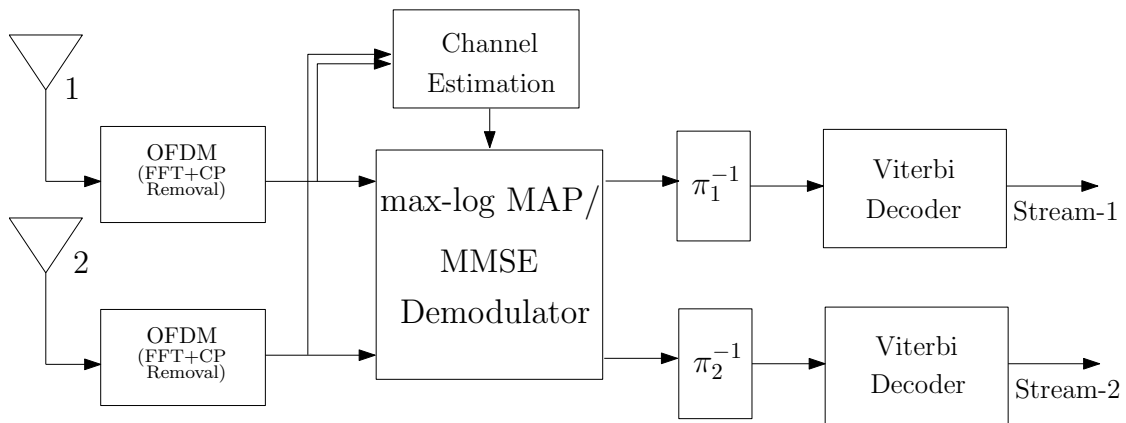
Figure 2.7: Dual-stream receiver structure.

## Receiver Architecture

The overall receiver structure is shown in Figure 2.7. After the CP removal and the FFT, a channel estimation based on the least squares algorithm is performed for CH $i$ using the corresponding synchronization symbol (CHSCH$_i$). Further, the frequency offset is estimated using the pilot subcarriers in the CHBCH. The main block of the receiver is either the spatial MMSE filter or the reduced complexity max-log MAP receiver described in the following subsections. Finally we perform inverse bit interleaving and Viterbi decoding.

## Signal Model

Consider the scenario depicted in Figure 2.2 with two clusterheads but only one MR (MR2). We assume that each CH has $n_t$ antennas and MR2 has $n_r$ antennas. Let $\mathbf{x}_{m,q}^{(j)}$ denote $n_t \times 1$ vector of the transmit symbols for subcarrier $q$ of OFDM symbol $m$ of CH $j$, $j = 1, 2$. We assume that the transmit symbols are taken from a signal set $\chi_j \subseteq \mathbb{C}$ of size $|\chi_j| = M_j$ with a Gray labeling map $\mu_j : \{0, 1\}^{\log|M_j|} \to \chi_j$.

Cascading the IFFT and the CP extension at the CHs and the FFT and the CP removal at MR2, the received signal at MR2 at $q$-th frequency tone and the $m$-th OFDM symbol can be expressed as:

$$\mathbf{y}_{m,q} = \mathbf{H}_q^{(1)} e^{2\pi j \phi_1 m} \mathbf{x}_{m,q}^{(1)} + \mathbf{H}_q^{(2)} e^{2\pi j \phi_2 m} \mathbf{x}_{m,q}^{(2)} + \mathbf{z}_{m,q} \tag{2.1}$$

where $\mathbf{H}_q^{(1)}$ and $\mathbf{H}_q^{(2)}$ denote the $n_r \times n_t$ MIMO channel between CH1 and MR2 and between CH2 and MR2. The channel is assumed to be frequency selective (i.e., it varies with subcarrier index $q$) and block fading (i.e., constant over the OFDM symbols of a frame). $\phi_1$ is the frequency offset between CH1 and MR2 and $\phi_2$ is the one between CH2 and MR2 in radians (to convert them to Hertz, multiply by the OFDM symbol

29

rate). $\mathbf{z}_{m,q} \in \mathbb{C}^{n_r}$ is the vector of circularly symmetric complex white Gaussian noise of variance $\sigma^2$.

Since each clusterhead transmits only one spatial stream and antenna cycling is used, only one element of $\mathbf{x}_{m,q}^{(j)}$, $j = 1, 2$ is non-zero for every $m$ and $q$. We identify this non-zero element with $x_{m,q}^{(j)}$, $j = 1, 2$ and can rewrite (2.1) equivalently as

$$\mathbf{y}_{m,q} = \mathbf{h}_q^{(1)} \mathrm{e}^{2\pi j\phi_1 m} x_{q,m}^{(1)} + \mathbf{h}_q^{(2)} \mathrm{e}^{2\pi j\phi_1 m} x_{m,q}^{(2)} + \mathbf{z}_{m,q}, \tag{2.2}$$

where $\mathbf{h}_q^{(1)}$ and $\mathbf{h}_q^{(2)}$ are the equivalent channel vectors for the non-zero elements. The complex symbols $x_{m,q}^{(1)}, x_{m,q}^{(2)}$ of the 2 streams are assumed to be independent and of variances $\sigma_1^2$ and $\sigma_2^2$ respectively. Assuming that the first stream is the desired stream, the signal to noise ratio (SNR) is given by $\sigma_1^2/\sigma^2$ and the signal to interference ratio (SIR) by $\sigma_1^2/\sigma_2^2$.

## MMSE Receiver

Linear spatial filters such as minimum mean square error (MMSE) and zero forcing (ZF) filters can be used to minimize the level of interference in the former case while nulling out the interference in the latter case. Linear MMSE filters exhibit better performance compared to ZF ones and are thus being considered as favorable candidates for future wireless systems [36, 37]. However, it is well known that MMSE detection for non Gaussian alphabets in low dimensional systems (low number of interferers) is sub-optimal [38] and moreover MMSE detection cannot exploit the interference structure.

The frequency domain MMSE filter $\mathbf{M}_q$ is given as

$$\mathbf{M}_q = \left(\sigma^2 \mathbf{P}^{-1} + \mathbf{H}_q^H \mathbf{H}_q\right)^{-1} \mathbf{H}_q^H$$

where $\mathbf{P}$ is the diagonal power distribution matrix with the diagonal as $\left[\sigma_1^2, \sigma_2^2\right]$ and $\mathbf{H}_q = \left[\mathbf{h}_q^{(1)} \; \mathbf{h}_q^{(2)}\right]$.

The estimates of the transmitted symbols $\hat{\mathbf{x}}_{m,q} = \left[\hat{x}_{m,q}^{(1)}, \hat{x}_{m,q}^{(2)}\right]^T$ are computed in three steps. Firstly, the frequency offset needs to be compensated by computing $\mathbf{y}_{m,q}' = \mathrm{e}^{-2\pi j\phi_1 m} \mathbf{y}_{m,q}$. Secondly the spatial filter $\mathbf{M}_q$ is applied to $\mathbf{y}_{m,q}'$ by computing $\tilde{\mathbf{x}}_{m,q} = \mathbf{M}_q \mathbf{y}_{m,q}'$. Finally an unbiasing operation is performed by computing $\hat{\mathbf{x}}_{m,q} = \Gamma_q^{-1} \tilde{\mathbf{x}}_{m,q}$ where $\Gamma_q = \mathrm{diag}\left(\mathbf{M}_q \mathbf{H}_q\right)$.

Post detection interference is assumed to be Gaussian which on one hand reduces the computational complexity but on the other adds to the sub-optimality of MMSE detection. MMSE pre-processing decouples the spatial streams and the bit metric for the $i$-th bit for bit value $b$ of the symbol $x_{m,q}^{(k)}$ on $k$-th stream is given as

$$\lambda_k^i \left(\mathbf{y}_{m,q}, b\right) \approx \max_{x_{m,q}^{(k)} \in \chi_{k,b}^i} \left[-\frac{\gamma_k^2}{N_0} \left|\hat{x}_{m,q}^{(k)} - x_{m,q}^{(k)}\right|^2\right] \tag{2.3}$$

for $k = 1, 2$ where $\gamma_k$ is the $i$-th diagonal element of $\Gamma_q$. $\chi_{k,b}^i$ denotes the subset of the signal set $x_{m,q}^{(k)} \in \chi_k$ whose labels have the value $b \in \{0, 1\}$ in the position $i$. Based

on these bit metrics, bit log likelihood ratios (LLRs) are calculated which after de-interleaving are passed to the channel decoder.

**Implementation**   The core of the MMSE receiver is the matrix inversion that is needed to calculate the filter

$$\mathbf{M}_q = \underbrace{(\sigma^2 \mathbf{P}^{-1} + \mathbf{H}_q^H \mathbf{H}_q)}_{=: \mathbf{A}_q}{}^{-1} \mathbf{H}_q^H.$$

$\mathbf{M}$ needs to be calculated for every subcarrier and every frame, but we drop the indices for notational convenience.

Since we are limited to a $2 \times 2$ MIMO system, the matrix inversion can be calculated directly using Cramer's rule $A_q^{-1} = \frac{1}{\det(\mathbf{A}_q)} \operatorname{adj}(\mathbf{A}_q)$, where $\operatorname{adj}(\mathbf{A}_q)$ denotes the adjoint of the matrix $\mathbf{A}_q$. Care has to be taken to properly scale the intermediate results in a fixed point implementation. The entries of the channel matrices $\mathbf{H}_q$ are stored in signed 16bit-wide variables, but their resolution is limited to 14 bit due to the A/D convertors. Since the calculation of the determinant $\det(\mathbf{A}_q)$ involves terms up to the fourth power, the dynamic range of the determinant can reach up to 48 bit. In order to handle this high dynamic range we first use a 64bit-wide variable to calculate $\det(\mathbf{A}_q)$ thus not loosing any accuracy. This intermediate result is then shifted such that $\max \det(\mathbf{A}_q)$ uses 16 bits.

In order to calculate the inverse of $\det(\mathbf{A}_q)$, we interpret all numbers as fractional Q15 numbers and use standard fixed-point arithmetic. Intermediate results are stored in double precision. The inverse is scaled back by the mean (over all subcarriers) of $\det(\mathbf{A}_q)$ and saturating to 16bit. Finally, the MMSE filter matrix is calculated according to $\mathbf{M}_q = \frac{1}{\det(\mathbf{A}_q)} \operatorname{adj}(\mathbf{A}_q) \mathbf{H}_q^H$, scaling the intermediate results always to 16 bits.

The high dynamic range of the determinant can cause severe problems. Especially in a frequency selective channel its inverse may saturate on some carriers and can be zero on some other frequencies. This is one of the reasons why the MMSE receiver has a worse performance than the max-log MAP detector described in the next subsection.

### Low Complexity max-log MAP Detector

This detector is a low complexity version of max-log MAP detector and is based on the matched filter outputs [32]. Its low complexity is based on the reduction of one complex dimension. Instead of attenuating the interference this detector exploits its structure and mitigates its effect. Without loss of generality, consider the first stream being the desired stream.

Contrary to the MMSE detection we do not compensate the frequency offsets in the received signal, but instead we integrate them in the channel estimates. Therefore define $\mathbf{h}_{m,q}^{(k)} = \mathbf{h}_q^{(k)} \mathrm{e}^{2\pi j \phi_k m}, k = 1, 2$. For clarity we omit the subindices $m, q$ in the following derivation. The max-log MAP bit metric for bit $b$ of the desired stream $x_1$ is given as

$$\lambda_1^i\left(\mathbf{y}, b\right) \approx \min_{x_1 \in \chi_{1,b}^i, x_2 \in \chi_2} \left\| \mathbf{y} - \mathbf{h}_1 x_1 - \mathbf{h}_2 x_2 \right\|^2$$

$$= \min_{x_1 \in \chi_{1,b}^i, x_2 \in \chi_2} \left\{ \|\mathbf{y}\|^2 + \|\mathbf{h}_1 x_1\|^2 - (2y_1 x_1^*)_R \right.$$

$$\left. + (2p_{12} x_1^* x_2)_R - (2y_2 x_2^*)_R + \|\mathbf{h}_2 x_2\|^2 \right\} \tag{2.4}$$

where $y_1 = \mathbf{h}_1^H \mathbf{y}$ be the matched filter output for the first stream and $p_{12} = \mathbf{h}_1^H \mathbf{h}_2$ be the cross correlation between the first and the second channel. Note that subscripts $(.)_R$ indicates the real part. Writing terms in their real and imaginary parts, we have

$$\lambda_1^i\left(\mathbf{y}, b\right) \approx \min_{x_1 \in \chi_{1,b}^i, x_2 \in \chi_2} \left\{ \|\mathbf{h}_1 x_1\|^2 - (2y_1 x_1^*)_R \right.$$

$$+ \left( 2\left( p_{12,R} x_{1,R} + p_{12,I} x_{1,I} \right) - 2y_{2,R} \right) x_{2,R} + \|\mathbf{h}_2\|^2 x_{2,R}^2$$

$$\left. + \left( 2\left( p_{12,R} x_{1,I} - p_{12,I} x_{1,R} \right) - 2y_{2,I} \right) x_{2,I} + \|\mathbf{h}_2\|^2 x_{2,I}^2 \right\} \tag{2.5}$$

where $(.)_I$ indicates imaginary part. For $x_2$ belonging to the equal energy alphabets (such as QPSK), the values of $x_{2,R}$ and $x_{2,I}$ which minimize (2.5) need to be in the opposite directions of $2\left( p_{12,R} x_{1,R} + p_{12,I} x_{1,I} \right) - 2y_{2,R}$ and $2\left( p_{12,R} x_{1,I} - p_{12,I} x_{1,R} \right) - 2y_{2,I}$ respectively thereby evading search on alphabets of $x_2$ and reducing one complex dimension of the system. The bit metric is therefore written as

$$\lambda_1^i\left(\mathbf{y}, b\right) \approx \min_{x_1 \in \chi_{1,b}^i, x_2 \in \chi_2} \left\{ \|\mathbf{h}_1 x_1\|^2 - (2y_1 x_1^*)_R \right.$$

$$- \left| \left( 2\left( p_{12,R} x_{1,R} + p_{12,I} x_{1,I} \right) - 2y_{2,R} \right) \right| |x_{2,R}|$$

$$\left. - \left| \left( 2\left( p_{12,R} x_{1,I} - p_{12,I} x_{1,R} \right) - 2y_{2,I} \right) \right| |x_{2,I}| \right\} \tag{2.6}$$

For non equal energy alphabets (such as 16-QAM), it is the minimization problem of a quadratic function again trimming one complex dimension of the system. In that case, the real and imaginary parts of $x_2$ which minimizes (2.4) are given as

$$x_{2,R} \to -\frac{\left( p_{12,R} x_{1,R} + p_{12,I} x_{1,I} \right) - y_{2,R}}{\|\mathbf{h}_2\|^2}$$

$$x_{2,I} \to -\frac{\left( p_{12,R} x_{1,I} - p_{12,I} x_{1,R} \right) - y_{2,I}}{\|\mathbf{h}_2\|^2} \tag{2.7}$$

where $\to$ indicates the quantization process in which amongst the finite available points, the point closest to the calculated continuous value is selected.

The reduced complexity max-log MAP detector has a much lower complexity than the MMSE receiver [33]. Furthermore, it can be implemented without any division and therefore it is numerically more stable than the MMSE receiver.

### 2.4.2 Network Synchronization

The dual-stream MIMO receiver described above requires timing and frequency synchronization. It has to be assured that the transmit frames are aligned and that the carrier frequency offsets between different nodes are small. The accuracy of the timing, i.e., the time difference between signals coming from the two different CHs, has to be smaller than the CP length of the OFDM system. Altough carrier frequency offsets are compensated in the receiver, large frequency offsets cause intercarrier interference and thus degrade the performance of the receiver. We will evaluate the maximum allowable frequency offset in Section 2.5 by simulation.

Timing synchronization can be achieved by using high accuracy reference clocks, such as rubidium oscillators or global positioning system (GPS) receiver. However, the rubidium oscillators are very expensive (in comparison with other components of the receiver) and very large. GPS receivers on the other hand are not able to operate indoors. Therefore we will take a distributed network synchronization approach.

In nature, distributed synchronization scheme can be observed on the flashing of fireflies [40]. Recently, this nature-inspired scheme has been applied to synchronization in wireless networks [41–44]. However, most of these works consider the isolated synchronization problem and neglect the actual data communication. The pulse-coupled oscillator model (the model inspired by firefly synchronization) assumes that nodes have to be listening to all other nodes except during its own transmission of the synchronization pulse and immediately afterwards (refractory period). Therefore data transmission can only take place in the refractory period. However, this period must not be very long because otherwise the system becomes unstable [43].

In OpenAirMesh we follow a similar approach as in [15] for distributed timing synchronization. It is based on the two physical channels CHSCH and MRSCH (see Table 2.5) which are transmitted in alternating TTIs from the CHs and MRs respectively. Initially we declare one CH to be the primary CH, which is the reference clock in the system. The primary CH continuously sends out a synchronization signal (the CHSCH) that allows every MR within the CH's broadcast region to synchronize to the network. As soon as a MR is synchronized (i.e., when it can detect the CHBCH successfully), it sends out a synchronization signal itself (the MRSCH). A secondary CH not within the broadcast domain of the primary CH can use the MRSCH to synchronize to the network. As soon as a secondary CH is synchronized to the network, it also sends out a CHSCH, allowing further MRs to synchronize, and so on. A positive side-effect of this method is that several MRs form a distributed antenna array when sending out the MRSCH. This means that the secondary CH can benefit from this array gain when detecting the MRSCH.

For the carrier phase synchronization, we use off-line calibration prior to the system deployment. However, the granularity of the calibration on the CBMIMO1 cards is in the order of 500Hz, causing residual frequency offsets.

### 2.4.3 Integration

The dual-stream MIMO receiver and the distributed network synchronization procedure described above enables the implementation of a single-frequency mesh network. Since all CHs are synchronized and transmit on the same frequency, MRs that are in the broadcast domain of two such clusters must use the dual-stream MIMO receiver to decode the CHBCHs of both CHs concurrently. But the receiver can also be used for the SACH (both in the uplink and in the downlink) allowing the CHs to schedule their resources independently (and thus significantly reducing the signalling overhead). For the downlink SACH, the receiver is used exactly the same way as for the CHBCH. On the uplink the MR transmit two independent data streams as described in Section 2.3.3 and the CHs decode only the stream dedicated for them, treating the other one as interference.

## 2.5 Experiments and Results

In this section we investigate the performance of the two dual-stream receiver structures described in the previous section. Firstly, in Subsection 2.5.1, we perform computer simulations of the two receiver structures using a simple synthetic channel model. Secondly, in Subsection 2.5.2 we present performance results from the real-time implementation on the OpenAirInterface platform. Last but not least, in Subsection 2.5.3 we present field trial experiments that were conducted within the CHORIST project[4] close to Barcelona, Spain in February 2009.

All performance comparisons (both for simulation and lab tests) were done using the broadcast channel (BCH) of the primary clusterhead (CH1) with interference from the BCH from the secondary clusterhead (CH2). The BCH uses QPSK modulation and rate 1/2 convolutional code. The block length is 1056bits, which corresponds to 8 OFDM symbols with 132 data subcarriers each. We use 2 antennas on all nodes.

### 2.5.1 Computer Simulations

In the computer simulations we isolate and study the effect of the following phenomena on the performance of the receiver: ($i$) channel state information at the receiver (CSIR), ($ii$) frequency selective fading vs. frequency flat fading, ($iii$) Rayleigh fading vs. Ricean fading, ($iv$) receive antenna correlation, and ($v$) frequency offsets.

**Channel Model**

For the simulations the $2 \times 2$ MIMO channel matrices $\mathbf{H}_q^{(1)}$ and $\mathbf{H}_q^{(2)}$ are modeled as spatially white and independent. The channel is assumed to be constant during a block and varies independently between blocks. We use both a frequency flat fading model as well as a frequency selective model. In the frequency flat case the channel matrices stay constant over all subcarriers $q$ with channel coefficients drawn from a Rayleigh

---

[4]http://www.chorist.eu

distribution with unit variance. In the frequency selective case we model the channel as a tapped delay line with 8 sample-spaced taps with an exponential decaying power delay profile. Each tap undergoes Rayleigh fading. If line-of-sight (LOS) is present, the first tap undergoes Ricean fading. Receive correlation is modeled by multiplying (from the left) the MIMO channel matrices with the square root of the receive correlation matrix $\mathbf{R}_{\mathrm{Rx}} = \begin{pmatrix} 1 & \rho \\ \rho & 1 \end{pmatrix}$.

## Simulation Results

The two receiver structures described in Section 2.4.1 were implemented in fixed-point C. The simulation model follows the model (2.1) with the difference that the C simulator includes the IFFT and CP insertion at the transmitter and the corresponding FFT and CP removal at the receiver. The channel is thus simulated in the time domain rather than in the frequency domain. Further, we can simulate carrier frequency offsets. By not adding any noise on the pilot symbols we can also simulate the case of perfect CSIR. This allows us to study the impact of imperfect channel estimates on the two receiver structures.

We perform Monte Carlo simulations with the MMSE receiver and the max-log MAP receiver. We fix the SNR for the first stream and vary the interference from the second stream on the y-axis. Each figure shows the frame error rates of the first stream for both receivers and several SNR values. We only show a representative subset of the simulation results:

- Figure 2.8 shows results for the frequency flat Rayleigh fading channel with perfect CSIR.

- Figures 2.9, 2.10, and 2.11 show results for the frequency flat and the frequency selective Rayleigh fading channel as well as for a frequency selective Ricean fading channel with a Ricean K-factor of $K = 10$.

- Figure 2.12 shows results for a frequency flat Rayleigh fading channel with a receive antenna correlation of $|\rho| = 0.75$.

- Figure 2.13 shows results for the frequency selective channel, where CH2 has a frequency offset of 1500 Hz w.r.t. the receiver.

We can make the following observations. First of all the max-log MAP receiver always performs better than the MMSE receiver. Together with the fact that the max-log MAP receiver has actually less complexity that the MMSE receiver [33], it is clearly the first choice for such a system. Also note that the performance of the max-log MAP receiver actually gets better when the interference gets stronger. Channel estimation errors have a stronger impact on the max-log MAP receiver than on the MMSE receiver. On the other hand it can be seen that in a frequency selective channel the max-log MAP receiver profits most from the the additional diversity, while the performance of the MMSE receiver hardly improves. This is due to the fact that the max-log MAP receiver has full diversity gain while MMSE receiver loses one order of diversity [45].

Figure 2.8: Frame error rate of the first stream of the of the MMSE and max-log MAP receiver for a frequency flat Rayleigh fading channel with perfect CSIR. Results are plotted for different SNR levels of the first stream. The $x$ axis denotes the interference of the second stream w.r.t. the first stream.
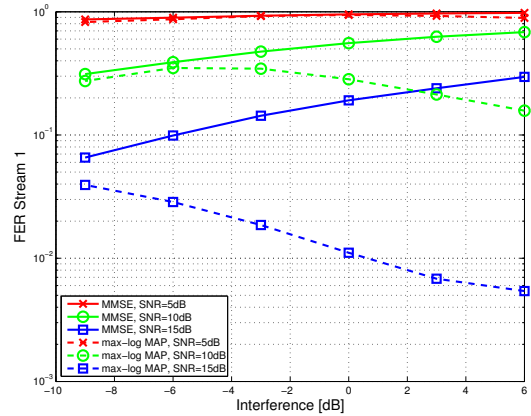


Figure 2.9: Frame error rate of the first stream of the of the MMSE and max-log MAP receiver for a frequency flat Rayleigh fading channel. Results are plotted for different SNR levels of the first stream. The $x$ axis denotes the interference of the second stream w.r.t. the first stream.
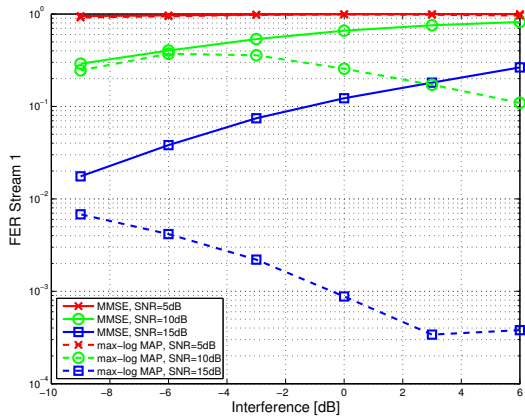


Figure 2.10: Frame error rate of the first stream of the of the MMSE and max-log MAP receiver for a frequency selective Rayleigh fading channel. Results are plotted for different SNR levels of the first stream. The $x$ axis denotes the interference of the second stream w.r.t. the first stream.
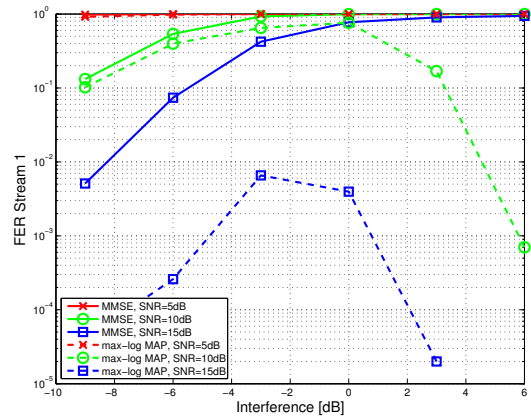


Figure 2.11: Frame error rate of the first stream of the of the MMSE and max-log MAP receiver for a frequency selective Ricean fading channel with a K-factor of $K = 10$. Results are plotted for different SNR levels of the first stream. The $x$ axis denotes the interference of the second stream w.r.t. the first stream.
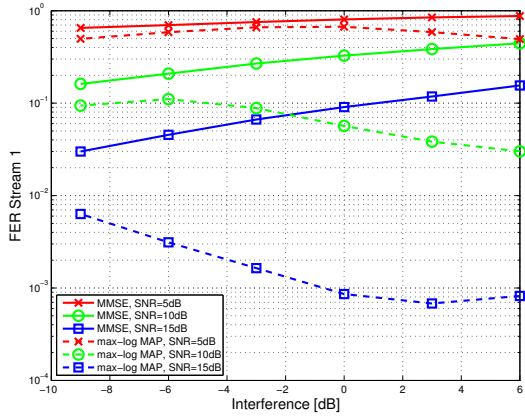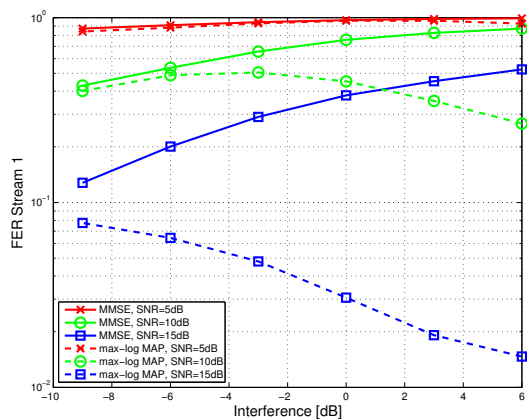
Figure 2.12: Frame error rate of the first stream of the of the MMSE and max-log MAP receiver for a frequency flat Rayleigh fading channel with a receive correlation of $|\rho| = 0.75$. Results are plotted for different SNR levels of the first stream. The $x$ axis denotes the interference of the second stream w.r.t. the first stream.
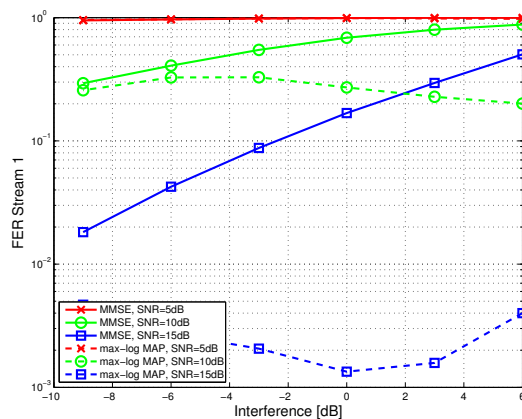
Figure 2.13: Frame error rate of the first stream of the of the MMSE and max-log MAP receiver for a frequency selective Rayleigh fading channel. CH2 has a frequency offset of $1500\,\mathrm{Hz}$ w.r.t. the receiver. Results are plotted for different SNR levels of the first stream. The $x$ axis denotes the interference of the second stream w.r.t. the first stream.

In a LOS Ricean fading channel, the performance of the max-log MAP receiver is better than in a Rayleigh fading channel only if the power of the interference is either stronger or weaker than the desired signal. If the powers are similar, a LOS component is not beneficial for the performance. Frequency offsets also have a very strong negative impact on the performance of the system. In fact as the interference gets stronger the max-log MAP receiver is not able to cancel out the interference as good as in the case with no frequency offsets. Last but not least, receive correlation also degrades the performance of the system.

### 2.5.2 Lab Tests

**Test Setup**

The dual stream receiver was tested in the lab using an extended version of the Eurecom MIMO OpenAir Sounder (EMOS) [4]. The EMOS can be seen as a stand-alone version of the physical layer of the OpenAirMesh testbed. Only the synchronization symbols (CHSCH, MRSCH) and the broadcast channels (CHBCH, MRBCH) are transmitted. Instead of the scheduled access channels (SACH), additional pilot symbols are transmitted that can be used for channel sounding purposes, but this functionality is not presented in this paper. Instead we record the frame error rates (based on the CRC check) of the CHBCH. Note that the real-time system uses the same fixed point code
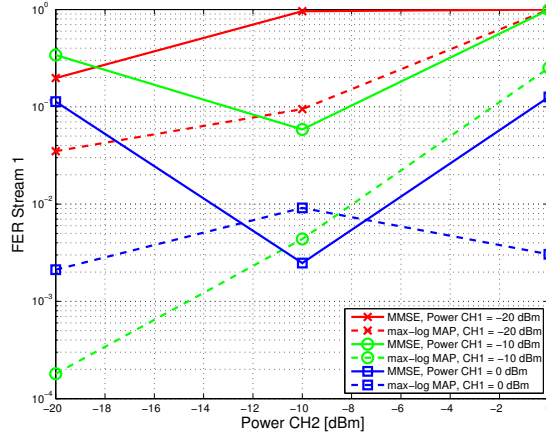
Figure 2.14: Measured frame error rate of the first stream using real-time MMSE and max-log MAP receiver in the Eurecom lab. Results are plotted for different power levels of the two clusterheads.



Figure 2.15: Five node mesh network trial in Bellaterra, Spain. MR1 is located at the roof of the red fire brigade building. CH1 and MR2 are located on opposite sides of the parking lot in front of the building. CH2 and MR3 are on the other side of the building.

for the receiver as the simulator.

For the experiments we set up three nodes (CH1, CH2 and MR2) in our lab. To simulate different SNR levels at the receiver we changed the transmit powers of the two CHs between -20 dBm and 0 dBm.

**Results**

Figure 2.14 show the FER of the first stream for different SNR values for the max-log MAP and the MMSE receiver respectively. It is worth noting that in the test setup we encountered a frequency offset of the second stream of around 500 Hz, while there was very little offset on the first stream (less than 10 Hz). This is very likely the reason why the interference cannot be cancelled out that well at a high interference level. Another difference to the simulations is the correlation of the MIMO channel, which was approximately $|\rho| = 0.9$ in the measurements. As we have seen in the simulations this has a very strong impact on the results. Nevertheless, we can still observe similar trends in the measurements as in the simulations, such as that the MMSE receiver has in general a worse performance than the max-log MAP receiver.

### 2.5.3 Field Trials

One major application of OpenAirMesh platform is the demonstration of rapidly-deployable broadband ad-hoc communications systems for public safety units in interventions following natural disasters and industrial accidents. Such a demonstration took place in February 2009 in Bellaterra, Spain in the context of the European project CHORIST, which is funded by the 6th framework program of the European Commission.

During the trials we set up a mesh network with five nodes as depicted in Figure 2.2 on the parking lot of the fire brigade building in Bellaterra (see Figure 2.15). MR1 was placed on the roof of the building and served as an edge router establishing the connection to the core network and the control room. CH1 and MR2 were placed on the parking lot in front of the building. CH2 and MR3 were placed behind the building, such that there was no connection between CH1 and MR3 as well as between CH2 and MR1. MR2 was in the broadcast domain of both CHs, relaying traffic between them.

Both MR2 and MR3 were used as gateways to other networks. Two different end-to-end applications were tested on the network: a video surveillance application and a push-to-talk VoIP application. During the trials we managed to establish a reliable connection (in the sense that both applications were running smoothly) between MR1 and MR3. See the CHORIST website[5] for more details and a video of the demo.

## 2.6 Conclusions

In this paper we have shown the feasibility of distributed network synchronization and distributed MIMO on the real-time open-source OpenAirInterface platform. We conclude this paper by describing a few lessons we have learned during the implementation and the field trials.

Synchronization is a prerequisite for the dual-stream MIMO receiver described in this paper and other cooperative communication schemes. We have seen that the proposed synchronization is feasible for small scale networks in indoor and medium-range outdoor scenarios. For larger networks, the requirement of a single reference clock is somewhat restrictive, since when it fails the whole network fails. Also it is not proven that the algorithm is stable in larger networks. We are planning to investigate this issue in future works.

As for the implementation of the dual-stream MIMO receiver we have seen that the reduced complexity max-log MAP detector has several advantages over the linear MMSE receiver. First of all its performance is much better (both diversity and coding gain), especially when the interference level is high. Further it can be implemented without any divisions which is very advantageous on a fixed point processor. The implementation of the MMSE receiver on the other hand requires a matrix inversion, which is not trivial using fixed point arithmetic.

During the trials we have also seen that the dual-stream MIMO receiver is very sensitive to channel conditions. The best performance is achieved if the two transmitters

---

[5]`http://www.chorist.eu`

have a line of sight to the receiver and if the receive correlation is small. However, positioning the nodes and their antennas in such a way is not trivial. In case of the max-log MAP receiver significant differences in the received powers form the two sources can also improve the performance.

In future work we would like to include distributed space-time coding and collaborative beamforming into OpenAirInterface. This could for example be used in a multiple relay channel, when several relays are placed between two clusterheads. One particular aspect we would like to investigate are the consequences of such scenarios on design aspects related to spatial HARQ and channel coding mechanisms.

# Chapter 3

# On the trade-off between feedback and capacity in measured MU-MIMO channels

In this chapter we study the capacity of multi-user multiple-input multiple-output (MU-MIMO) downlink channels with codebook-based limited feedback using real measurement data. Several aspects of MU-MIMO channels are evaluated. Firstly, we compare the sum rate of different MU-MIMO precoding schemes in various channel conditions. Secondly, we study the effect of different codebooks on the performance of limited feedback MU-MIMO. Thirdly, we relate the required feedback rate with the achievable rate on the downlink channel. Real multi-user channel measurement data acquired with the Eurecom MIMO OpenAir Sounder (EMOS) is used.

To the best of our knowledge, these are the first measurement results giving evidence of how MU-MIMO precoding schemes depend on the precoding scheme, channel characteristics, user separation, and codebook. For example, we show that having a large user separation as well as codebooks adapted to the second order statistics of the channel gives a sum rate close to the theoretical limit. A small user separation due to bad scheduling or a poorly adapted codebook on the other hand can impair the gain brought by MU-MIMO. The tools and the analysis presented in this paper allow the system designer to trade-off downlink rate with feedback rate by carefully choosing the codebook.

## 3.1  Introduction

Multiple-input multiple-output (MIMO) wireless communication systems can substantially improve the spectral efficiency in wireless point-to-point links. Early theoretical results [46, 47] are beginning to be successfully implemented in systems and standards [48, 49].

Recently there has also been a great deal of interest on how to carry these perfor-

mance gains over to the system level. Multi-user MIMO (MU-MIMO) refers to a system where a transmitter equipped with multiple antennas is communicating with several users simultaneously on the same physical resources. The users can have multiple antennas too, but this is not a necessity. Especially the downlink (or broadcast) channel of such systems has received a lot of attention in the context of emerging cellular systems, such as the IEEE worldwide inter-operability for microwave access (WiMAX) [50] or the 3GPP long term evolution (LTE) [49]. The downlink channel is also the focus of this paper.

By regarding the set of antennas of the users as one virtual antenna array, results from conventional MIMO can be readily applied to the MU-MIMO case. However, since the users cannot cooperate, all the space-time processing has to be done at the transmitter side in the form of precoding. The performance of MU-MIMO depends on a variety of factors such as ($i$) the precoding scheme used, ($ii$) the quality of the channel state information at the transmitter, and ($iii$) the channel characteristics and the user separation.

Information theory reveals that if there is full channel state information at the transmitter (CSIT) and the receiver (CSIR), the optimum transmit strategy for the MU-MIMO broadcast channel involves a theoretical pre-interference cancellation technique known as dirty paper coding (DPC) combined with an implicit user scheduling and power loading algorithm [51, 52]. Since DPC is computationally expensive and hard to implement also simpler, sub-optimal transmit strategies based on user scheduling together with linear precoding have been proposed [53, 54].

CSIT can be achieved either by exploiting channel reciprocity in a time division duplex (TDD) system or by means of a limited feedback channel in a frequency division duplex (FDD) system. In the latter case, which is also the focus of this paper, channel vector quantization (CVQ) based on predefined codebooks can be used to feed back a quantized version of the channel [55]. The codebook has to be designed in a way to minimize the quantization error of the channel matrices as well as the feedback overhead. However, minimizing the quantization error requires large codebooks which require a large amount of feedback [56]. In a real system, the best trade-off between these two design criteria has to be found.

Most of the current literature studies MU-MIMO systems in ideal simulation environments using independent and identically distributed (i.i.d.) Rayleigh fading channel models. Compared to a single-user MIMO (SU-MIMO) time division multiple access (TDMA) system, DPC with perfect CSIT can bring a theoretical performance gain of up to $\max(\min(M/N, K), 1)$ in an i.i.d. Rayleigh fading channel, where $M$ and $N$ is the number of transmit antennas and receive antennas respectively and $K$ is the number of users [57]. If all users experience the same transmit correlation matrix and the number of users is large, [58] showed that the rate loss due to correlation is $M \log c$, where $c$ depends on the scheduling scheme and the eigenvalues of the covariance matrix.

However it was shown in [59, 60] that neither the i.i.d. assumption nor the assumption of a common transmit correlation matrix for one user holds true in real measured MU-MIMO channels. From a system level perspective it is interresting to see the performance

of MU-MIMO with limited feedback in realistic conditions with a small number of users.

Thus, in this paper we use real channel measurements to study MU-MIMO systems with $K = M$ users. We compare the performance of different linear MU-MIMO precoding schemes, such as zero-forcing (ZF) and regularized channel inversion (also called Minimum Mean Square Error (MMSE) precoder) [53] with the achievable capacity in such channels (the DPC region) [61]. We also study the impact of limited feedback based on CVQ using a Fourier codebook, a Grassmannian codebook, a random codebook, and a random codebook exploiting the second order statistics of the channel. Last but not least we evaluate the information rate on the feedback channel using a first order Markov chain model for the temporal evolution of the feedback [62]. Relating this feedback rate to the achievable rate on the broadcast channel provides a mean to evaluate different codebooks.

MU-MIMO channel measurements have been obtained using the Eurecom MIMO OpenAir Sounder (EMOS) [63]. The EMOS can perform real-time channel measurements synchronously over multiple users moving at vehicular speed. The measured channels are stored to disk for offline analysis. For this paper, we have used four transmit antennas and four users with one antenna each.

**Related Work**  Many measurement campaigns for point-to-point MIMO channels have been carried out to date, but MU-MIMO measurements are still rare in the literature. A common practice is to conduct SU-MIMO measurements and later combine them into a MU-MIMO channel. Such an approach has for example been reported in [64–67]. Recently, [68] has claimed that under certain conditions this method is feasible. However, this is definitely not the case for rapidly changing environments and the high-mobility measurements as considered in this paper. To the best of the authors knowledge, real synchronized MU-MIMO channel measurements have only been described in [69]. The measurements were conducted using a MEDAV-LUND channel sounder with its corresponding receiver as well as the receiver of an Elektrobit channel sounder. The measurements of the two receivers are synchronized in a post-processing step using a dummy channel that was inserted between snapshots. The authors present capacity results for the uplink channel, as well as path-loss and delay spreads for the measured scenarios. However, the measurements in [69] are limited to a two-user case while also being very costly and time-consuming.

**Contributions and Outline**  The contributions of this work are as follows

- We assess the performance of different MU-MIMO schemes using several different channel measurements.

- We study the effect of limited feedback using different codebooks in real world conditions.

- We introduce a novel way how to relate feedback rate to capacity of MU-MIMO channels thus providing a mean to evaluate different codebooks.
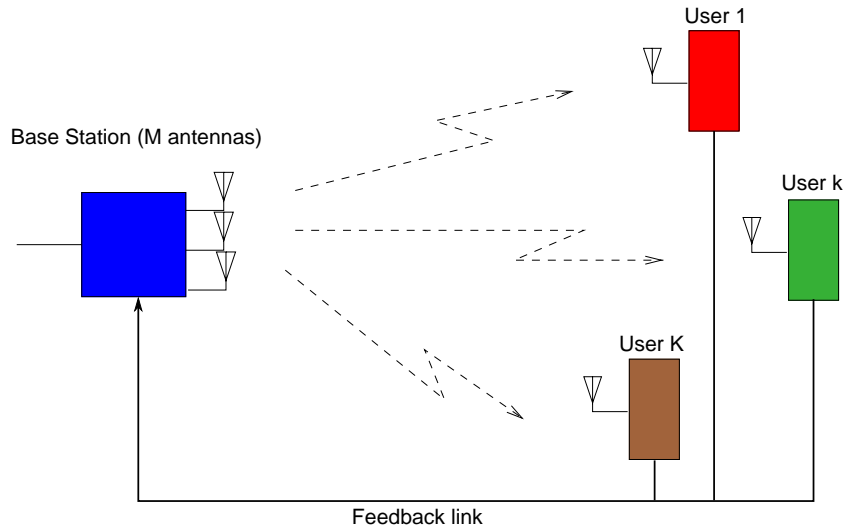
Figure 3.1: Multi-user MIMO System Model.

- We present the EMOS platform and show how the challenge of performing MU-MIMO measurements synchronously over multiple users can be addressed.

The chapter is organized as follows. In Section 3.2 we describe the MU-MIMO system model. Section 3.3 reviews results on the capacity of MU-MIMO channels and describes the different linear precoding schemes studied in this paper. In Section 3.4 we describe how to obtain partial CSIT by means of limited feedback. The measurements and their results are discussed in Section 3.5. Finally conclusions are drawn in Section 3.6. The Eurecom MIMO OpenAir Sounder (EMOS) is described in Section 3.7 .

**Notation**   Column vectors and matrices are denoted by $\mathbf{a}$ and $\mathbf{A}$ respectively. $\mathbf{I}_M$ is the identity matrix of size $M$ and $\mathbf{0}_M$ is an $M$-dimensional vector of zeros. The Euclidean ($\ell_2$) norm of a vector $\mathbf{a}$ is denoted by $\|\mathbf{a}\|$ and the Frobenius norm of a matrix $\mathbf{A}$ is denoted by $\|\mathbf{A}\|_F$. $\mathbb{E}$ denotes expectation, and $\mathcal{CN}(\mathbf{m}, \mathbf{C})$ denotes a multivariate proper complex normal distribution with mean vector $\mathbf{m}$ and covariance matrix $\mathbf{C}$.

## 3.2   System Model

We consider a multi-user, multi-antenna wideband downlink channel in which a base station (BS) equipped with $M$ antennas communicates with $K \leq M$ user equipments (UEs), each equipped with one antenna (see Fig. 3.1). Such a channel is also called a broadcast channel (BC) in the information theory literature. We use orthogonal frequency division multiplexing (OFDM) and thus the sampled received signal $y_{k,m,q} \in \mathbb{C}$ of the $k$-th user at time $m$ and subcarrier $q$ is mathematically described as

$$y_{k,m,q} = \mathbf{h}_{k,m,q}^T \mathbf{x}_{m,q} + n_{k,m,q} \quad \text{for} \quad k = 1, \ldots, K \tag{3.1}$$

44

where $\mathbf{h}_{k,m,q} \in \mathbb{C}^M$ represents the $k$-th user channel response and $n_{k,m,q} \in \mathcal{CN}(0, \sigma^2)$ represents the circularly symmetric additive white Gaussian noise with zero mean and variance $\sigma^2$. The vector of transmit symbols $\mathbf{x}_{m,q} \in \mathbb{C}^M$ is a function of the multiple users' transmit symbols $\mathbf{x}_{k,m,q}$ with covariance matrix $\mathbf{\Sigma}_{k,m,q} = \mathbb{E}\{\mathbf{x}_{k,m,q}\mathbf{x}_{k,m,q}^H\}$. The sub-indices $m$ and $q$ always refer to the time and subcarrier indices, respectively.

The transmitter is subject to a power constraint per subcarrier, i. e., $\mathbf{x}_{m,q}^H \mathbf{x}_{m,q} \leq P$. The total transmit power is not dependent on the number of transmit antennas. Note that we always assume that we transmit to exactly $K = M$ users and we do not study the impact of user scheduling or power control. Further we assume that the noise power $\sigma^2 = 1$.

Equation (3.1) can also be written in matrix notation by defining $\mathbf{H}_{m,q} = [\mathbf{h}_{1,m,q} \dots \mathbf{h}_{K,m,q}]^T$ and the vectors $\mathbf{y}_{m,q}$ and $\mathbf{n}_{m,q}$ accordingly:

$$\mathbf{y}_{m,q} = \mathbf{H}_{m,q}\mathbf{x}_{m,q} + \mathbf{n}_{m,q}. \tag{3.2}$$

We assume that each of the receivers has perfect and instantaneous knowledge of its own channel. Further we assume a zero-delay error-free feedback channel and denote the channel matrix fed back at the transmitter with $\hat{\mathbf{H}}$. We consider two cases for the feedback: $(i)$ full feedback, i.e., the bandwidth is large enough to feed back the full channel estimate and $(ii)$ limited feedback with a resolution of $B$ bits for each subcarrier $q$ and time $m$. For notation convenience, we drop the time and subcarrier indices $m$ and $q$ when their dependence is not needed.

## 3.3 Sum Rates of Multi-user MIMO channels

In this section we review the capacity of multi-user MIMO channels (Subsection 3.3.1) as well as the sum rate of linear precoding schemes (Subsection 3.3.2). For comparison we will also review the sum rate of a multi-user system employing single-user multiple-input single-output (SU-MISO) TDMA in Subsection 3.3.3.

### 3.3.1 Capacity

From the results in [51, 70], the sum capacity of the MU-MIMO downlink channel can be expressed by the following maximization:

$$\mathcal{C}_{\mathrm{BC}}(\mathbf{H}, P) = \max_{\mathbf{\Sigma}_k \geq 0, \sum_{k=1}^K \mathrm{tr}(\mathbf{\Sigma}_k) \leq P} \sum_{k=1}^K \log_2 \frac{1 + \mathbf{h}_k^H \left(\sum_{j=1}^K \mathbf{\Sigma}_j\right) \mathbf{h}_k}{1 + \mathbf{h}_k^H \left(\sum_{j \neq k} \mathbf{\Sigma}_j\right) \mathbf{h}_k}, \tag{3.3}$$

where the maximization is over the set of all positive semidefinite transmit covariance matrices $\mathbf{\Sigma}_k, k = 1, \dots, K$. The objective function of the maximization in (3.3) is a non-convex function of the covariance matrices, making it very difficult to deal with. Fortunately, due to the duality of the BC and the multiple access channel (MAC) [61],

the sum rate capacity of the MIMO BC is equal to the sum rate capacity of the dual MAC with power constraint $P$

$$\mathcal{C}_{\text{BC}}(\mathbf{H}, P) = \mathcal{C}_{\text{MAC}}(\mathbf{H}, P) = \max_{\mathbf{Q}_k \geq 0, \sum_{k=1}^{K} \text{tr}(\mathbf{Q}_k) \leq P} \log_2 \left( 1 + \sum_{k=1}^{K} \mathbf{h}_k^H \mathbf{Q}_k \mathbf{h}_k \right), \qquad (3.4)$$

where each of the matrices $\mathbf{Q}_i$ is a positive semidefinite covariance matrix. Since (3.4) involves the maximization of a convex function, efficient numerical algorithms exist. In this paper, we use the specialized algorithm developed in [71] to calculate $\mathcal{C}_{\text{BC}}(\mathbf{H}, P)$.

It has been shown [52] that the sum rate capacity given in Equation (3.4) is actually achieved by using DPC. However, DPC is complex to implement in practical systems and thus we also study linear precoding schemes in the next section.

### 3.3.2 Linear Precoding

Let $s_k \in \mathbb{C}$ denote the $k$-th user data symbol. Under linear precoding, the transmitter multiplies the data symbols $s_k$ by the precoding vectors $\mathbf{w}_k \in \mathbb{C}^M$ and combines them to the transmit symbol $\mathbf{x}$, i.e., $\mathbf{x} = \sum_{k=1}^{K} \mathbf{w}_k s_k$. In order to fulfill the transmit power constraint, the transmitter further normalizes $\mathbf{x}$, such that $\mathbf{x}^H \mathbf{x} = P$. From (3.1) the resulting received signal vector for user $k$ is then given by

$$y_k = \mathbf{h}_k^T \mathbf{w}_k s_k + \sum_{j \neq k} \mathbf{h}_k^T \mathbf{w}_j s_j + n_k, \qquad (3.5)$$

where the first term is the desired signal, the second term represents the multi-user interference, and the last term the noise. The signal to noise plus interference ratio (SINR) at each user $k$ is thus given by

$$\text{SINR}_k = \frac{\left| \mathbf{h}_k^T \mathbf{w}_k \right|^2}{\sum_{j \neq k} \left| \mathbf{h}_k^T \mathbf{w}_j \right|^2 + \sigma^2}. \qquad (3.6)$$

If the user codes are drawn from an i.i.d. Gaussian distribution, the sum rate of linear precoding is thus given by

$$\mathcal{R}_{\text{BC}}(\mathbf{H}, P) = \sum_{k=1}^{K} \log_2 \left( 1 + \text{SINR}_k \right). \qquad (3.7)$$

In this paper we use a regularized channel inversion with equal power allocation based on the feedback channel to design the precoding vectors $\mathbf{w}_k$ [53]. The regularized channel inverse is given by

$$\mathbf{W} = \hat{\mathbf{H}}^H (\hat{\mathbf{H}} \hat{\mathbf{H}}^H + \beta \mathbf{I})^{-1}, \qquad (3.8)$$

where $\hat{\mathbf{H}} = [\hat{\mathbf{h}}_1, \ldots, \hat{\mathbf{h}}_K]^T$ is the fed back channel matrix and $\beta$ is the regularization factor. The precoding vectors $\mathbf{w}_k$ are finally given by the columns of $\mathbf{W}$.

The above scheme is often referred to as MMSE precoding with equal power allocation due to the analogy with MMSE beamforming weight design criterion if the noise is spatially white. If $\beta = 0$, Equation (3.8) reduces to the ZF precoder. However, when the channel matrix is ill-conditioned, at least one of the singular values of $(\hat{\mathbf{H}}\hat{\mathbf{H}}^H)^{-1}$ is very large, resulting in a very low signal to noise ratio (SNR) at the receivers.

A non-zero $\beta$ value on the other hand allows for a certain amount of multi-user interference. The amount of interference is determined by $\beta > 0$ and an optimal tradeoff between the condition of the channel matrix inverse and the amount of crosstalk ought to be found. In practice, the regularization factor is commonly chosen as $\beta = M\sigma^2/P$ motivated by the results in [53] that show that it approximately maximizes the SINR at each receiver, and leads to linear capacity growth with $M$. The performance of MMSE is certainly significantly better at low SNR and converges to that of ZF precoding at high SNR. However, MMSE does not provide parallel and orthogonal channels and thus power allocation techniques cannot be performed in a straightforward manner.

### 3.3.3   Time Division Multiple Access

In a TDMA system, the BS only serves one user at a time. We analyze the case when full CSIT and with no CSIT. In the case of full CSIT, the capacity of a particular user $k$ is given by

$$\mathcal{C}_{\text{SU-CSIT}}(\mathbf{h}_k, P) = \log_2\left(1 + \frac{P}{\sigma^2}\|\mathbf{h}_k\|^2\right). \tag{3.9}$$

The capacity is achieved by transmit maximum ratio combining [72].

If full CSIT is available the sum rate of the system can be optimized by transmitting to the user with the largest single-user capacity only, exploiting multi-user diversity [73]. However, with multiple transmit antennas and a small number of users (which is the case considered in this paper) the gains of multi-user diversity are reduced. Therefore, we assume that all users are allocated an equal amount of time (round robin scheduling). This also allows a more fair comparison to the linear precoding schemes considered in the previous section. The sum rate of the system is thus given by

$$\mathcal{C}_{\text{TDMA-CSIT}}(\mathbf{H}, P) = \sum_{k=1}^{K} \frac{1}{K}\mathcal{C}_{\text{SU-CSIT}}(\mathbf{h}_k, P). \tag{3.10}$$

When no CSIT is available, the capacity of a particular user $k$ is given by

$$\mathcal{C}_{\text{SU-noCSIT}}(\mathbf{h}_k, P) = \log_2\left(1 + \frac{P}{\sigma^2 M}\|\mathbf{h}_k\|^2\right). \tag{3.11}$$

Again, we assume that multiple users are served using a round robin scheduler and thus the sum rate $\mathcal{C}_{\text{TDMA-noCSIT}}(\mathbf{H}, P)$ can be defined similar to (3.10).

## 3.4 Obtaining CSIT through Limited Feedback

The linear precoding schemes described in the last section require CSIT in the form of the matrix $\hat{\mathbf{H}}$. When a feedback channel with a limited bandwidth (as described in Section 3.2) is available, channel vector quantization can be used to feed back a quantized version of the channel, providing partial CSIT. Such a scheme has also been proposed for LTE [49] and is outlined in Section 3.4.1.

By exploiting time-correlation in the channel, the actual feedback rate can be reduced. Recently, it has been pointed out in [62] that the actual required feedback rate is given by the *CSI source rate*. This measure is introduced in Subsection 3.4.2.

### 3.4.1 Channel Vector Quantization

For each subcarrier $q$ and every time index $m$, the UE $k$ selects a quantization vector with index $I_{k,m,q}$ from a codebook $\mathcal{C} = \{\mathbf{c}_1, \ldots, \mathbf{c}_C\}$ of size $C = 2^B$, such that the angle between the actual channel $\mathbf{h}_{k,m,q}$ and the codeword $\mathbf{c}_{I_{k,m,q}}$ is minimized. This is equivalent to writing

$$I_{k,m,q} = \underset{i=1,\ldots,C}{\operatorname{argmax}} |\mathbf{c}_i^H \mathbf{h}_{k,m,q}|. \qquad (3.12)$$

For every subcarrier, the UE then feeds back the index $I_{k,m,q}$ along with a channel quality information (CQI). In this paper we use the channel vector norm $\|\mathbf{h}_{k,m,q}\|$ as CQI. Note that this choice of CQI is not suitable for multi-user scheduling, since it does not take the multi-user interference and the quantization error into account. However, in this paper we are only interested in the precoder design and do not consider scheduling. Moreover, we assume that the channel vector norm is not quantized, since we are only interested in the ability of the codebook to capture the spatial properties of the channel.

The transmitter, which also knows the codebook, can then reconstruct the channel by a simple lookup table: $\hat{\mathbf{h}}_{k,m,q} = \mathbf{c}_{I_{k,m,q}}\|\mathbf{h}_{k,m,q}\|$. The codebook $\mathcal{C}$ is designed off-line and there are several well-known possibilities. In this paper we consider a Grassmannian codebook, a Fourier codebook, a random codebook and a correlated random codebook.

#### Grassmannian Codebook

The Grassmannian codebook derives its name from the Grassmannian line packing problem, which is defined as follows [74]: how should $C$ one-dimensional subspaces of the $M$-dimensional (complex) Euclidean space be arranged so that they are as far apart as possible? This problem is equivalent to finding the optimal quantization vectors of a source with uniform distribution on the (complex) $M$-dimensional unit sphere. Therefore the resulting codebook is optimal if the elements of the channel vectors $\mathbf{h}_k$ are i.i.d. complex Gaussian distributed [75]. In this work we use the Grassmannian codebook available for download at [76].

**Fourier Codebook**

The Fourier codebook is obtained by defining $\mathbf{c}_i$ as the top $M$ rows of the $i$-th column of the discrete Fourier transform (DFT) matrix of size $C$, i.e.,

$$\mathbf{c}_i = \frac{1}{\sqrt{M}}[1, e^{-2\pi ji/C}, \ldots, e^{-2\pi ji(M-1)/C}]^T. \tag{3.13}$$

Each entry of the codebook can be interpreted as a beamforming vector of a linear antenna array with one fixed beam. This codebook is therefore well suited for line of sight (LOS) channels with linear antenna arrays.

The Fourier codebook index calculation (3.12) can be implemented efficiently (in terms of memory and computation) by means of an inverse fast Fourier transform (IFFT). Also, the codebook does not need to be stored at the transmitter, as it can be easily reconstructed [77].

**Random Codebook**

The quantization vectors of the random codebook are constructed by drawing $\mathbf{c}_i$ randomly from an i.i.d. complex Gaussian distribution on the $M$-dimensional unit sphere, i.e., $\mathbf{c}_i \in \mathcal{CN}(\mathbf{0}_M, \mathbf{I}_M)$ and subsequent normalization, i.e., $\|\mathbf{c}_i\| = 1$.

**Correlated Random Codebook**

The quantization vectors of the correlated random codebook are drawn from complex Gaussian distribution on the $M$-dimensional unit sphere, whose covariance matrix matches the transmit correlation matrix of the channel, i.e., $\mathbf{c}_i \in \mathcal{CN}(\mathbf{0}_M, \mathbf{R}_{\mathrm{Tx}}^{(k)})$ and $\|\mathbf{c}_i\| = 1$. The transmit correlation matrix is defined as

$$\mathbf{R}_{\mathrm{Tx}}^{(k)} = \mathbb{E}\{\mathbf{h}_k \mathbf{h}_k^H\}. \tag{3.14}$$

The application scenario of correlated codebooks considered in this paper is that different BSs or even different sectors of a BS employ codebooks that are adapted to their environment. The transmit correlation matrix should thus be estimated over a wide frequency range and several locations. In this paper we estimate $\mathbf{R}_{\mathrm{Tx}}^{(k)}$ from the measurements by taking the mean of $\mathbf{h}_k \mathbf{h}_k^H$ over all frequencies $q$ and all frames $m$ in one measurement.

For both the random and the correlated random codebook we assume that each user has a different and independently generated quantization codebook as in [56].

### 3.4.2 Feedback Rate

In order to evaluate the intrinsic rate of information brought by the measured channel, we follow [62] and model the time variation of $I_{k,m,q}$ as a finite-state Markov chain of order 1 with $C$ states (see Fig. 3.8 for an example). Let $\mathbf{P}^{(k,q)}$ be the transition probability matrix with elements $P_{l,n}^{(k,q)} = \Pr(I_{k,m,q} = l | I_{k,m-1,q} = n)$. Also define the

| Parameter | Meas. 1–3 | Meas. 4 |
|---|---|---|
| Center Frequency | 1917.6 MHz | 1917.6 MHz |
| Useful Bandwidth | 4.8 MHz | 4.0625 MHz |
| BS Transmit Power | 30 dBm | 30 dBm |
| Number of Antennas at BS ($M$) | 4 | 2 |
| Number of UE ($K$) | 4 | 2 |
| Number of Antennas at UE ($N$) | 1 | 1 |
| Number of Subcarriers ($Q$) | 40 | 80 |

Table 3.1: Parameters of the Eurecom MIMO OpenAir Sounder for the four measurement campaigns.

stationary probability vector $\pi^{(k,q)}$ with elements $\pi_l^{(k,q)} = \Pr(I_{k,m,q} = l)$. $\mathbf{P}^{(k,q)}$ and $\pi^{(k,q)}$ are estimated from the measurements.

We now use Proposition 1 of [62] to calculate the normalized CSI source bit rate per user and per subcarrier

$$\mathcal{R}_{\text{CSI}}(k,q) = B \sum_{l=1}^{C} \pi_l^{(k,q)} (1 - P_{l,l}^{(k,q)}). \tag{3.15}$$

When evaluating the measurements we take the mean over all frequencies $q$ like we do for the capacity evaluations. Further, in the multi-user case we are interested in the sum rate and thus sum over all users $k$

$$\mathcal{R}_{\text{CSI}} = \frac{1}{Q} \sum_{k=1}^{K} \sum_{q=1}^{Q} \mathcal{R}_{\text{CSI}}(k,q). \tag{3.16}$$

## 3.5 Measurements and Results

In this section we present results using real channel measurement data. We first describe the measurement scenarios in Subsection 3.5.1 and the normalization of the recorded channel matrices in 3.5.2. Finally, in Subsection 3.5.3 we apply the metrics for the MU-MIMO sum rate from Section 3.3 and the feedback rate from Section 3.4 directly to the recorded and normalized channel matrices.

### 3.5.1 Measurement Description

The measurements were conducted using the Eurecom MIMO OpenAir Sounder (EMOS) [59, 63, 78] in the vicinity of the Eurecom institute in Sophia-Antipolis, France. The scenario is characterized by a semi-urban hilly terrain, composed by short buildings and vegetation. Fig. 3.2 shows a map of the environment. The BS is located at the roof of Eurecom's southmost building. The antenna is directed towards Garbejaire, a small nearby village. The colors indicate the received signal strength along the measurement
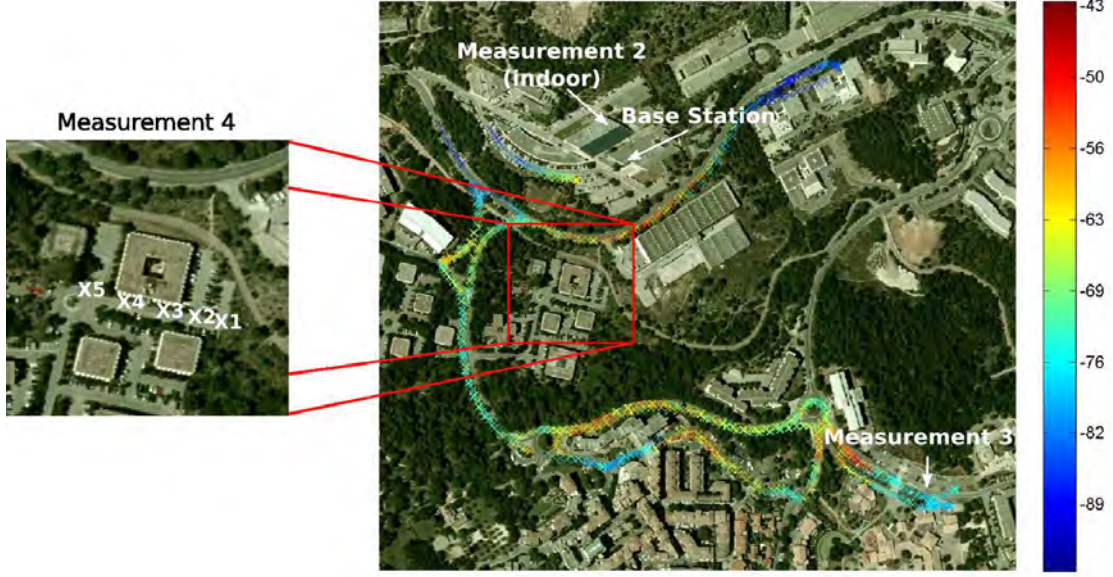
Figure 3.2: Map of the measurement scenario. In measurement 1 the users were driving in cars along the indicated routes (the colors show the received signal strength in dBm along the routes). Measurements 2–4 are indicated on the map.

routes. The measurement parameters are summarized in Table 3.1. A more detailed description of the EMOS can be found in Section 3.7.

In the first three measurements, we use all four transmit antennas (arranged in 2 cross-polarized pairs) and four users with one antenna each. In the first measurement, the UEs were placed inside standard passenger cars which were being driven along the routes shown in Fig. 3.2. The cars had no fixed routes and thus the distance between them was changing. In the second measurement, the users were indoors in the same room, walking around slowly. In the third measurement, the users were parked close together in a parking lot.

In the fourth measurement we use only two co-polarized antennas at the transmitter and two users with one antenna each. The first user is always at position $x_1$ and the second user is at position $x_i, i = 1, \ldots, 5$. Positions $x_1, x_2$, and $x_5$ are LOS while positions $x_3$ and $x_4$ are behind an office building. During the measurements the users were moving only within a few wavelengths in order to get a sufficient number of samples for the evaluation of the statistics of the small scale fading.

### 3.5.2 Normalization

In order to control the average SNR at the UEs, we have to re-normalize the recorded MIMO channel matrices. One measurement results in the set of MIMO channel matrices

$$\{\mathbf{H}_{k,m,q} \in \mathbb{C}^{N \times M}, k = 0, \ldots, K - 1, m = 0, \ldots, N_\mathrm{F} - 1, q = 0, \ldots, Q - 1\},$$
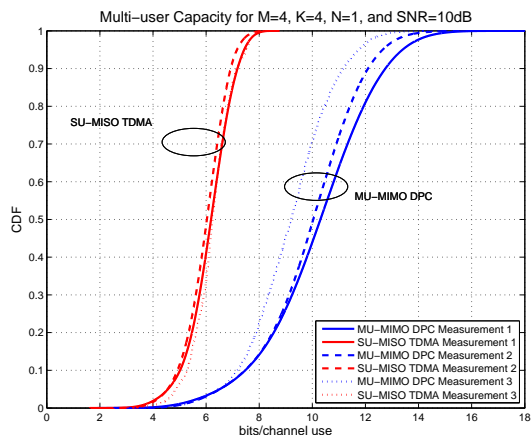
Figure 3.3: CDF of the sum rate of SU-MISO TDMA compared to MU-MIMO with DPC for measurements 1-3. The average SNR is fixed to 10dB for each user.
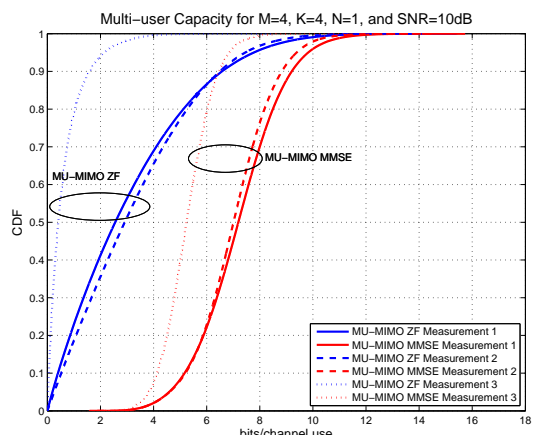
Figure 3.4: CDF of the sum rate of MU-MIMO with ZF and MMSE precoding for measurements 1-3. The average SNR is fixed to 10dB for each user.

where $k$ denotes the user index, $m$ the snapshot index, and $q$ the frequency (or subcarrier) index. $N, M,$ and $K$ are the number of receive antennas, number of transmit antennas and number of users respectively. $N_\mathrm{F}$ is the total number of snapshots per measurement after removing erroneous frames (on average $N_\mathrm{F} \approx 18.000$, corresponding to approx. 50 sec). The total number of channel estimates in the frequency domain is given by $Q = 160/M$, since there are 160 subcarriers in total and the pilots are multiplexed over the $M$ transmit antennas. The MIMO matrices are normalized by

$$\mathbf{H}'_{k,m,q} = \mathbf{H}_{k,m,q} \sqrt{\frac{N N_\mathrm{F} Q}{\sum_{m,q} \|\mathbf{H}_{k,m,q}\|_F^2}} \tag{3.17}$$

such that $\mathbb{E}\{\|\mathbf{H}'_k\|_F^2\} = N$. Since the noise variance $\sigma^2 = 1$, the average SNR at each UE $k$ is thus $\frac{NP}{K}$.

### 3.5.3 Results

#### Comparing different scenarios

Firstly, we compare the performance of MU-MIMO using DPC, ZF precoding, and MMSE precoding as well as SU-MISO TDMA based on the empirical cumulative density function (CDF) of the sum rate (Equations (3.4), (3.7), and (3.10)). We assume an average SNR at the users of 10 dB, which corresponds to the average SNR at the cell edge. The results are plotted in Figures 3.3 and 3.4 for measurements 1-3. Secondly, we compare the mean MU-MIMO sum rate for all the above mentioned schemes with respect to the inter-user distance. The results are plotted in Fig. 3.5 for measurement 4.
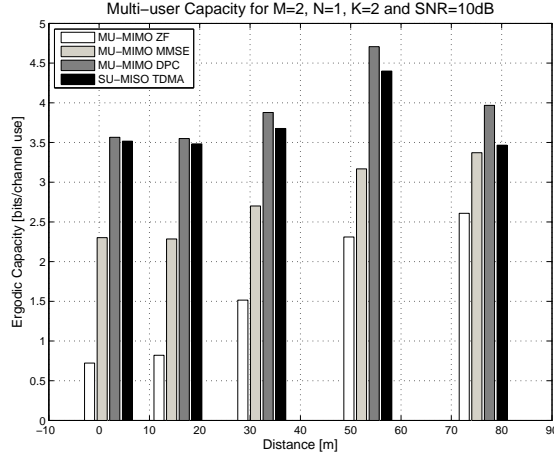
Figure 3.5: Comparison of mean MU-MIMO sum rate for DPC and SU-MISO TDMA, as well as ZF and MMSE precoding with respect to inter-user distance for measurement 4. The average SNR is fixed to 10dB for each user.

It can be seen from Fig. 3.3 that MU-MIMO DPC as well as SU-MISO TDMA do not show a very high variability with respect to the different measurements. However, the linear MU-MIMO precoding schemes (see Fig. 3.4) are very sensitive to the channel conditions. Especially the performance of the ZF precoder drops significantly in the outdoor scenario where the users are close together. In the indoor scenario and the other outdoor scenario where all users are well separated, the performance of the linear MU-MIMO schemes is comparable.

The effect of the inter-user distance on the capacity of the different schemes can be observed more closely in Fig. 3.5. It can be seen that there is a clear relationship between the distance and the capacity of linear precoding schemes: the further apart the users are, the higher the capacity. In fact, for inter-user distances up to 55m, the SU-MISO TDMA scheme always performs better than the linear MU-MIMO schemes. Only in the last measurement at 75m, the MMSE precoder shows a slightly better performance than the TDMA scheme.

The poor performance of linear precoders in scenarios with a small inter-user distance can be explained by looking at the channel correlation matrix of the different scenarios [60, 79]. When the channel is strongly correlated it means that the channel matrix is ill-conditioned. Thus at least one of the singular values of $(\mathbf{HH}^H)^{-1}$ is very large, resulting in a very low SNR at the receivers, when ZF precoding is used. The MMSE precoder can alleviate this problem, but still suffers from the high correlation at the transmitter.

**Comparing Different Codebooks**

Fig. 3.6 and 3.7 compare the CDF of the MU-MIMO sum rate using MMSE precoding based on quantized feedback using different codebooks of size 64 (6 bit) and size 4096 (12

53
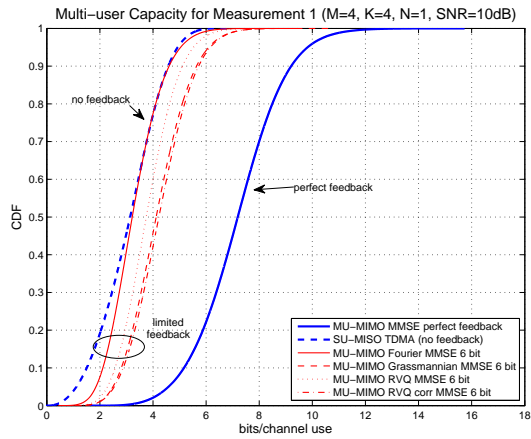
Figure 3.6: CDF of the sum rate of MU-MIMO with MMSE precoding with different feedback schemes for measurement 1. The average SNR is fixed to 10dB for each user. We compare the performance under several codebooks of size 64 (6 bit) with the perfect feedback case as well as to the case with no feedback, which is equivalent to SU-MISO TDMA.

Figure 3.7: CDF of the sum rate of MU-MIMO with MMSE precoding with different feedback schemes for measurement 1. The average SNR is fixed to 10dB for each user. We compare the performance under several codebooks of size 4096 (12 bit) with the perfect feedback case as well as to the case with no feedback, which is equivalent to SU-MISO TDMA.
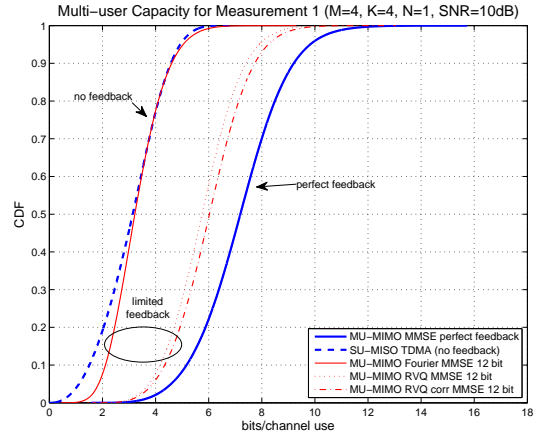
bit) respectively. We also plot the cases with perfect feedback (cf. Equation (3.7)) and no feedback (cf. Equation (3.11)) as lower and upper bounds for comparison. Measurement 1 are used for both plots.

It can be seen that the performance of MU-MIMO with MMSE precoding depends strongly on the chosen codebook. For the evaluated outdoor channel, the Fourier codebook exhibits the worst performance, being only slightly better than a SU-MISO TDMA scheme with no feedback at all. Further, its performance does not increase with the number of feedback bits. The correlated random codebook performs better than the Fourier codebook. The random codebook and the Grassmannian codebook perform best. However, for 6 bits of feedback the gap to the perfect feedback case is still significant (3 bits/sec/Hz at 50% outage rate). Doubling the number of feedback bits to 12 reduces the gap to 1.2 bits/sec/Hz (at 50% outage rate), which is comparable to the theoretical results achieved in [56]. The gain to the SU-MISO TDMA system is 2.9 bits/sec/Hz (at 50% outage rate).

The poor performance of the Fourier codebook can be explained by the fact that ($i$) the BS does not use a linear antenna array and ($ii$) the investigated channel does not have a LOS component. Further, the fact that the performance of the Fourier codebook does not increase with the codebook size can be explained by looking at the maximum cross-correlation between codebook entries, $f(C) = \max_{\mathbf{c}_i, \mathbf{c}_j \in C, i \neq j} |\mathbf{c}_i^H \mathbf{c}_j|$. In the case of a Fourier codebook, $f(C)$ will converge to one as the codebook size increases (just choose two neighboring codebook entries $\mathbf{c}_i$ and $\mathbf{c}_{i+1}$). For the random codebook on the other hand $f(C)$ will converge to zero, since any two codewords are uncorrelated with probability one [80].

**Feedback Rate vs Capacity**

For illustration purposes we plot the quantized channel indices $I_{k,m,q}$ (3.12) for measurement 1 for user $k = 1$ in Fig. 3.8. It can be seen that for some frequencies $q$ the channel remains quite constant whereas for other frequencies it varies more.

In Fig. 3.9 we plot the CSI source rate $\mathcal{R}_{\text{CSI}}$ (3.16) vs. the MU-MIMO sum rate $\mathcal{R}_{\text{MMSE}}$ (3.7) for measurements 1–3, three different codebooks and two codebook sizes. This figure gives an indication of how well the codebook is able to exploit the temporal correlation in the channel (low feedback rate) with respect to the gain in capacity it brings. Points further to the top left of the figure are the best (low feedback rate while having high capacity).

It can be seen that the results are quite different for different codebooks and for the different measurements. Looking at the Fourier codebook (black markers), it can be seen that this codebook requires the largest feedback rate while providing the lowest sum rate. Increasing the number of feedback bit just increases the feedback rate and not the capacity. Considering the Grassmannian codebook (blue markers) on the other hand, it can be seen that this codebook requires much less feedback than the Fourier codebook for the same codebook size while having a larger capacity. Further, increasing the codebook size increases the capacity significantly.

The random codebook has similar properties as the Grassmannian codebook. A 4 bit
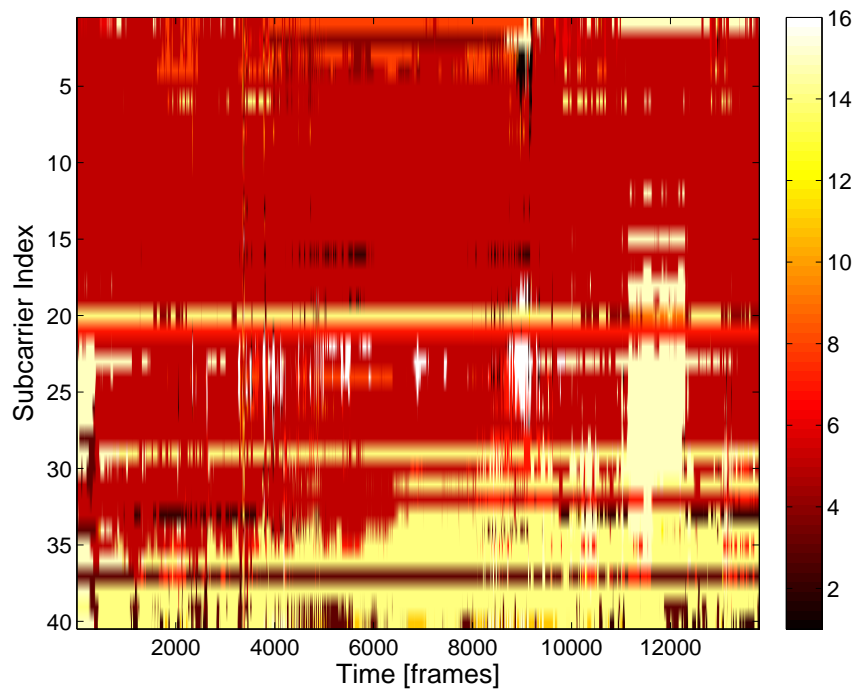
Figure 3.8: Calculated codebook indices $I_{1,m,q}$ using a 4 bit Grassmannian codebook on measurement 1. The different shades of gray correspond to different codebook indices. It can be seen that for some subcarriers the volatility of the codebook indices is quite high (resulting in a higher feedback rate) while for other subcarriers it is rather low (resulting in a low feedback rate).
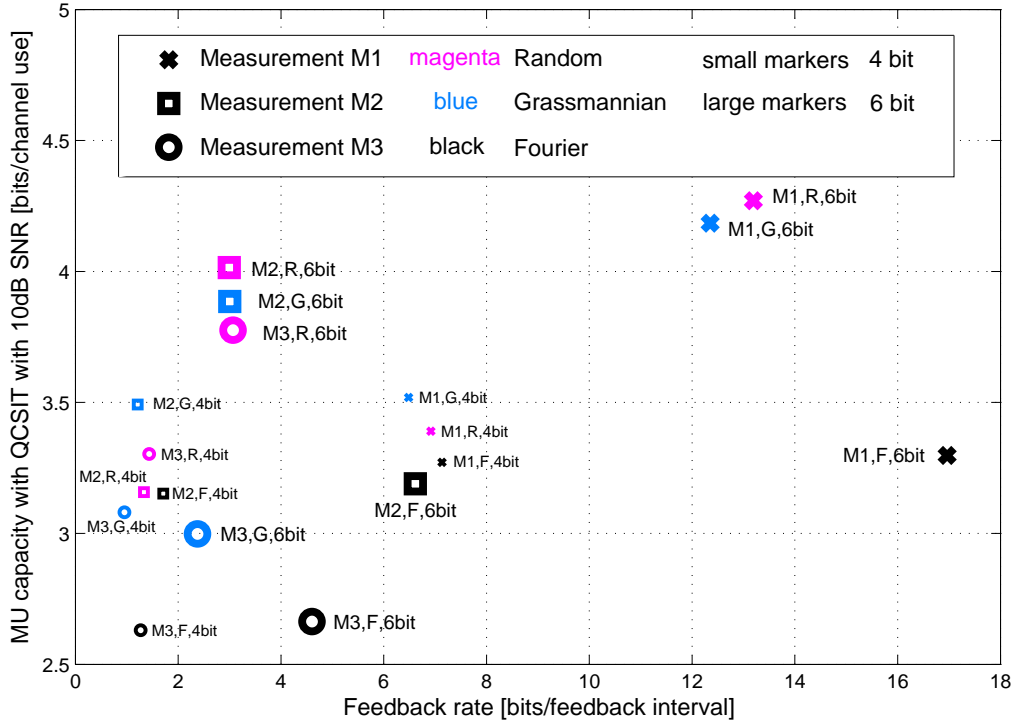
Figure 3.9: CSI source rate of the output of the channel quantizer $\mathcal{R}_{\text{CSI}}$ vs. MU-MIMO sum rate $\mathcal{R}_{\text{MMSE}}$. Each point in the graph represents the result for one measurement, one codebook and one codebook size. This figure allows us to compare different codebooks with respect to their ability to capture the spatial and temporal properties of the channel. The used measurements, codebooks and codebook sizes are given in the legend as well in the figure next to the data point.

random codebook offers a lower capacity than a 4 bit Grassmannian codebook, whereas a 6 bit random codebook offers higher capacity than a 6 bit Grassmannian codebook. Also interesting to note is that the higher mobility measurements require more feedback than the low mobility measurements, but at the same time have a higher capacity.

## 3.6  Conclusions

We have presented an extensive evaluation of different MU-MIMO schemes with perfect and limited feedback in various channel conditions. The data was acquired using Eurecom's MU-MIMO channel sounder EMOS.

From the results we can derive two important criteria that need to be considered when designing MU-MIMO schemes. Firstly, spatial separation of users has a very strong impact on the performance of linear precoding schemes. In particular, the performance of a ZF precoder drops significantly in outdoor scenarios, when the users are close together. Therefore it is necessary to design proper scheduling algorithms that select users with different spatial signatures.

Secondly, the performance of limited feedback MU-MIMO schemes crucially depends on the codebook. It was seen that the performance of the Fourier codebook is hardly better than that of a SU-MISO TDMA scheme with no feedback at all, even for a high number of feedback bits. Further this codebook does not allow any feedback reduction in time-correlated channels. We thus conclude that the Fourier codebook is not able to capture the spatial properties of the measured outdoor wideband channel appropriately. The performance of the random codebook, the Grassmannian codebook and especially the correlated random codebook increases with the number of feedback bits. Also, these codebooks allow for a feedback reduction in time-correlated channels. Thus, these codebooks are able to represent the channel more appropriately.

It can be concluded that the codebook design for MU-MIMO systems remains a hot topic. The tools and the analysis presented in this paper allow to carefully evaluate different codebooks and to choose the codebook that provides a good trade-off between feedback and downlink rate.

## 3.7  The Eurecom MIMO OpenAir Sounder

This Appendix describes the Eurecom MIMO OpenAir Sounder (EMOS). We start by giving an overview of the hardware architecture, followed by a description of the sounding signal, the synchronization procedure, and the channel estimation procedure [59, 79, 80].

### 3.7.1  Hardware Description

The EMOS is based on the OpenAirInterface[1] hardware/ software development platform at Eurecom. The platform consists of a BS that continuously sends a signaling frame,

---

[1]`http://www.openairinterface.org`

(a) BS with PLATON boards

(b) Power amplifiers and Powerwave antenna

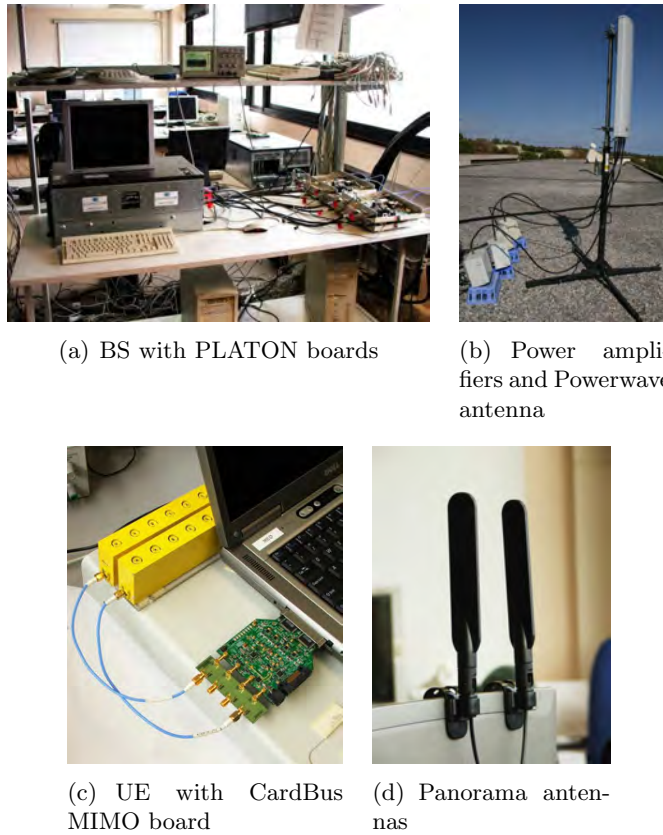(c) UE with CardBus MIMO board

(d) Panorama antennas

Figure 3.10: EMOS base station and user terminals [63].
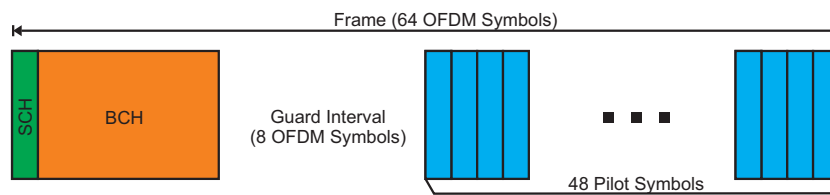


Figure 3.11: Frame structure of the OFDM Sounding Sequence. The frame consists of a synchronization channel, (SCH), a broadcast channel (BCH), and several pilot symbols used for channel estimation.

and one or more UEs that receive the frames to estimate the channel. The BS consists of a workstation with four baseband data acquisition cards, which are connected to four radio-frequency (RF) boards (called PLATON, see Fig. 3.10(a)). The RF signals are amplified and transmitted by a Powerwave 3G broadband antenna composed of four elements which are arranged in two cross-polarized pairs (part no. 7760.00, see Fig. 3.10(b)). The UEs consist of a laptop computer with Eurecom's dual-RF data acquisition card (called CardBus MIMO, see Fig. 3.10(c)) and two clip-on 3G Panorama Antennas (part no. TCLIP-DE3G, see Fig. 3.10(d)). Both equipments operate at 1.900–1.920 GHz with 5 MHz channels[2]. The platform is designed for a full software-radio implementation, in the sense that all protocol layers run on the host PCs under the control of the real-time application interface (RTAI), which is an extension to the Linux operating system.

### 3.7.2 Sounding Signal

The EMOS is using an orthogonal frequency division multiplexing (OFDM) modulated sounding sequence with 256 subcarriers (out of which 160 are non-zero) and a cyclic prefix length of 64. One transmit frame is 64 OFDM symbols (2.667 ms) long and consists of a synchronization symbol (SCH), a broadcast data channel (BCH) comprising 7 OFDM symbols, a guard interval, and 48 pilot symbols used for channel estimation (see Fig. 3.11). The pilot symbols are taken from a pseudo-random quadrature phase-shift keying (QPSK) sequence defined in the frequency domain. The subcarriers of the pilot symbols are multiplexed over the four transmit antennas to ensure orthogonality in the spatial domain. We can therefore obtain one full MIMO channel estimate for one group of $M$ subcarriers. The BCH uses QPSK modulation and rate 1/2 convolutional code and contains (among other information) the frame number of the transmitted frame that is used for synchronization among the UEs.

### 3.7.3 Synchronization

Transmitter and receiver must be synchronized in order to conduct usefull measurements. Synchronization is taking place at three different levels, which are described below.

**Initial Synchronization**

Initial synchronization is performed using a sliding window correlator on the SCH symbol in the frequency domain. After successfull detection of the SCH, a channel estimate is performed on the SCH. This channel estimate is used for coherent detection of the BCH with a Viterbi decoder. Synchronization is declared only if the BCH can be detected successfully, i.e., the cyclic redundancy check (CRC) is positive.

---

[2]Eurecom has a frequency allocation for experimentation around its premises.

**Synchronization Tracking**

Due to the drifts of the sampling clocks of transmitter and receiver, as well as the movement of the user, the synchronization needs to be adjusted constantly. This is done by tracking the peak of the channel estimate of the SCH in the time domain. To avoid jitter, the peak position is passed through a low-pass filter. If the peak position drifts from the target position by more than 5 samples, the timing offset of the hardware is increased (decreased) by one sample.

The receiver also continues to decode the BCH. If the BCH cannot be detected successfully for 100 consecutive frames or more, the receiver declares itself out of sync and the initial synchronization procedure is stared again. For successful decoding of the BCH, a SNR of approximately 10 dB or more is required.

**Multi-user Synchronization**

In order to conduct multi-user measurements, all the UEs need to be frame-synchronized to the BS. This is important for ($i$) synchronized start and stop of the data acquisition and ($ii$) for the proper alignment of the measurement data from multiple users in the post processing. Multi-user synchronization is achieved by using the frame number encoded in the BCH. This frame number is also stored along with the measured channel at the UEs for post processing.

### 3.7.4   EMOS Channel Estimation Procedure

Once the receiver is fully synchronized to the transmitter, the EMOS channel estimation procedure is started. Note that this procedure uses all the 48 pilot symbols of a frame (cf. Fig. 3.11) and thus provides a more accurate channel estimate than the one based on the SCH symbol at the beginning of the frame, which is only used for synchronization and coherent decoding of the BCH.

The EMOS channel estimation procedure consists of two steps. Firstly, the pilot symbols are derotated with respect to the first pilot symbol to reduce the phase-shift noise generated by the CardBus MIMO card. Secondly, the pilot symbols are averaged to increase the measurement SNR. The channel is then estimated in the frequency domain by multiplication of the derotated and averaged symbols with the complex conjugate of the pilot symbol. The estimated MIMO channel is finally stored to disk. For a more detailed description of the synchronization and channel estimation procedure see [63, 78].

# Chapter 4

# Exploiting Channel Reciprocity in MIMO TDD systems

Channel state information at the transmitter (CSIT) can greatly improve the capacity of a wireless MIMO communication system. In a time division duplex (TDD) system CSIT can be obtained by exploiting the reciprocity of the wireless channel. This however requires calibration of the radio frequency (RF) chains of the receiver and the transmitter, which are in general not reciprocal. In this chapter we investigate different methods for relative calibration in the presence of frequency offsets between transmitter and receiver. We show results of theses calibration methods with real two-directional channel measurements, which were performed using the Eurecom MIMO Openair Sounder (EMOS). We demonstrate that in a single-user MIMO channel and for low signal-to-noise (SNR) ratios, the relative calibration method can increase the capacity close to the theoretical limit.

## 4.1   Introduction

In a wireless communication system using antenna arrays, channel state information at the transmitter (CSIT) can greatly improve the capacity of the wireless link. This gain becomes even more significant in multi-user MIMO systems. CSIT can be acquired in several ways. In time division duplex (TDD) systems, the physical forward and the backward channel are reciprocal since they operate on the same carrier frequency [81]. In reality however, the communication channel does not only consist of the physical channel, but also the antennas, RF mixers, filters, A/D converters, etc., which are not necessarily identical for all devices. Therefore the system needs to be calibrated before channel reciprocity can be exploited.

Contrarily to absolute calibration [82] where external reference sources are used to measure and compensate for the imperfections of each RF chain independently, we focus here on approaches relying on relative calibration [83]. In this context, the calibration relies on the devices exchanging channel measurements, rather than on extra hardware.

Relative calibration can be formulated as a total least squares (TLS) problem either

in the time domain or in the frequency domain. Efficient solutions exist for a couple of special cases, such as SIMO or MISO or when the reciprocity matrices are assumed to be diagonal (which is equivalent to having negligible cross-talk between the different RF chains). In this work we include the effect of frequency offsets in the reciprocity model and investigate their effect on the relative calibration. For the analysis in this paper we use real two-directional channel measurements, which were performed using the Eurecom MIMO Openair Sounder (EMOS) [4].

## 4.2   Reciprocity model

The investigated reciprocity model is based on the technique introduced in [83], whereby the characteristics of the amplifiers at the transmitter and receiver are modeled with linear time-invariant filters. Compared to [83] the model presented in this section also contains the effects of up- and down-conversion and is thus able to model frequency offsets between transmitter and receiver.

Let us consider a point-to-point TDD communications system involving two devices denoted A and B. Denote the number of antennas at side A and B with $N_A$ and $N_B$ respectively. As depicted in Fig. 4.1, the channel as seen by transceivers in the digital domain, is comprised of the effective electromagnetic channel ($C(t)$), assumed identical in both directions, and filters modeling the imperfections of the power amplifiers ($T_A$, $T_B$) and low-noise amplifiers ($R_A$, $R_B$). In the case where antenna arrays are used, those are vector-input, vector-output filters.
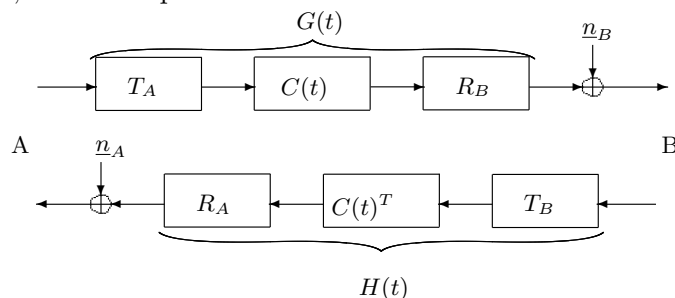


Figure 4.1: Reciprocity model for the point-to-point case

In the ideal case, often considered in the literature, $T_A$, $T_B$, $R_A$ and $R_B$ are all identity filters and carrier frequency at both sides are identical. In that case, the channels are perfectly reciprocal without requiring calibration. Conversely, we investigate practical methods applying to non-ideal cases. As the notations imply, the filters modeling the amplifiers ($T_A$, $T_B$, $R_A$, $R_B$) are assumed to remain constant over the observed time horizon. Let $f_A$ and $f'_A$ denote the up-conversion and down-conversion frequencies at side A, and $f_B$ and $f'_B$ the up- and down-conversion frequencies at node B. It is very likely that $f_A = f'_A$ and $f_B = f'_B$ since the mixers are normally driven by the same clock. However, $f_A$ can differ significantly from $f_B$, typically by up to one kHz.

For a given frequency $f$, the channel impulse response as measured by the digital signal processor is the cascade of the up-conversion, the transmit filter, the electromag-

netic channel, the receive filter, and the the down-conversion. The measured uplink and downlink channel are thus modeled as:

$$G(t, f) = R_B(f)e^{2\pi j f'_B t} C(t, f) T_A(f) e^{-2\pi j f_A t}, \tag{4.1}$$

$$H(t, f) = R_A(f)e^{2\pi j f'_A t} C(t, f)^T T_B(f) e^{-2\pi j f_B t}. \tag{4.2}$$

Note that in the sequel, we will omit the dependency on $f$, although it should be kept in mind that that the flat-fading models used below hold independently for each frequency, in typical OFDM fashion.

In the time domain, a similar set of equations is obtained by replacing products by convolutions and matrices by linear filters in the Eqs. (4.1) and (4.2).

Departing from classical calibration techniques whereby $T_A$, $T_B$, $R_A$ and $R_B$ are estimated and compensated individually, [83] introduced the concept of *relative* calibration. It consists in introducing the filters $P_A = R_A^{-T} T_A$ and $P_B = T_B^T R_B^{-1}$. Eliminating $C$ from Eqs. (4.1) and (4.2), one obtains

$$(G(t)e^{-2\pi j(f_A - f'_B)t}) = P_B^{-1}(H(t)^T P_A e^{-2\pi j(f_B - f'_A)t}). \tag{4.3}$$

$f_A - f'_B$ and $f_B - f'_A$ are residual frequency offset in the channel estimations of both directions. There are two main methods on how to deal with the frequency offsets: ($i$) Estimate the frequency offsets, compensate them, and apply a standard estimator to estimate the reciprocity factors or ($ii$) estimate both the frequency offsets and the receprocity factors jointly. Both methods are detailed in the following.

## 4.3   Estimation of the calibration factors without frequency offsets

The frequency offsets can be estimated using several consecutive channel estimates of $G(t)$ and $H(t)$. The problem is equivalent to the one of estimating the frequency of a single complex sinusoid in noise-corrupted discrete-time samples. One efficient solution is proposed in [84]. Once $f_A - f'_B$ and $f_B - f'_A$ are estimated, we compensate each channel measurements which eliminates the effect of frequency offset. The problem therefore reduces to an estimation problem without frequency offsets

$$G(t) = P_B^{-1} H(t)^T P_A. \tag{4.4}$$

In the considered point-to-point scenario, relative calibration consists in estimating directly $P_A$ and $P_B$, using eq. (4.4) and the measured values of $G(t)$ and $H(t)$. Once these are known, the channel can be estimated through reciprocity using (4.4).

### 4.3.1   Design of reciprocity estimators for the point-to-point case

Let us consider a series of $K$ bi-directional channel measurements, i.e. both $G(t)$ and $H(t)$ are assumed to be measured simultaneously (or with negligible time difference) at

times $t_i$, $i = 1 \ldots K$. We wish to design an estimator for $(P_A, P_B)$ based on the noisy channel measurements $(\hat{G}(t_i), \hat{H}(t_i))$, $i = 1 \ldots K$. Considering one single frequency, and dropping the index $f$ for notational simplicity, the following estimator minimizes the objective function suggested by the reciprocity relationship $P_B G(t) - H(t)^T P_A = 0$. Since this relationship only applies to the true channels, we allow for compensation terms $\tilde{G}(t)$ and $\tilde{H}(t)$ to be added to $\hat{G}(t)$ and $\hat{H}(t)$, in the spirit of the Total Least-Squares (TLS) technique [85], in order to account for the uncertainty due to the estimation noise:

$$(\hat{P}_A, \hat{P}_B) =$$

$$\underset{\substack{(P_A, P_B, \tilde{G}_i, \tilde{H}_i), \\ \text{s.t.} \|P_A\|_2^2 = 1}}{\operatorname{argmin}} \sum_{i=1}^{K} \left\| P_B \left( \hat{G}(t_i) + \tilde{G}_i \right) - \left( \hat{H}(t_i) + \tilde{H}_i \right)^T P_A \right\|_2^2 + \left\| \tilde{G}_i \right\|_2^2 + \left\| \tilde{H}_i \right\|_2^2. \quad (4.5)$$

It can be seen from eq. (4.5) that if the compensation terms $\tilde{G}$ and $\tilde{H}$ are exactly equal to the measurement noise, the first norm vanishes. The condition $\|P_A\|_2^2 = 1$ ensures that the trivial solution $(P_A, P_B) = (0,0)$ is avoided. This condition is added without loss of generality since the set of parameters $(P_A, P_B)$ is over-determined: it can be seen from eq (4.4) that the family of solutions where $P_A$ and $P_B$ are multiplied with the same scalar factor indeed represents a single solution to the problem at hand.

### 4.3.2 Approaches to solve the minimization problem

The quartic (note e.g. the product between $P_B$ and $\tilde{G}_i$, which are both components of the variable under optimization) objective function defined in (4.5) makes the solution of the optimization problem non trivial. For relatively small problem sizes, this is solvable by standard non-convex optimization methods, although the complexity currently prevents any real-time exploitation. Another avenue to reduce the complexity of the considered estimation problem is to simplify the model above.

**Frequency-flat SISO case**

In the SISO case, the filters $P_A$ and $P_B$ are scalars and thus the products in (4.4) commute. Letting $P = P_B^{-1} P_A$ yields $G(t) = H(t)P$. Since both $G(t)$ and $H(t)$ are affected by estimation errors, the estimate of $P$ can be estimated as the classical total least-squares solution: collecting $K$ pairs of measurements in the vectors $\hat{\mathbf{g}} = [\hat{G}(t_1), \ldots, \hat{G}(t_K)]^T$ and $\hat{\mathbf{h}} = [\hat{H}(t_1), \ldots, \hat{H}(t_K)]^T$, $\hat{P}$ is estimated as

$$\underset{\tilde{\mathbf{h}}, \tilde{\mathbf{g}}, P}{\operatorname{argmin}} \|\tilde{\mathbf{h}}\|_2^2 + \|\tilde{\mathbf{g}}\|_2^2 \quad \text{s.t.} \quad (\hat{\mathbf{h}} + \tilde{\mathbf{h}})P = (\hat{\mathbf{g}} + \tilde{\mathbf{g}}). \quad (4.6)$$

This TLS problem can be easily solved using the classical solution based on the singular value decomposition (SVD) [86].

**MIMO with Diagonal Reciprocity Matrices**

The model of eqs. (4.1) and (4.2) incorporates cross-talk between all antenna pairs in an array. In reality, the effect of this phenomenon is negligible, making $P_A$ and $P_B$ diagonal. This decouples the MIMO problem (4.4) into $N_A N_B$ SISO problems

$$[G(t)]_{i,j} = [P_B^{-1}]_{i,i}[H(t)]_{j,i}[P_A]_{j,j}, \qquad (4.7)$$

which are solved as in Section 4.3.2.

**Frequency-selective SISO case**

The case of the frequency selective channel is not conceptually different from the flat-fading problem, except for the added complexity due to the increased dimensions. Two approaches can be envisioned:

1. A per-subband approach, in which the reciprocity estimator is applied independently to each subband, i.e.,

$$G(t,f) = H(t,f)P(f). \qquad (4.8)$$

   The complexity of this approach scales linearly with the transmission bandwidth, however it fails to exploit the correlation across subbands between the reciprocity parameters. This correlation is expected to be high, since the impulse responses of $P_A$ and $P_B$ are expected to be extremely short in practice.

2. Estimating the reciprocity parameters in the time domain by transforming (4.8) into the time domain:
$$G(t,\tau) = H(t,\tau) * P(\tau), \qquad (4.9)$$

   Under the assumption that $P(\tau)$ is a FIR filter such that $P_B(\tau) * P(\tau) = P_A(\tau)$, a solution to this problem is proposed in [83], based on the deconvolution algorithm of [87].

Those two approaches outlined above are compared in Section 4.3.3 with simulation and Section 4.5 over real measured data.

### 4.3.3 Accuracy and Complexity Comparison

In this section, we compare the numerical performance of the two methods envisioned in Section 4.3.2.

Method 1: Consider the estimation of one $P(f)$ from $K = 20$ channel estimations for each subcarrier($N_c$ in total). The main part of computation is to find the right singular vectors of a $N_c$ by 2 matrix $[\hat{g}, \hat{h}]$ [86], which are also the right eigenvectors of a 2 by 2 matrix $[\hat{g}, \hat{h}]^H \cdot [\hat{g}, \hat{h}]$. The latter can be calculated analytically and requires $8K$ complex multiplications/additions, and a few other operations. Thus the complexity of estimating all the subcarriers is around $\mathcal{O}(K \cdot N_c)$

Method 2: Essentially, this method constructs a STLS (Structured Total Least Square) problem and uses numerical computation to solve a LS (Least Square) problem within each iteration. According to the fast algorithm provided in [87], it takes $(M_1 \cdot M_2)$ flops to solve an $M_1$ by $M_2$ LS problem. So in our case, the complexity will be $\mathcal{O}(L_p \cdot L_{\text{ch}} \cdot K \cdot N_{\text{iter}})$ FLOPS (real floating point operations, multiplication or addition), where $L_p$ is the length of the impulse response of the reciprocity filter $P(t)$, $L_{\text{ch}}$ is the length of the channel impulse response, $N_{\text{rl}}$ is the number of estimations we use for the estimator, and $N_{\text{iter}}$ stands for the average number of iterations. Fig. 4.2 shows the average complexity while setting the stop criterion to $10^{-5}$ and $10^{-7}$ .

For the evaluation of the accuracy comparison, we perform a Monte Carlo simulation consisting 1000 runs. The 2 methods are then applied to estimate the reciprocity $P(f)$ and $P(\tau)$ in frequency and time domain respectively. As another comparison of Method 2, a frequency domain filter which nulls out the non-used subband is applied upon the estimation result of the FIR filter $P(\tau)$. The relative errors defined by $\frac{\|\hat{P}(f) - P(f)\|^2}{\|P(f)\|^2}$ are briefly shown in Fig. 4.2 and 4.3. It can be seen in Fig. 4.3 that the performance curve of the unfiltered time domain estimate turns flat in high SNR because the influence of the filter dominates the relative error. It's obvious that despite of close accuracy, the estimator in frequency domain significantly outperform its counterpart in time domain in the aspect of complexity.
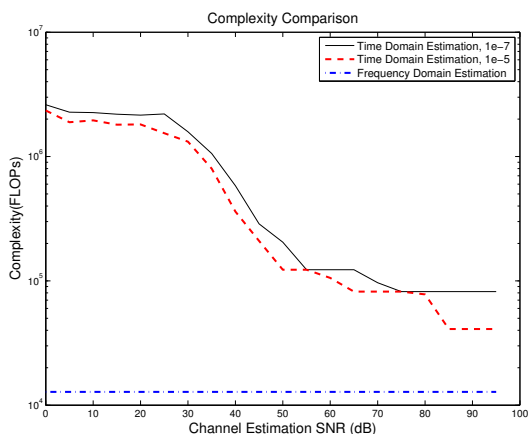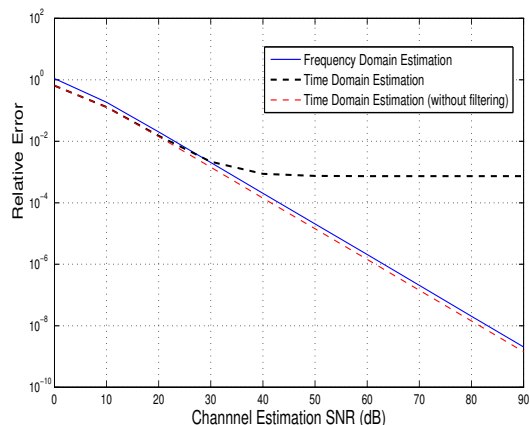


Figure 4.2: Complexity

Figure 4.3: Accuracy Comparison

## 4.4 Joint estimation of frequency offset and reciprocity factors

Another way of dealing with the frequency offsets is by including them in the estimation procedure. Therefore we rewrite Equation 4.3 as

$$(G(t)e^{-2\pi j f_o t}) = P_B^{-1}(H(t)^T P_A), \tag{4.10}$$

where $f_o = (f_A - f'_B + f'_A - f_B)$ is the frequency offset between transmitter and receiver. Taking channel estimates at time instances $t_1, \ldots, t_K$ results in

$$G(t_k)e^{-j\phi_k} = P_B^{-1}(H(t_k)^T P_A), \quad t_1, \ldots, t_K, \tag{4.11}$$

where $\phi_k = 2\pi f_o(t_k - t_0)$, $k = 1 \ldots K$ is the unknown phase offset due to the frequency offset at measurement $k$. We observe the following:

- the $\phi_k$ are only significant *modulo* $2\pi$,

- if $t_k - t_0$ gets large, the estimation accuracy of $f_o$ must be extremely high in order to guarantee acceptable accuracy on the $\phi_k$. Indeed, let $\widehat{f_o} = f_o + \epsilon$ and $\widehat{\phi}_k = 2\pi \widehat{f_o}(t_k - t_0)$, thus $\widehat{\phi}_k - \phi_k = 2\pi \epsilon(t_k - t_0)$. Since the $\phi_k$ are only significant *modulo* $2\pi$, it is clear that the desired accuracy lies in the regime where $|\widehat{\phi}_k - \phi_k| \ll 2\pi$, i.e. $\epsilon \ll \frac{1}{t_k - t_0}$. In practice, since $t_k - t_{k-1}$ should be larger than the channel coherence time for the reasons mentioned above, we expect $t_K - t_0$ to be measured in seconds. It is therefore clear that the sub-Hz accuracy required for $\widehat{f_o}$ is out of reach for state-of-the-art frequency offset estimators.

In light of the above, we choose to consider the over-parameterized model in (4.11), and treat $\phi_1 \ldots \phi_K$ as nuisance parameters. Similar to the case without frequency offsets, we now need to introduce a noisy version of (4.11), formulate relative calibration as a structured TLS estimation problem, and propose an iterative solution. Please refer to [6] for details.

## 4.5 Validation Using Measured Data

In order to check the validity of the model in (4.11), and to assess the performance of relative calibration in a practical system, the proposed algorithm was applied to measurements collected using the Eurecom MIMO OpenAir Sounder (EMOS), a subsystem of the OpenAirInterface LTE testbed (`http://www.openairinterface.org`).

### 4.5.1 EMOS Hardware

The hardware used for the user equipment (UE) is depicted in Fig. 4.4. It consists of PC running the software modem, the Express MIMO board, the LIME RF front-end, and an antenna. The base station (eNB) is similar with the difference that the RF front-end and the antennas are duplicated.

Express MIMO is a baseband processing board, which comprises two FPGAs: one Xilinx XC5VLX330 for real-time embedded signal processing applications and one Xilinx XC5VLX110T for control. The card uses an eight-way PCI express interface to communicate with the host PC. The card employs four high-speed A/D and D/A converters from Analog Devices (AD9832) allowing to drive four RF chains using quadrature modulation. In the current setting the ADAC are configured to 7.68 MSPS (corresponding to the LTE 5MHz bandwidth allocation).
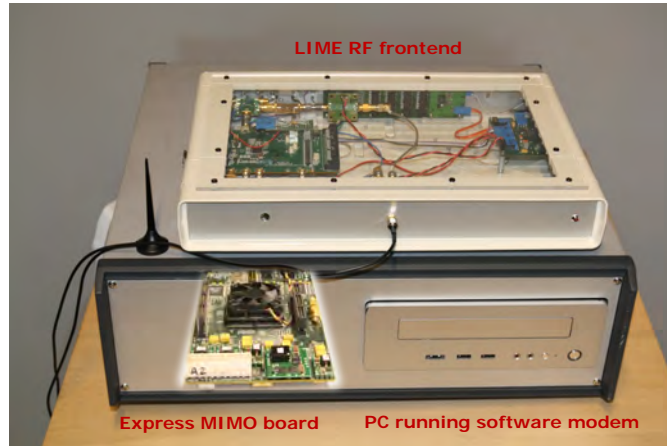
Figure 4.4: User equipment (UE) used in the measurements.
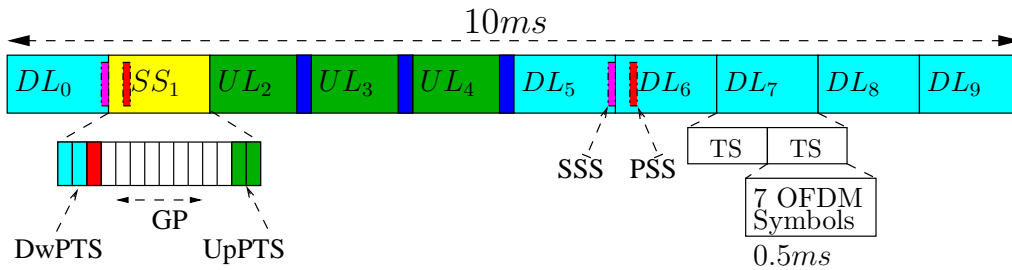


Figure 4.5: Frame structure for LTE TDD type 3

As an RF front-end we have used a custom design based on the LMS6002D evaluation boards from Lime Microsystems. Up to four such front-ends can be connected, each independently tunable from 300 MHz to 3.8 GHz with a maximum output power of 0dBm. However, the current filters limit the carrier frequency to the band around 1.9GHz.

### 4.5.2 Measurement methodology

**System overview** A software modem running under the control of the real-time application interface (RTAI) of a standard Linux operating system uses the Express MIMO card as a baseband signal acquisition and transmission subsystem. The software modem implements a large part of the 3GPP LTE Rel 8.6 standard. For the measurements we used TDD configuration 3, depicted in Fig. 4.5. It consists of 6 downlink (DL) subframes, 3 uplink (UL) subframes, and one special subframe (SS).

On the DL, we use the cell specific LTE reference symbols (CS-RS) to estimate the channel. We use linear interpolation in the frequency domain to obtain a channel estimate for the whole bandwidth. On the UL, we allocate the whole bandwidth to one

single UE in subframe 4 and use the corresponding demodulation reference symbols (DM-RS) to estimate the channel. Since these RS are available over the whole bandwidth, we do not need interpolation. More details on the measurement methodology can be found in [88].

**Measurement Collection**  For the measurements we set up one eNB with two antennas and one UE with one antenna in Eurecom's lab (static setup). The eNB was collecting channel measurements for the UL while the UE was collecting channel measurements from the DL. The measured data was processed offline in Matlab. To estimate the reciprocity parameters, we used 10 consecutive samples of from the DL channel estimates from subframe 4 and the UL channel estimate from subframe 5.

**Measurement Post-processing**  Apart from the frequency offset, timing drifts are also present due offset between the clocks of the UE and eNB. The UE therefore needs to continuously adjust the frame start in order to stay synchronized with the eNB. These drifts and the resulting adjustments do not harm the normal (frame-based) modem operations. However, for the reciprocity calibration procedure they need to be reverted. Since these timing drifts are logged by the UE, they can be simply compensated by resampling the impulse responses (using a standard Lanczos filter) so that the peaks of the impulse responses are always on the same sample.

### 4.5.3  Performance Metrics

The metric adopted here to evaluate the quality of the reciprocity-based CSIT estimation is again the achieved mutual information. Since MISO channels are considered, CSIT is exploited by doing maximum-ratio combining at the transmitter independently for each frequency of the 512 subcarriers of the OFDM modulation. The transmitter power is assumed constant over the considered bandwidth. The following mutual information expressions should be understood to be applied on a subcarrier basis. Denote the MISO channel for one subcarrier as $\mathbf{h}_F$ and its estimate with $\hat{\mathbf{h}}_F$ Assume that we want to transmit from A to B. We can distinguish three cases, depending on whether perfect, partial, or no channel state information is available at the transmitter (CSIT). For each case we evaluate the maximum achievable mutual information:

1. The channel is known only at B: The optimal transmission strategy is Alamouti coding which has capacity $C_1 = \log_2\left(1 + \frac{E_S}{N_A N_0}\mathbf{h}_F\mathbf{h}_F^H\right)$, where $E_S/N_0$ the SNR and $N_A = 2$ is the number of transmit antennas.

2. The channel is known to A and B: here we can do optimal beamforming and the capacity is $C_2 = \log_2\left(1 + \frac{E_S}{N_0}\mathbf{h}_F\mathbf{h}_F^H\right)$.

3. A has only knowledge of $\hat{\mathbf{h}}_F$ (estimated from the reciprocity matrices) and B knows $\mathbf{h}_F$. We assume that we use the same transmission scheme as in case 2, but now the beamforming vector does not match the actual channel. Denote with $\mathbf{v}$ the

right singular vector of $\hat{\mathbf{h}}_F$ corresponding to the largest singular value (optimal beamforming vector). Then $C_3 = \log_2\left(1 + \frac{E_S}{N_0}\mathbf{h}_F\mathbf{v}\mathbf{v}^H\mathbf{h}_F^H\right)$.

Fig. 4.6 depicts the above performance metrics obtained by applying the estimated calibration factors to a part of the measurements taken 3 seconds after the calibration period. Additionally we also show the performance for the following cases: ($i$) we do not perform any calibration, i.e., we assume that $h = g$; ($ii$) we use the calibration algorithm from [83] and ignore the frequency offset; and ($iii$) we compensate the frequency offset before using the algorithm from [83]. Remarkably, the capacity curve obtained with the channel reconstructed from the estimated calibration factors is almost as good as the one obtained for perfect CSIT. Furthermore, we see that the method of compensating the frequency offset before the reciprocity estimation also works somehow, but none of other methods work well - their performance is almost the same as the case where there is no CSIT at all.

## 4.6  Conclusions

In this chapter we have shown how to practically exploit channel reciprocity in a MIMO TDD system in order to obtain channel state information at the transmitter. We have verified the method using real two-way MIMO channel measurements that were conducted using the Eurecom MIMO Openair Sounder (EMOS). It was shown that the method is able to increase the capacity of a single-user MIMO system close to the theoretical limit.

The channel measurements used in this paper are synchronized over the air as in a real system. This kind of synchronization results in frequency offsets since the clocks at the two nodes are not identical. The frequency can be compensated using standard methods, but residual frequency offsets will always remain. While these residual offsets might not have an impact on standard receiver design, they do have a big impact on the exploitation of channel reciprocity, since even the smallest offset of a few Hz will accumulate and make the UL and DL channels non-reciprocal within a few seconds.

We have therefore introduced a time-domain relative calibration algorithm that jointly estimates the frequency offsets and the reciprocity factors. The proposed method and has been shown to provide accurate reciprocity-based CSIT in the presence of realistic impairments due to offsets between clock frequencies.
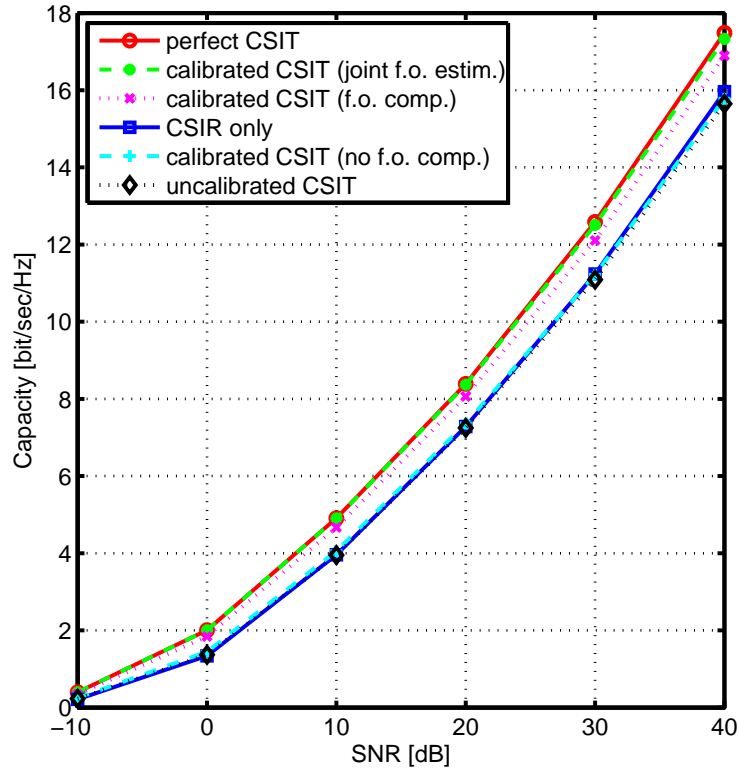
Figure 4.6: Mutual information of the six cases (from top to bottom): $G$ is known at A and B (perfect CSIT); A has only knowledge of $G_{est}$ (estimated using the joint estimator), and B knows $G$ (CSIR + estimated CSIT (joint f.o. estim.)); A has only knowledge of $G_{est}$ (estimated using the standard estimator after frequency offset compensation), and B knows $G$ (CSIR + estimated CSIT (f.o. comp.)); $G$ is known only at B (CSIR only); A has only knowledge of $G_{est}$ (estimated using the standard estimator with no frequency offset compensation), and B knows $G$ (CSIR + estimated CSIT (no f.o. comp.)); A uses $H$ as an estimate for $G$, and B knows $G$ (uncalibrated CSIT).

# Chapter 5

# Interference-Aware Receiver Design for MU-MIMO in LTE: Real-Time Performance Measurements

Multiuser (MU) MIMO is a promising technique to significantly increase the cell capacity in LTE systems. However, users scheduled for MU-MIMO may still experience strong MU interference if the channel state information at the basestation is outdated or in small cells with a limited number of users available. To tackle the MU interference, an interference-aware (IA) receiver design is employed. Unlike the interference-unaware (IU) receiver, the IA receiver exploits the information about the interfering data stream in the decoding process, resulting in a significant performance gain while maintaining a moderate complexity. We evaluate the performance of both receivers in terms of throughput through real-time measurements carried out with the OpenAirInterface, an open-source hardware/software development platform created by Eurecom. The measurement results show that the IA receiver achieves significantly higher data rates compared to the IU receiver if the user has multiple receive antennas.

## 5.1  Introduction

It is wellknown that multiuser (MU) multiple-input multiple-output (MIMO) transmission can significantly increase the cell throughput compared to single-user (SU) MIMO transmission due to MU diversity. Therefore, MU-MIMO is already implemented in the 3GPP long-term evolution (LTE) standard Rel 8[89], where it is referred to as transmission mode (TM) 5. However, since TM5 only supports two co-scheduled user equipment (UE) with a single data stream each, the MU-MIMO mode has been extended in TM8 and TM9 in LTE Rel 9 and 10, respectively, by introducing UE-specific (precoded) reference signals (RS) [90, 91]. In TM8 and TM9 the base station (referred to as eNB in

the context of LTE) can schedule up to four users with a single data stream where both precoding technique and number of co-scheduled users are entirely transparent to the UE.

In MU-MIMO, the throughput at the UEs greatly depends on the amount of interference from co-scheduled users. This MU interference can be managed at the eNB through efficient precoding or at the UE via interference cancellation. If the precoding is effective, there will not be any significant MU interference at the UEs and thus no need to cancel that residual interference. However, in TM5 where the precoding is based on a very limited set of possible precoding vectors, efficient precoding can only be achieved if the number of users in the cell is large. The same holds true for non-based precoding schemes as enabled in TM8 and TM9, unless very accurate channel state information is available at the eNB, which in turn is very difficult to obtain.

Consequently, the precoding is likely to be incapable of efficiently mitigating the MU interference at the UEs especially in small cells with a very limited number of users. Therefore, it is of paramount importance that the UEs are able to effectively mitigate the residual MU interference by exploiting its structure.

To achieve effective interference mitigation at the UE, different receiver designs have been proposed in the literature. [92] propose an optimal simplified interference-aware (IA) receiver based on the maximum likelihood (ML) criterion. However, the optimal IA receiver requires knowledge of the interfering symbol constellation, which is unavailable to the UE. Therefore, [92] propose to use a fixed constellation and shows that the performance degradation of the sub-optimal IA receiver is acceptable. [93] try to overcome this disadvantage of the IA receiver by implementing an interference modulation estimator prior to the IA receiver. It is shown through simulations that this joint receiver outperforms the IA receiver with fixed interfering modulation especially when the interference power is high. The question of the performance-complexity tradeoff of different receivers is addressed [94], where a linear receiver termed interference rejection combiner (IRC) is applied to MU-MIMO. Based on simulation results under various channel conditions, the authors conclude that the IRC achieves the best performance-complexity tradeoff. However, it is important to note that the simulation results [94] assume an infinite number of potential users suggesting that the MU interference is rather low. Under higher interference levels, the simulation results [93] show a significant performance loss of the IRC compared to the IA receiver. However, in practice, the amount of MU interference is highly dependent on the algorithms (scheduling, precoding) implemented at the eNB and it is therefore difficult to identify a "typical" MU-MIMO scenario.

In this chapter, we focus on TM5 applied in small-cell scenarios with few users in the cell resulting in high residual MU interference at the UEs. The focus on TM5 is further motivated by the fact that at lower bandwidths (5 MHz and lower), the number of possible UE-specific downlink control information (DCI) in the PDCCH is limited and it is very likely that the eNB is unable to co-schedule more than two UEs. We implemented the IA receiver proposed [92] on the OpenAirInterface real-time platform[95] and evaluate its performance through measurements under realistic channel conditions.

The remainder of this chapter is organized as follows. Section 5.2 introduces the

system model and briefly reviews the IA receiver design. In Section 5.2.3 we carry out simulations to evaluate the IA receiver performance under false assumptions on the interfering symbol constellation. Section 5.4 describes the real-time measurement setup and presents our results. Finally, Section 5.5 gives conclusions.

*Notation*: In the following, boldface lower-case and upper-case characters denote vectors and matrices, respectively. The operators $(\cdot)^{\mathsf{H}}$ and $\mathsf{E}[\cdot]$ denote conjugate transpose and expectation, respectively. The $N \times N$ identity matrix is denoted $\mathbf{I}_N$, $\Re(z)$ and $\Im(z)$ are the real and imaginary part of $z \in \mathbb{C}$, respectively. The imaginary unit is denoted $\mathbf{i}$. A random vector $\mathbf{x} \sim \mathcal{CN}(\mathbf{m}, \boldsymbol{\Theta})$ is complex Gaussian distributed with mean vector $\mathbf{m}$ and covariance matrix $\boldsymbol{\Theta}$.

## 5.2   System Model

Consider a system with an $n_{\mathrm{t}}$-antenna eNB and $K$ scheduled UEs, each endowed with $n_{\mathrm{r}}$ receive antennas. We assume that the eNB transmits a *single* stream $s_k$ to UE $k$ ($k = 1, 2, \ldots, K$) and applies a linear precoding technique. Under narrow-band transmission, the received signal $\mathbf{y}_k \in \mathbb{C}^{n_{\mathrm{r}}}$ of user $k$ takes the form

$$\mathbf{y}_k = \underbrace{\mathbf{H}_k \mathbf{g}_k s_k}_{\text{useful signal}} + \underbrace{\mathbf{H}_k \sum_{j=1, j\neq k}^{K} \mathbf{g}_j s_j}_{\text{MU interference}} + \underbrace{\mathbf{n}_k}_{\text{noise}}, \tag{5.1}$$

where $\mathbf{H}_k = [\mathbf{h}_{k1}, \mathbf{h}_{k2}, \ldots, \mathbf{h}_{kn_{\mathrm{r}}}]^{\mathsf{H}} \in \mathbb{C}^{n_{\mathrm{r}} \times n_{\mathrm{t}}}$ is the channel from the eNB to UE $k$, $\mathbf{G} = [\mathbf{g}_1, \mathbf{g}_2, \ldots, \mathbf{g}_K]^{n_{\mathrm{t}} \times K}$ is the concatenated precoding matrix and $\mathbf{n}_k \sim \mathcal{CN}(0, \sigma^2 \mathbf{I}_{n_{\mathrm{r}}})$ is the noise vector. Defining the *effective* channels of user $k$ as $\bar{\mathbf{h}}_i \triangleq \mathbf{H}_k \mathbf{g}_i$ ($i = 1, 2, \ldots, K$), the received signal reads

$$\mathbf{y}_k = \bar{\mathbf{h}}_k s_k + \sum_{j=1, j\neq k}^{K} \bar{\mathbf{h}}_j s_j + \mathbf{n}_k. \tag{5.2}$$

The key challenge in MU-MIMO is to minimize the MU interference. This interference can be mitigated at the eNB by computing an appropriate precoder $\mathbf{G}$ or the interference can be accounted for in the receiver by exploiting its potential structure. It is well-known that efficient interference mitigation at the eNB requires precise downlink channel knowledge which can only be acquired through extensive user feedback. On the other hand, interference management at the receiver necessitates an estimate of the effective channels $\bar{\mathbf{h}}_i$ as well as the interfering symbol alphabet $\mathcal{A}_j$, $s_j \in \mathcal{A}_j$ ($j \neq k$). In the following sections, we discuss the LTE MU-MIMO mode in more detail.

### 5.2.1   MU-MIMO in LTE Release 8

LTE Release 8 [89] defines MU-MIMO in TM 5 where two UEs can be scheduled simultaneously each receiving a single data stream. The UEs are aware of a co-scheduled user

through the downlink power offset value signaled in the DCI. Moreover, LTE Release 8 adopts a codebook-based precoding scheme as a compromise between performance and feedback overhead. The codebook $\mathcal{G}$ for $n_t = 2$ is defined as

$$\mathcal{G} = \frac{1}{\sqrt{2}} \left\{ \begin{pmatrix} 1 \\ 1 \end{pmatrix}, \begin{pmatrix} 1 \\ -1 \end{pmatrix}, \begin{pmatrix} 1 \\ \mathbf{i} \end{pmatrix}, \begin{pmatrix} 1 \\ -\mathbf{i} \end{pmatrix} \right\} \tag{5.3}$$

and $\mathbf{g}_k \in \mathcal{G}$. Since this codebook only offers a very limited choice of precoding vectors, there will remain a significant amount of MU interference at the UEs especially in small cells with few users. Therefore, it is crucial to implement an IA receiver which exploits the knowledge about the MU interference, as opposed to an IU receiver that treats the interference as noise.

## 5.2.2 MU-MIMO in LTE Release 9 and Beyond

The LTE Releases 9 and beyond allow for MU-MIMO transmission with UE-specific reference symbols (RS) defined as TM8 (Rel 9) and TM9 (Rel 10). Transmission modes 8 and 9 enable the scheduling of up to four users with a single data stream or up to two users with two data streams each. The UE-specific RS are precoded the same way as the data, thus leaving the actual precoding open to implementation and entirely transparent to the UEs. Hence, the users are completely oblivious to whether the eNB applied a linear precoding technique like zero-forcing (ZF) or regularized ZF[53, 96] or even a nonlinear technique as Tomlinson-Harashima precoding. However, note that such non-codebook-based approaches require accurate downlink channel estimate at the eNB which can only be obtained via quantized codebook-based feedback in FDD systems. Furthermore, with UE-specific RS the UE does not know if there are any co-scheduled users or if it is operating in SU-MIMO mode. If the precoding is working well, there will not be any significant MU interference and thus an IA receiver will not improve the performance compared to an IU receiver. The UE can monitor the power of the interfering streams by estimating the effective channel $\bar{h}_j$ since the UE-specific RS among the potentially co-scheduled users are quasi-orthogonal. Subsequently, if the interference power $\|\bar{h}_j\|^2$ exceeds some given threshold, the UE will cancel this interference with an IA receiver.

Recently [8] to study the potential advantages of providing additional information to the UE in order to support its interference cancellation abilities. In the context of MU-MIMO, such information could include the interfering modulation order and the number of interferers (co-scheduled users). If the UE receiver is capable of decoding and subtracting the interfering data stream, then information about the interfering MCS and resource allocation is required. This could be achieved by providing the UE with the RNTI of the interfering users to decode the interfering DCIs and subsequently the data for successive interference cancellation.

In our context of TM5 and the IA receiver, only information the interfering modulation order (QPSK, 16QAM or 64QAM). The measurements presented in this how valuable this is under different propagation environments.

### 5.2.3 Interference-Aware Receiver

The IA receiver design has been proposed in [92] and exploits the potentially available information about the MU interference, i.e., the interfering effective channels $\bar{\mathbf{h}}_j$ ($j \neq k$) and the interfering symbol constellation $\mathcal{A}_j$. In the following, we briefly review the principle of the IA receiver. As discussed in the previous section, each user has access to the effective channels $\bar{\mathbf{h}}_j$ either through cell-specific RS and the a-priori known codebook like in LTE Rel. 8, or through UE-specific RS as in LTE Rel. 9 and beyond. Concerning the interfering symbol constellations $\mathcal{A}_j$, this information is not readily available to the UEs. The symbol alphabets $\mathcal{A}_j$ could be estimated from the statistics of the received signal but this approach is rather difficult and computationally complex. However, through simulations in the subsequent section, we show that assuming identical alphabets, i.e., $\mathcal{A}_j = \mathcal{A}_k \forall j$ performs very well even if the true interfering constellation is different.

To compute the log-likelihood ratios (LLRs) $\Lambda$, we apply the classical maximum-likelihood (ML) criterion with subsequent Max-log approximation. We focus on UE $k$ and hence drop the index $k$. The minimum distance $\lambda$ reads

$$\lambda = \max_{s_i \in \mathcal{A}_i} \left\{ - \left\| \mathbf{y} - \sum_{i=1}^{K} \bar{\mathbf{h}}_i s_i \right\|^2 \right\}. \tag{5.4}$$

For $n_\mathrm{t} = K = 2$, omitting the common term $\|\mathbf{y}\|^2$ and separating into real and imaginary parts we obtain

$$\begin{aligned} \lambda = \max_{\substack{s_1 \in \mathcal{A}_1 \\ s_2 \in \mathcal{A}_2}} \Big\{ &- \|\bar{\mathbf{h}}_1\|^2 |s_1|^2 - \|\bar{\mathbf{h}}_2\|^2 |s_2|^2 \\ &+ 2[\Re(\bar{y}_1)\Re(s_1) + \Im(\bar{y}_1)\Im(s_1)] \\ &+ 2|\eta_1||\Re(s_2)| + 2|\eta_2||\Im(s_2)| \Big\}, \end{aligned} \tag{5.5}$$

with

$$\eta_1 = \Re(\rho_{12})\Re(s_1) + \Im(\rho_{12})\Im(s_1) - \Re(\bar{y}_2) \tag{5.6}$$

$$\eta_2 = \Re(\rho_{12})\Im(s_1) - \Im(\rho_{12})\Re(s_1) - \Im(\bar{y}_2), \tag{5.7}$$

where we defined the matched filter outputs $\bar{y}_1 \triangleq \bar{\mathbf{h}}_1^\mathsf{H}\mathbf{y}$, $\bar{y}_2 = \bar{\mathbf{h}}_2^\mathsf{H}\mathbf{y}$ and the correlation coefficient $\bar{\rho}_{12} \triangleq \bar{\mathbf{h}}_1^\mathsf{H}\bar{\mathbf{h}}_2$. Note that in (5.5) we do not require the sign of the interfering symbol $s_2$ since (5.5) is maximized if $\Re(s_2)$ and $\Im(s_2)$ have the opposite signs of $\eta_1$ and $\eta_2$, respectively. Moreover, the search space for the ML detection can be reduced by one complex dimension since both $\eta_1$ and $\eta_2$ are *independent* of $s_2$ and hence by equating the derivative of (5.5) to zero the optimal values of $|\Re(s_2)|$ and $|\Im(s_2)|$ are directly given. For detailed expressions of the LLRs under various symbol alphabets the reader is referred to [92].

The above IA receiver is able to cancel a *single* interferer. An extension to multi-interference cancellation is not straight-forward since the optimal interference amplitude

can only be directly computed for one interfering symbol. To cancel more than one interferer requires a full ML detection, which quickly increases the complexity of the receiver. The UE can monitor the strength of the interfering users and decide to cancel the strongest interferer if beneficial.

### 5.2.4 Precoder Selection

User $k$ selects the precoding vector $\mathbf{g}_k^\star$ that maximizes his desired *effective* channel magnitude $\|\mathbf{H}_k\mathbf{g}_k\|$, i.e.,

$$\mathbf{g}_k^\star = \arg\max_{\mathbf{g}\in\mathcal{G}}\{\|\mathbf{H}_k\mathbf{g}\|\}. \tag{5.8}$$

and sends the corresponding precoding matrix indicator (PMI) to the eNB. In the test configuration presented in this paper, we always assume that two users with orthogonal precoding vectors are scheduled for transmission. Moreover, the above maximization is carried out over the average channel per sub-band as opposed to wideband PMI [94].

## 5.3 Simulation Results

Before carrying out real-time measurements, we do link-level simulations to identify the performance loss incurred by a false assumption on the interfering constellation $\mathcal{A}_j$. Given various modulation and coding schemes (MCS), we measure the BLER for the SCM-C channel model and average over 10 000 independent channel realizations.

Figures 5.1,5.2 and 5.3 show the simulation results for QPSK, 16 QAM and 64 QAM interference, respectively. From these figures it can be observed that if the desired user has a QPSK constellation then the assumption on the interfering constellation has little impact on the IA receiver performance. Even the IU receiver performs almost as well as the IA receiver. If the desired user constellation is 16 QAM or 64 QAM, we observe that the performance loss is more significant, especially if the interfering modulation order is high but a low modulation order is assumed. From these simulations we conclude that the assumption $\mathcal{A}_j = \mathcal{A}_k \forall j$ is robust and results only in a small performance loss. Even under a false assumption on $\mathcal{A}_j$ the IA receiver always outperforms the IU receiver significantly.

We are now interested in the computational complexity of the IU and IA receiver and choose to measure the processing time of each receiver on an IntelR XeonT CPU E5-2690 core clocked at 3 GHz. It should be noted that the implementation makes heavy use of the Streaming SIMD Extension (SSE) 4 instruction set. The results are presented in Figure 5.4, where we assume that $\mathcal{A}_1 = \mathcal{A}_2$ and also plot the processing time of the Turbo decoder for comparison. From Figure 5.4, we observe that the processing time of the IU receiver increases only slightly with the modulation order whereas the IA receiver complexity increases significantly. For 64QAM the processing time of the IA receiver is almost 5 times that of the Turbo decoder and 12 times the amount of the IU receiver. Although the IA receiver greatly increases the computational complexity at
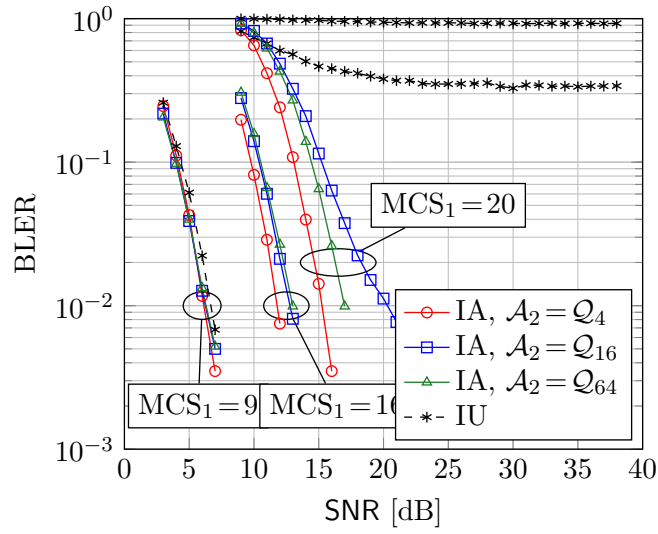
Figure 5.1: QPSK interference, BLER vs. SNR, $\mathrm{MCS}_1 = \{9, 16, 20\}$, $\mathrm{MCS}_2 = 9$, $n_\mathrm{r} = 2$, SCM-C, no HARQ, 10 000 channel realizations.
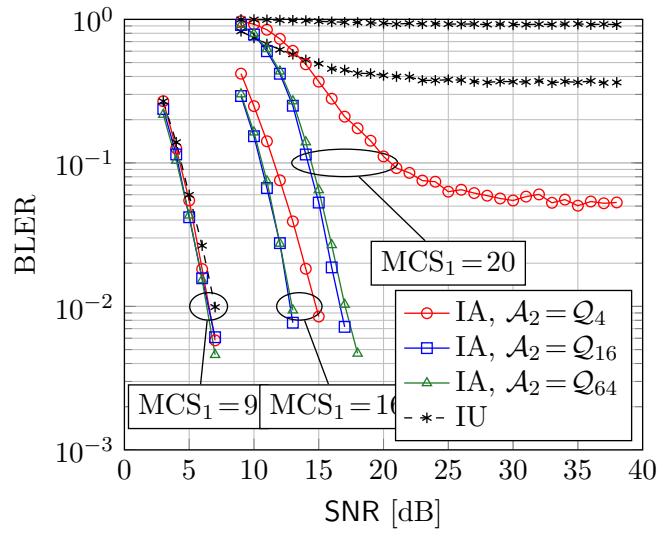


Figure 5.2: 16QAM interference, BLER vs. SNR, $\mathrm{MCS}_1 = \{9, 16, 20\}$, $\mathrm{MCS}_2 = 16$, $n_\mathrm{r} = 2$, SCM-C, no HARQ, 10 000 channel realizations.
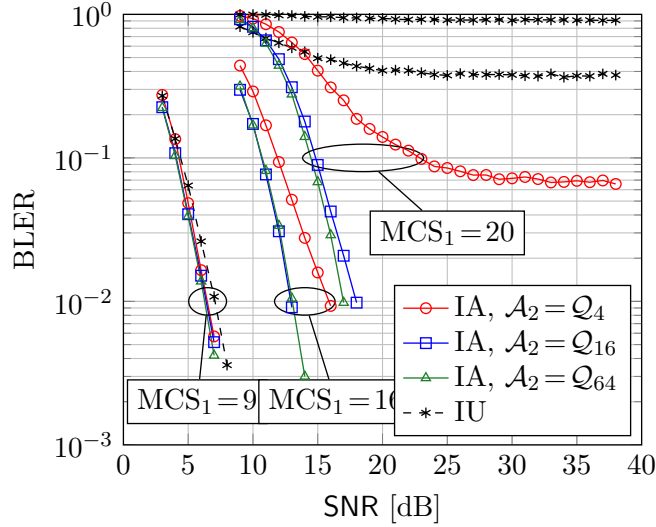
Figure 5.3: 64QAM interference, BLER vs. SNR, $MCS_1 = \{9, 16, 20\}$, $MCS_2 = 20$, $n_r = 2$, SCM-C, no HARQ, 10 000 channel realizations.

| Parameter | Value |
|---|---|
| Carrier Frequency | 1907.6 MHz |
| System Bandwith | 5 MHz |
| TDD Configuration | 3 |
| DL Transmit Subframe | 7 |
| UL Transmit Subframe | 3 |
| RB Allocation | 8191 (all 25 RBs) |
| Number of PDCCH symbols | 1 |

Table 5.1: System Configuration Parameters

high modulation orders, it is precisely in that region where the subsequent measurements show a tremendous performance gain over the IU receiver. Note that the real-time implementation of the LLR computation uses multiple threads to meet the real-time requirements.

## 5.4 Real-time Measurements

In this section we describe the real-time measurement setup and assumptions, the equipment and the different measurement scenarios. The throughput is measured for both IU and IA receivers in TM5.
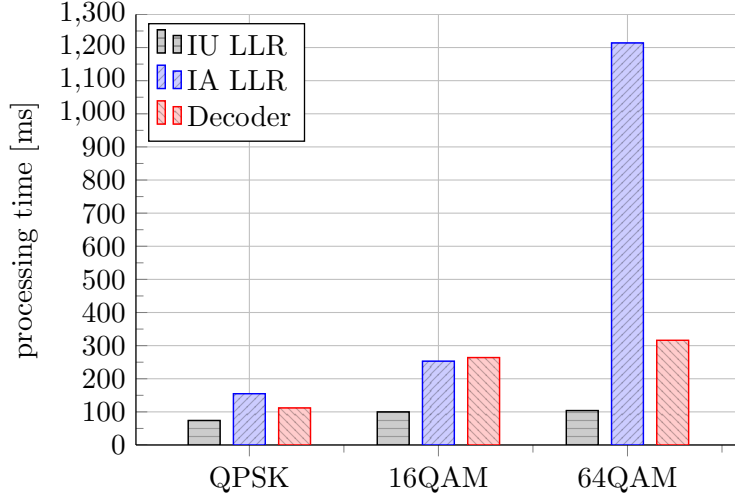
Figure 5.4: Processing time per subframe of the IA and IU receiver with $n_r = 2$

### 5.4.1  Setup

For the test setup, we configured Time-Division Duplex (TDD) mode on LTE band 33 (1900–1920MHz). The eNB has two antennas for transmission and reception whereas the UE uses one antenna for transmission and one or two antennas for reception. The important system configuration parameters are summarized in Table 5.1.

In subframe (SF) 3, the UEs transmit their measured PMIs on the PUSCH which is subsequently used in SF 7 by the eNB to precode the signals of both users. In our test setup, only SF 7 carries downlink data.

Note that in TM5, the data for the interfering UE (user 2) always occupies exactly the same time-frequency resources as the data for user 1, because the downlink (DL) power offset parameter, signaled in the DCI and indicating the presence of another user, is valid for the entire subframe. In TM8 and TM9, the interference could only be present partially within a codeword the IA receiver should only be applied to those resources with interference otherwise, in absence of interference, the IA receiver will perform worse than the IU receiver. As previously mentioned, the presence of an interfering user could be determined by monitoring the interference power and applying a suitable threshold to decide if interference cancellation is used.

In the measurements we use two IA receivers. One IA receiver assumes that the interference modulation order is the same as the desired modulation order. This receiver is simply termed "IA" The other receiver is assumed to obtain the correct interfering modulation order through network-aided (NA) signaling and is referred to as "NA-IA" receiver.

### 5.4.2 Assumptions

In the measurements, we consider the scenario where only users are available for TM5. The eNB always uses the PMI reported by user 1 (the desired user) and assigns orthogonal PMIs to user 2 regardless of the PMI report of user 2. This scheduling scheme is optimal for user 1 but suboptimal for user 2 and from a cell capacity point of view. However, since we focus on the throughput of user 1, this scheduling scheme is adequate. This assumption is realistic in small cells where the number of users is likely to be small and orthogonal PMIs might not be available which will result in higher MU interference.

Concerning the PMI feedback, we make several assumptions. First, we ensure that the uplink (UL) is always error-free by transmitting with sufficient power. This is necessary to avoid errors in the PMI would impair our receiver performance measurements. Secondly, we implement sub-band PMI measurements similarly to TM6, which is not foreseen in LTE Rel 8 but later in Rel 9 and beyond. However, this has no impact on the relative performance of IA and IU receiver.

Since the PMI is measured in SF 2 and applied in SF 7, the channel is supposed to be approximately constant during 5 SFs or equivalently 5 ms, which the case during the measurements.

The LTE modem ran without protocol stack (no Hybrid ARQ) and UL and DL resources were statically configured. Note that, although we disabled the higher layers for this measurements, a similar MU-MIMO setup has been successfully demonstrated with complete protocol stack during the SAMURAI project [97, 98].

During the measurements, the receiver type is changed per frame and $MCS_1$ is random and uniformly distributed between 0 and 27. To make $MCS_2$ available to the NA-IA receiver without explicit signaling, it is coupled to the system frame number (SFN) as $MCS_2 = SFN mod 28$. Although $MCS_2$ is not truly random, no significant change in performance compared to a random $MCS_2$ has been observed. Moreover, each of the subsequent results was obtained by measuring over a time period of about 2 minutes.

### 5.4.3 Equipment

The measurements are carried out with the EURECOM experimental OpenAirInterface (OAI) platform. The OAI implements a defined radio of the 3GPP LTE Rel 8.6 standard which runs on common x86 Linux machines. To ensure real-time operation, we utilize the real-time application interface (RTAI). Furthermore, the real-time signals are transmitted via the PCIxpress interface to the EURECOM Express MIMO 2 board (Figure 5.5), where the base-band signal is modulated and transmitted via an additional RF front-end as depicted in Figure 5.6. The Express MIMO 2 board is able to receive and transmit on channels independently and for a wide range of frequencies.

### 5.4.4 Scenarios

We consider three different scenarios

Figure 5.5: Express MIMO 2 board



Figure 5.6: User equipment with RF board
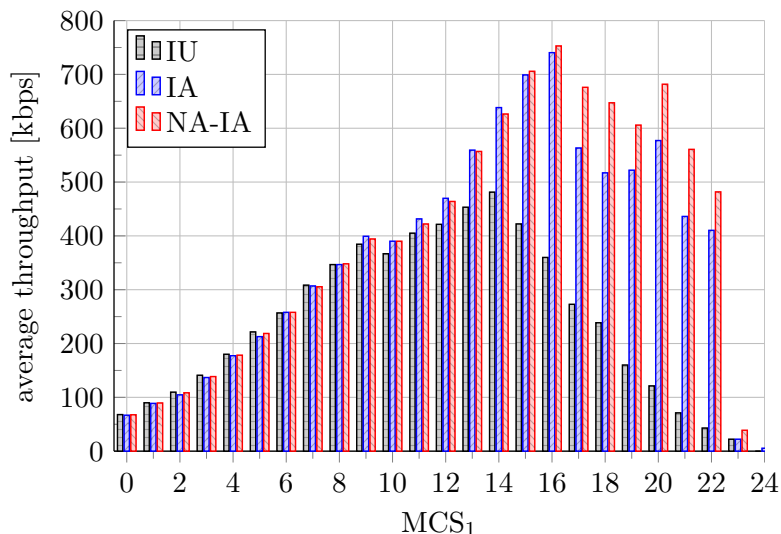
Figure 5.7: $MCS_1$ vs. average throughput with $n_r = 1$, indoor scenario.

1. Indoor scenario (UE is inside building, eNB is outside) to measure throughput for different number of receive antennas

2. Outdoor scenario with a strong line-of-sight (LOS) channel

3. Outdoor scenario with non-LOS (NLOS) channel conditions

In all scenarios the UE is moved at low speeds to avoid a strong Doppler effect but to allow for an averaging of the performance over sufficiently different channel realizations.

### 5.4.5 Measurement Results

The throughput measurements for all three scenarios are presented in the following sections.

**Scenario with Variable Number of Receive Antennas**

The measurement setup consists of an eNB situated outside on top of the EURECOM building and the UE placed inside the building.

Figure 5.7 and Figure 5.8 show the average throughput of IU, IA and NA-IA receivers with one or two receive antennas, respectively, for different values of $MCS_1$. From these figures we observe that, for QPSK (MCS 0,1,…,9), all receivers achieve about the same throughput irrespective of the number of receive antennas.

From Figure 5.7, we observe that the IA receiver does not offer a significant throughput increase if only a single receive antenna is available. However, the NA-IA can achieve moderately higher throughput for higher MCS.
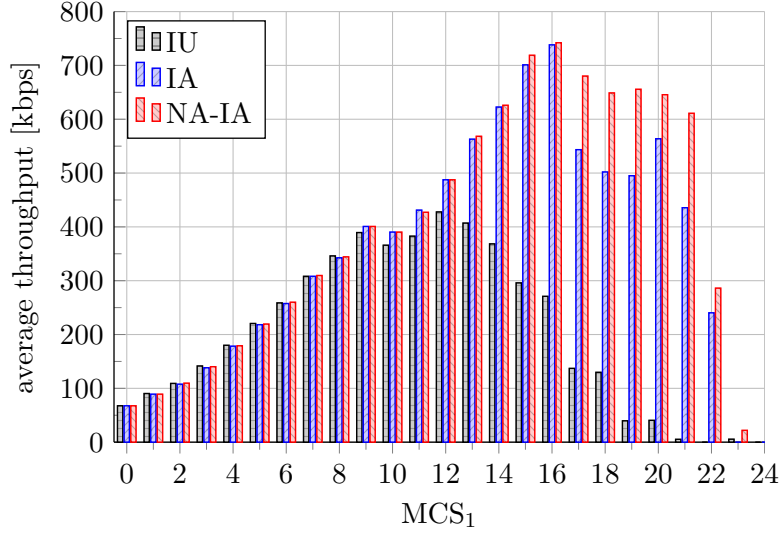
Figure 5.8: $MCS_1$ vs. average throughput with $n_\mathrm{r} = 2$, indoor scenario

With two receive antennas the performance of the IA and NA-IA receivers improve drastically (Figure 5.8), whereas the IU receiver shows a small performance loss which may be explained by the varying channel conditions. The NA-IA receiver outperforms the IA receiver for $MCS_1 > 16$, for 64QAM modulation.

We conclude that an IA receiver can significantly improve the performance of the UE in TM5, especially if an additional receive antenna is present to allow for effective interference mitigation. Furthermore, the NA-IA can improve the performance if 64QAM modulation is used.

### Outdoor scenario with strong line-of-sight component

Figure 5.9 shows the measurement environment with the UE in the foreground and the eNB on the roof in the background. During the measurement we move the UE slowly in one direction and back multiple times.

Figure 5.10 depicts the measurement results for all three receivers. It can be observed that both IA and NA-IA receiver achieve maximum throughput for $MCS_1 = 16$ and the IU receiver at $MCS_1 = 14$. Although the maximum throughput of IA and NA-IA receiver are almost identical, the NA-IA achieves a significantly higher throughput for $MCS_1 > 16$, for 64QAM modulation.

### Outdoor scenario without line-of-sight component

Figure 5.11 shows the NLOS environment, where the UE was slowly moved straight until the bridge.

The throughput results for a NLOS channel are presented in Figure 5.12. It can be seen that the difference in maximum throughput between IA and NA-IA receiver

Figure 5.9: Outdoor scenario with strong LOS channel
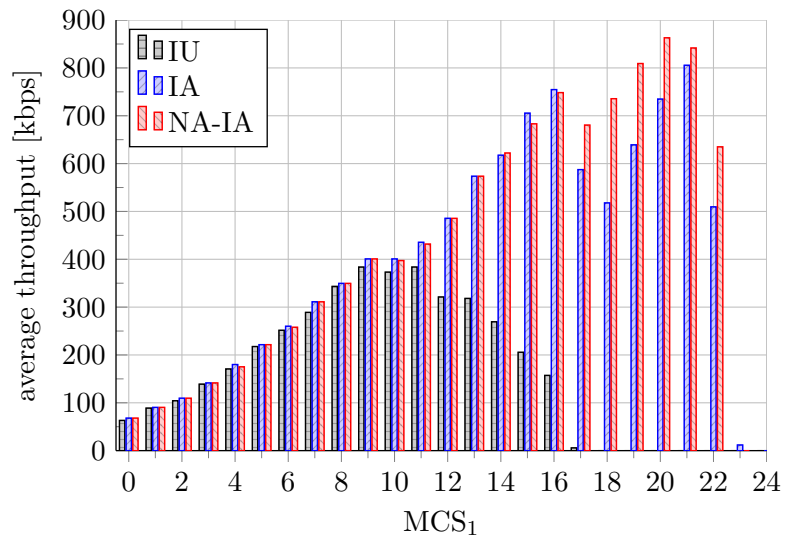


Figure 5.10: MCS$_1$ vs. average throughput with $n_r = 2$, outdoor scenario with strong LOS channel.

Figure 5.11: NLOS environment with eNB on the roof of left building

is negligible and almost identical compared to the results in the LOS environment. Moreover, as in the LOS channel, the NA-IA receiver significantly outperforms the IA receiver for 64QAM modulation. These results suggest that the relative performance of IA and NA-IA receiver is robust to the propagation environment, , their throughput difference is similar in LOS and NLOS channels.

Regarding the IU receiver, we observe significant performance degradation in NLOS compared to LOS channels especially for $MCS_1 > 12$. For instance, the maximum throughput in LOS of 481 kbps to 428 kbps in NLOS channel. Even more drastic is the loss at higher order modulations, for $MCS_1 = 17$ the throughput decreased from 273 kbps to 137 kbps. We conclude that the IU receiver benefits significantly from LOS environments especially at higher order modulations. This is in line with the findings [94], wh show that channel correlation is beneficial for MU-MIMO. The LOS component of the channel increases the channel correlation and hence renders the precoding more effective, resulting in lower MU interference.

## 5.5 Conclusion

This chapter evaluated the potential performance improvements of IA receiver designs over an IU receiver in TM5 through real-time field measurements in LOS and NLOS propagation environments.

In case of single receive antenna the measurements indicate that the IA receiver offers almost no advantage compared to the IU receiver.

However, for both single and dual antenna receivers, the measurements revealed that the NA-IA receiver significantly outperforms the IA receiver for higher order modulations, 64QAM. This result suggests that the signaling of the interfering modulation order can greatly improve performance in case 64QAM is applied. For lower order modula-
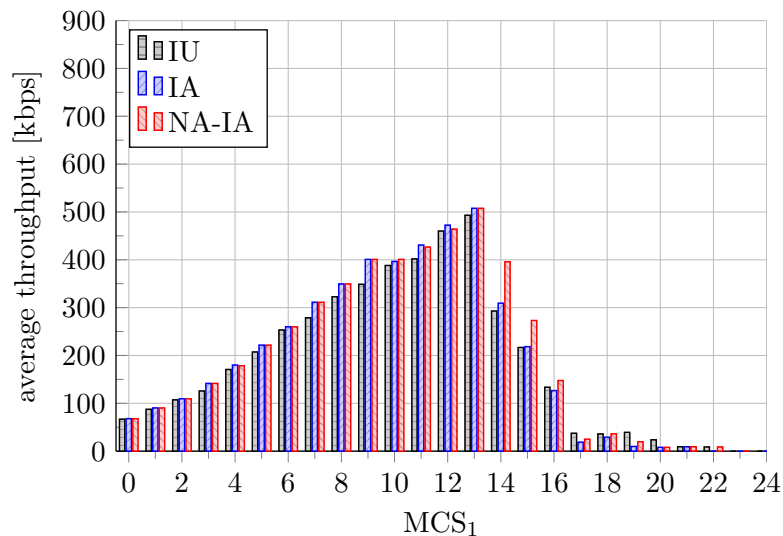
Figure 5.12: MCS$_1$ vs. average throughput with $n_r = 2$, outdoor scenario with non-LOS channel.

tions the simplified IA receiver without knowledge of the interfering modulation order performs equally well as the NA-IA.

Moreover, the measurements indicate that the IU receiver benefits significantly from LOS channels compared to the IA receivers especially at higher order modulations. In case of QPSK even the IU receiver achieves the same throughput as the IA receivers.

We conclude that a UE with IA receiver can greatly increase both cell and user throughput especially with additional network assistance.

# Chapter 6

# Physical layer abstraction for LTE

We present an in-depth performance analysis of the gains of physical layer (PHY) abstraction when compared to a full implementation of the physical layer. The abstraction model uses either effective signal to noise plus interference (SINR) mapping or mutual information effective SINR mapping and covers different transmission modes as well as support for hybrid automatic repeat request. Using the OpenAirInterface LTE system level simulator we show that for a simple network with one base station and two user equipments these PHY abstraction techniques decrease the simulation time by a factor of up to 100 while providing the same accuracy as with the full PHY implementation.

## 6.1 Introduction

System level simulations are an integral part of performance evaluations of mobile communication networks. Typically these system level simulators implement small networks with 10-20 base stations (called eNB in LTE) and several hundred user equipments (UEs). Also channel models, mobility models, and traffic models are often also included in such simulators. To motivate the use of physical layer (PHY) abstraction in system level simulators consider the following example experiment, carried out using the OpenAirInterface LTE system level simulator (oaisim) [95]. The top-level parameters of the experiment are given in Table 6.1. Note that the OpenAirInterface uses heavily optimized C code and single-input multiple-data (SIMD) instructions, both for the MODEM and for the channel convolution. The experiment has been carried out on a PC with an Intel Core i5 CPU running at 3.33GHz. The process has been pinned to one CPU and its priority has been set to the maximum to avoid swapping. An overview of where time is spent in the system level simulator is given in Figure 6.1, which shows the processing time needed for one subframe (1ms). It can be seen that 85% of the time is spent in the channel simulation, that is generation of the random channel, interpolation to the right sampling rate, and convolution of the signals with the channel. Although the UE's receiver is operating at its full capacity, it only makes up 10% of the total simulation time. In total 95 % of the simulation time is spent on the PHY and the channel.

| Parameter | Value |
|---|---|
| No. eNBs | 1 |
| No. UEs | 1 |
| Path loss model | $\text{PL}_{\text{dB}} = 128 + 36.7 \cdot \log_{10}(d_{\text{km}})$ |
| UE distribution | fixed at distance of $d = 0.32$km from eNB |
| TX power | 15dBm |
| RX noise figure | 0dBm |
| Antenna gains | 0dBm |
| Resulting SNR | 10dB |
| Large scale fading | none |
| Small scale fading | SCM-C |
| System bandwidth | 5MHz (25 ressource blocks) |
| TDD configuration | 3 (6 DL, 3 UL, 1 special subframe) |
| Cyclic Prefix | normal |
| Transmission Mode | 1 (SISO) |
| Antennas at eNB/UE | 1/1 |
| Link adaptation | fixed MCS 7 |
| Resulting max throughput | 1.867 Mbps |
| Trafic model | full buffer |

Table 6.1: Simulation Parameters

## 6.2 Overview of Physical Layer Abstraction Techniques

### 6.2.1 Introduction

PHY abstraction is the process of modeling the performance of the physical layer (in terms of block error rates or throughput) as a function of the radio channel without running the time consuming MODEM and the channel convolution. The model takes into account the power and resource allocation, the modulation and coding scheme (MCS) and the current channel state, i.e., path loss, shadowing, fading and interference. In case multiple antennas are used at the transmitter and/or receiver (creating a multiple-input multiple-output (MIMO) channel), also the precoding and the receive processing is taken into account. PHY abstraction models are useful for two different purposes: Firstly they can be used in the implementation of a UE to compute the feedback (channel quality information - CQI) and secondly they can be used in large-scale system level simulations to speed up simulation time.

The two most important PHY abstraction methods are Exponential effective SINR mapping (EESM) and Mutual Information based SINR mapping (MIESM). EESM was first introduced in [99] for system level evaluations and since then it has been extensively used for link quality modeling. In [100] it is shown that EESM is a suitable choice for 3GPP LTE wireless systems and it outperforms the other schemes. Further it was demonstrated that training of link abstraction is independent of the used channel model.

While EESM is very attractive because of its simplicity, MIESM is much better suited to model more advanced (non-linear) receiver architectures, hybrid automated repeat request (HARQ), and MIMO transmission modes [101]. In [102] the authors have used the observation that decoding of a codeword is independent of modulation so they have devised a two step method where received bit information rate is used as a link quality measure instead of effective SINR. This method is also mutual information based and does not require the calibration for convolution and turbo decoders and was selected as an evaluation methodology in the WINNER project [103] and the WiMAX standard [104]. MIESM is also very well suited to model HARQ as shown in [11, 105, 106].

An important work in the field of MIMO communications was presented in [107] where the authors have presented a semi-analytical performance prediction model based on MIESM for iterative minimum mean squared error (MMSE) interference cancellation detection. Experimental results for this method for an LTE-compliant system are shown in [108]. Another important work was presented in [109] for MIMO-OFDM systems with maximum likelihood (ML) receivers. Their model is also based on a variant of MIESM (based on work by [102]) and they model the effects of channel mismatch and correlation in the abstraction model. They show results for the rate compatible punctured convolution codes and different MIMO antenna configurations. A new method for PHY abstraction for multi-user MIMO (MU-MIMO) in the framework of LTE using non-linear interference aware receivers has been proposed in [10]. Although the scheme is targeted towards MU-MIMO systems but it can also be applied to MIMO systems employing non-linear receivers.

## 6.2.2 PHY abstraction in LTE systems

The 3GPP long-term evolution (LTE) is a 4th generation cellular communications standard. On the downlink (DL), LTE employs orthogonal frequency division multiple access (OFDMA) and defines several physical transport channels. The most important one, the physical downlink shared channel (PDSCH) uses turbo-codes with adaptive modulation and coding as well as hybrid automatic repeat request (HARQ) protocol. The PDSCH can also make use of MIMO techniques through the so called transmission modes. For example, transmission mode 2 refers to Alamouti precoding, while transmission mode 4 means closed-loop spatial multiplexing with up to two spatial streams. The challenge for PHY abstraction for the PDSCH is to have a system that can flexibly adapt to the different code rates and takes into account the HARQ and the MIMO transmission mode.

In addition to the PDSCH, the downlink also defines a physical control channel (PDCCH), which uses a variable rate tail-biting convolutional code and the physical broadcast channel (PBCH), which uses a fixed rate turbo code.

On the uplink (UL), LTE uses single carrier frequency division multiple access (SC-FDMA) and defines the physical uplink shared channel and the physical uplink control channel. The first one uses–like the downlink–adaptive turbo codes, while the latter uses either simple spreading codes for small payloads (format 1, 1a, and 1b) or Reed-Muller linear codes for larger payloads (format 2, 2a, 2b).
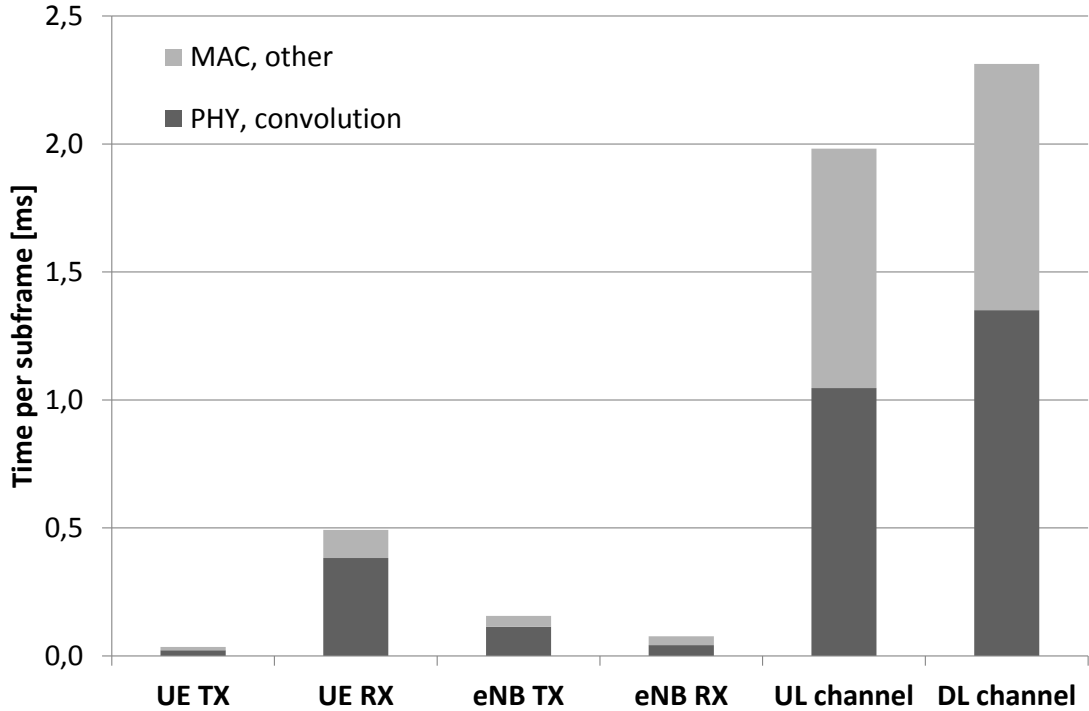
Figure 6.1: Computation time spent in the different elements of a system level simulator.

In the following chapter we describe the abstraction procedure for the PDSCH.

### 6.2.3 PHY Abstraction Overview

In the following we give a brief overview of the PHY abstraction process based on effective SINR mapping (ESM). The procedure can be divided into three steps as shown in Figure 6.2: SINR calculation, SINR Compression, and Link Quality Mapping.

**SINR calculation** The first step of the PHY abstraction procedure consists of the SINR calculation per resource element (RE). This step depends on the transmission mode and the used receiver architecture. The most simple case is transmission mode 1 (SISO), where the signal model is given by

$$y_n = h_n \cdot x_n + z_n, \quad n = 0, \ldots, N-1 \tag{6.1}$$

where $x_n \in \chi_M$ are the modulated resource elements (RE) of the encoded codeword, taken from a finite constellation of order $M$ (QPSK, 16QAM, or 64QAM), $h_n$ is the channel at RE $n$, $y_n$ is the received signal at RE $n$, and $z_n$ is the circularly symmetric additive white Gaussian noise (AWGN) with zero mean and variance $\sigma^2$. $N$ is the total number of REs occupied by the codeword. The SINR $\gamma_n$ is for every RE $n = 0, \ldots, N-1$
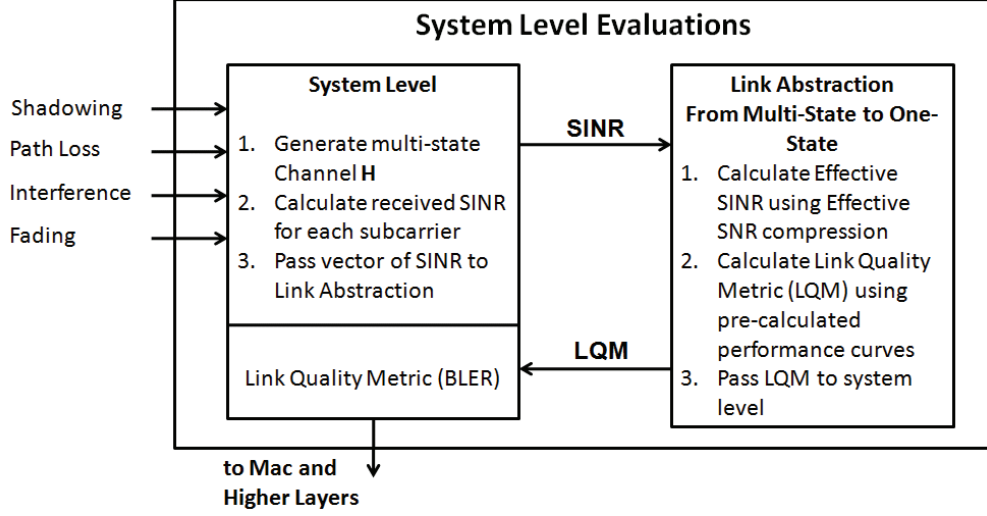
Figure 6.2: PHY abstraction model

is then given by

$$\gamma_n = \frac{|h_n|^2}{\sigma^2}, \quad n = 0, \ldots, N - 1. \tag{6.2}$$

Transmission mode 2 uses Alamouti precoding on two transmit antennas to achieve transmit diversity. In the first symbol time $x_1$ and $x_2$ are transmitted from antenna 1 and 2, whereas in the second symbol time $-x_2^*$ and $x_1^*$ are transmitted from antenna 1 and 2 respectively. At the receiver, the two received signals are combined and the SINR for the $n$-th resource element is given by

$$\gamma_n = \frac{||\mathbf{H}_n||^2}{2\sigma^2}, \tag{6.3}$$

where $\mathbf{H}_n$ is the MIMO channel at RE $n$.

Beamforming is implemented in LTE in transmission modes 6 and 7. The signal model for these modes is given by

$$\mathbf{y}_n = \mathbf{H}_n \mathbf{p}_n \cdot x_n + \mathbf{z}_n, \quad n = 0, \ldots, N - 1, \tag{6.4}$$

where $\mathbf{p}_n$ is the beamforming (precoding) vector. The SINR per RE at the receiver is given by

$$\gamma_n = \frac{||\mathbf{H}_n \mathbf{p}_n||^2}{\sigma^2}. \tag{6.5}$$

Closed loop spatial multiplexing is implemented in LTE in transmission modes 4, 8, and 9. A general signal model for those transmission modes can be written as

$$\mathbf{y}_n = \mathbf{H}_n \mathbf{P}_n \cdot \mathbf{x}_n + \mathbf{z}_n, \quad n = 0, \ldots, N - 1, \tag{6.6}$$

93

where $\mathbf{x}_n = [x_{1,n}, \ldots, x_{C,n}]^T$ is the vector of codewords and $\mathbf{P}_n = [\mathbf{p}_{1,n}, \ldots, \mathbf{p}_{C,n}]$ is the precoding matrix. The SINR depends on the receiver architecture and has to be computed for each codeword $c$. In the ideal case, where the receiver is able to do perfect interference cancellation we would have

$$\gamma_{n,c}^{\text{PIC}} = \frac{||\mathbf{H}_n \mathbf{p}_{c,n}||^2}{\sigma^2}. \tag{6.7}$$

If an MMSE receiver architecture is used, then

$$\gamma_{n,c}^{\text{MMSE}} = \frac{1}{\left[\left(\mathbf{I} + \frac{1}{\sigma^2}\mathbf{p}_{c,n}^H \mathbf{H}_n^H \mathbf{H}_n \mathbf{p}_{c,n}\right)^{-1}\right]_{c,c}} - 1. \tag{6.8}$$

For maximum-likelihood receivers, [109] has recently shown that the SINR can be modeled as

$$\gamma_n^{\text{ML}} = (1 + \gamma_{n,c}^{\text{PIC}})^{\alpha\beta}(1 + \gamma_{n,c}^{\text{MMSE}})^{1-\alpha\beta}, \tag{6.9}$$

where $\alpha$ and $\beta$ are factors that need to be calibrated in advance.

Multi-user MIMO (transmission modes 5 or 9) is a special case of the above, where different codewords are destined for different users. Here the signal model can be written as

$$\mathbf{y}_n = \mathbf{H}_{1,n}\mathbf{p}_{1,n} \cdot x_{1,n} + \mathbf{H}_{1,n}\mathbf{p}_{2,n} \cdot x_{2,n} + \mathbf{z}_n, \quad n = 0, \ldots, N-1, \tag{6.10}$$

where the first term is the desired signal for user 1 and the second term is the interfering signal destined for user 2. A standard or interference unaware (IU) receiver would treat the interfering signal as noise and thus the SINR would be given by

$$\gamma_{n,c}^{\text{IU}} = \frac{||\mathbf{H}_n \mathbf{p}_{1,n}||^2}{||\mathbf{H}_n \mathbf{p}_{2,n}|| + \sigma^2}. \tag{6.11}$$

A more intelligent, interference aware (IA) receiver (such as the one described in [92]) however is able to take this interference into account and perform optimal detection. In this case the abstraction procedure is a bit different since instead of the SINR we now need to calculate the signal to noise ratio (SNR) and the signal to interference ratio (SIR) separately. Please refer to [10, 110] for details.

**SINR Compression**   Secondly, the multi-state channel described by the post-processing SINR $\gamma_n, n = 0, \ldots, N-1$ is compressed into a single *effective* SINR value $\gamma_{\text{eff}}$ using an information measure function $I$:

$$\gamma_{\text{eff}} = \beta_1 I^{-1}\left[\frac{1}{N}\sum_{n=1}^{N} I\left(\frac{\gamma_n}{\beta_2}\right)\right]. \tag{6.12}$$

$\beta_1$ and $\beta_2$ are called an adjustment factor that need to be calibrated [12, 110]. The reverse information mapping function $I^{-1}$ does not necessarily have to be the same as the forward function $I$, for example if the interference aware receiver abstraction is used [10].
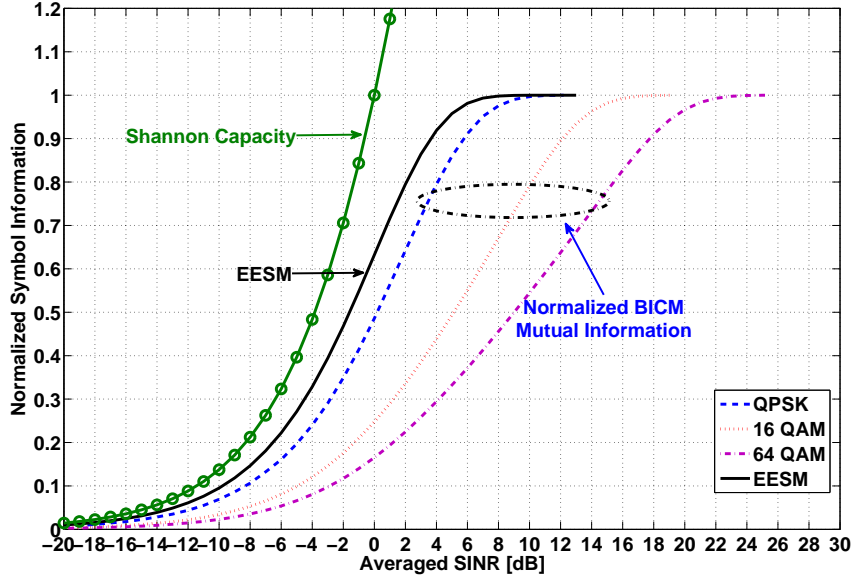
Figure 6.3: Comparison of different information mapping functions.

For turbo codes, several choices for the information mapping function $I$ are available (other codes might require other functions):

**EESM.** The exponential effective SINR mapping (EESM) function is calculated using Chernoff union bound of error probabilities, i.e.,

$$I_{\text{EESM}}(\gamma_n) = 1 - \exp(-\gamma_n) \tag{6.13}$$

**MIESM.** The mutual information based effective SINR mapping (MIESM) function is on the mutual information of bit-interleaved coded modulation (BICM) [39].

$$I_{\text{MIESM}}(\gamma_j, M_1) = \log M_1 -$$

$$\frac{1}{M_1} \sum_{x_1 \in \chi_1} \mathcal{E}_{z_1} \log \frac{\sum_{x_1' \in \chi_1} \exp\left[-\left|\gamma_j\left(x_1 - x_1'\right) + z_1\right|^2\right]}{\exp\left[-|z_1|^2\right]}, \tag{6.14}$$

where $\chi_1$ is the set of constellation points, $M_1 = |\chi_1|$ is the modulation order, and $z_1$ is a circularly symmetric white Gaussian noise with zero mean and unit variance.

A comparison of the information mapping functions is given in Figure 6.3. Note that we plot the MIESM functions in a normalized way to allow a better comparison with the EESM function. It can be seen that the EESM function is a good approximation and advantageous due to its simplicity. However, best results are achieved with the mutual information function. The only problem is these functions need to be pre-computed using Monte-Carlos simulations since no closed form expressions exist.

95

|  | Full PHY | Abstraction |
|---|---|---|
| Throughput | 1.75 Mbps | 1.73 Mbps |
| BLER | 4% | 4% |

Table 6.2: System performance for full PHY and abstraction.

|  | Full PHY | Abstraction | Improvement |
|---|---|---|---|
| **UE TX** | 0.035 | 0.010 | 4 |
| **UE RX** | 0.493 | 0.026 | 19 |
| **eNB TX** | 0.157 | 0.012 | 13 |
| **eNB RX** | 0.077 | 0.012 | 6 |
| **UL channel** | 1.982 | n/a | n/a |
| **DL channel** | 2.313 | 0.012 | 192 |
| **total** | 5.056 | 0.072 | 70 |

Table 6.3: Simulation times per subframe (in ms) for full PHY and abstraction.

**Link Quality Mapping**  The final step of PHY abstraction computes the block error rate (BLER) of the channel as a function of the effective SINR $\gamma_{\text{eff}}$ based on pre-computed AWGN reference curves for the effective coderate of the codeword $r_{\text{eff}}$, and the modulation order $Q_m$.

$$\text{BLER} = \text{BLER}_{\text{AWGN}}(r_{\text{eff}}, \gamma_{\text{eff}}, Q_m) \tag{6.15}$$

The number of reference curves can be reduced to three (one per modulation order) by appropriate shifting of the curve according to the effective code rate $r_{\text{eff}}$ [11]. This method is also applicable to HARQ.

## 6.3  Performance results

Both EESM and MIESM abstraction methodologies have been implemented in the OpenAirInterface LTE system level simulator (oaisim). In this section we analyze the applicability and the performance of MIESM compared to a full PHY implementation (EESM has already been analyzed in [12]). The simulation parameters used in this experiment[1] are the same as in Table 6.1. Table 6.2 shows a comparison of the throughput and their (BLER) for both the full PHY and the PHY abstraction. As expected, the PHY abstraction shows the same performance results as the full PHY, proving the applicability of the method.

Table 6.3 shows the simulation times per subframe (in ms) for full PHY and abstraction and the corresponding improvements factors. It can be seen that the abstraction

---

[1]The code used for this experiment has been tagged on our SVN server and can be found at `http://svn.eurecom.fr/openair4G/tags/asilomar2013`.
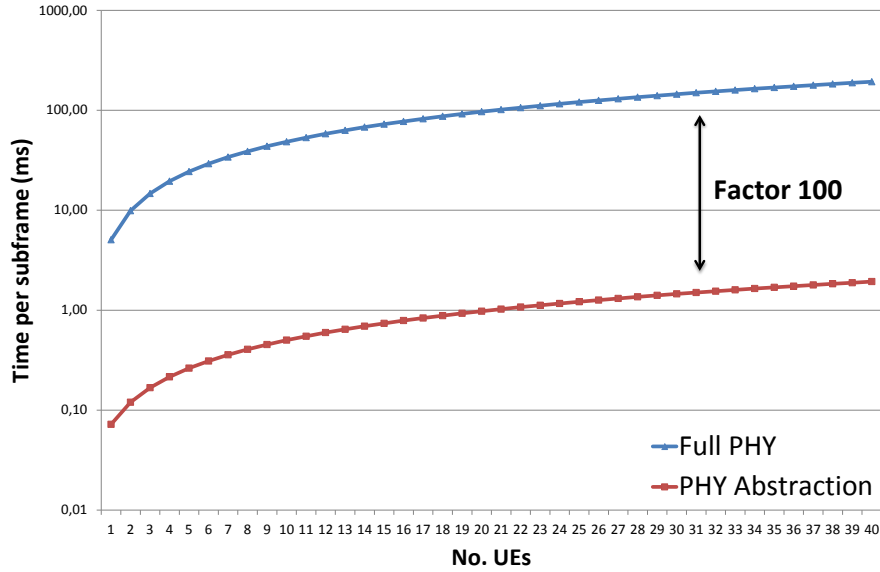
Figure 6.4: Comparison of the computation time of the system level simulator with full PHY and with abstraction.

provides performance improvements in the execution of both UE and eNB, but the most notable performance improvement is in the DL channel, since in the abstraction we do not need to carry out the channel convolution. The UL channel is not yet abstracted in oaisim (it is error free regardless of the channel), so the performance numbers are not yet available. However, the same numbers as for the DL can be expected. Figure 6.4 depicts an extrapolation of the execution time for a multi-user system. It can be seen that asymptotically a factor 100 can be saved in execution time, allowing the simulation of a 20 user system almost in real-time on a single core CPU.

## 6.4 Conclusions

We have shown in this paper that the physical layer and channel model take more than 80% of simulation time in state-of-the-art LTE system level simulators. To simulate large systems with several base stations and hundreds of users, the simulation time becomes prohibitively complex. Physical layer abstraction is a technique to predict the performance of a physical link without running the complex MODEM and the channel convolution. We have shown with the help of the OpenAirInterface system level simulator oaisim, which implements LTE release 8/9 both with full PHY and PHY abstraction, that PHY Abstraction can improve simulation time by a factor of 70 for a single link and by a factor of 100 for a multi-user system.

# Chapter 7

# Conclusions

The previous chapters have each treated a particular topic of experimental wireless communications and conclusions for that particular topic were given. In this chapter we would like to give some meta-conclusions in the form of lessons that we have learned during these research projects and experiments. Finally we give some future directions for research in experimental wireless communications.

## 7.1 Lessons learnt from OpenAirInterface

Developing and maintaining a testbed for wireless communications is not an easy task. In this section I would like to summarize some of the lessons learned. These are both a mix of my personal experience and of my colleague and mentor Raymond Knopp [111].

### 7.1.1 Personnel is key

One of the keys to a successful testbed is the team. A testbed like OpenAirInterface needs people with basic engineering knowledge in telecommunications (computer programming/architecture, computer science, electronics, etc.) as well as more advanced and recent knowledge in wireless communications standards (e.g., 3GPP LTE), signal processing, and networking. Such people are obviously very hard to find and even harder to keep. The latter is especially true in an academic environment like Eurecom, whose experimental activity is only financed through third party funding. This means we cannot provide the same salary and the same kind of contract as a comparable job in industry.

The OpenAirInterface core team comprises professors, assistant professors, and permanent research engineers that ensure the basic operation and continuity of the platform and are responsible for project acquisition and management. On top of that, depending on the amount of third party funding, there are post-docs and PhD students, carrying out the more innovative and experimental work. It is therefore very important that the permanent team takes care of the "hard-core" engineering work, while providing "simple tools" for the PhDs to perform experiments.

### 7.1.2 Experimentation and publishing are not necessarily mutually exclusive

One of the key performance indicators (KPI) of a researcher's output is their number of publications. Some people see this requirement as a counter-argument to do experimental research, as this requires a lot of preparation work. Most of the time, the actual development work of the experiment takes much longer than the experiment itself. Especially PhD students are often turned off by experimental activities, since they don't see how this can be accomplished in the relatively short time-frame of a PhD (In France the average length of a PhD thesis is 3.5 years).

However, excellent work can be both experimental and fundamental and the best for a PhD is a combination of both. The KPI should not only be measured in number of publications but also in the impact of the publication. Further also contributions to open-source software, teaching, industry collaboration should be taken into account.

### 7.1.3 Keep it simple, stupid

The "Keep it simple, stupid" (KISS) principle states that most systems work best if they are kept simple rather than made complex; therefore simplicity should be a key goal in design and unnecessary complexity should be avoided [1]. The same applies to the design of experiments on wireless testbeds.

First of all the platforms should be designed or chosen to suit realizable objectives. In OpenAirInterface for example, the 2nd generation platform CBMIMO (2005) was designed as a cheap radio front-end for software defined radio applications. It was used successfully in many projects including projects on networking and applications. The 3rd generation platform ExpressMIMO (2007) was no longer designed to be used as a purely software radio but it should also serve as a platform for system-on-chip (SoC) architecture exploration. At the same time wireless networking experimentation should still be possible. However, the complexity of HW and SW design for the SoC architecture was too high and only very simple MODEMs could be realized. This in turn was incompatible with the second objective of doing experimentation with advanced wireless networks and therefore lead to many failed objectives in projects. The 4th generation platform ExpressMIMO2 (2012) had the same objectives as CBMIMO, i.e., a purely software defined radio, but with an updated and more performant radio front-end.

Secondly, programming languages and implementation methodologies should be chosen as simple as possible to achieve the project objectives. For example, for many experiments, hard-real time is not necessary and simple off-line preparation of the signals and asynchronous reception are sufficient. In this case, the MATLAB/OCTAVE interface of OpenAirInterface can be used.

---

[1] http://en.wikipedia.org/wiki/KISS_principle

### 7.1.4 Development needs testing and review

A research testbed is in constant evolution. New features are added by different contributors all the time. Very often contributors are not even aware of any side effects their commit causes. Therefore it is of utmost importance that at least a minimum amount of regression testing is performed every time a new feature is added. These regression tests should not only be done on a software level, but also on a hardware/firmware level. Otherwise weeks might be lost trying to find a bug.

## 7.2 Future directions

### 7.2.1 Channel Reciprocity

In Chapter 4 we have used the assumption of diagonal calibration matrices when exploiting channel reciprocity. However, the calibration matrices are in fact only diagonal if there is neither mutual coupling nor cross-talk between the RF chains. A simple numerical experiment shows that if there is even only a small cross-talk, the off-diagonal elements of the calibration matrices become significant. In order to see how significant, we have done an experiment using one ExpressMIMO2 with 4 transciever chains, where 1 chain was used to emulate node A and the other 3 chains were used to emulate node B. This setup has the advantage of avoiding any synchronization and frequency offset issues. The reciprocity matrix is estimated using an alternate projection method and the results show that the resulting reciprocity matrix has off-diagonal elements which are only 10dB lower than the main diagonal elements. When applied to a simple beamformer the performance loss due to the assumption of diagonal reciprocity matrices can jeopardize the whole beamforming gain [112]. It is therefore of utmost importance to drop the assumption of diagonal reciprocity matrices when exploiting channel reciprocity. Moreover, efficient relative calibration mechanisms for this more complicated model need to be designed. This is especially true for the case of massive MIMO, which we will describe next.

### 7.2.2 Massive MIMO

The work on channel reciprocity is getting more and more attention these days with the development of massive MIMO systems. Massive MIMO takes MU-MIMO to the next level by scaling up the number of antennas at the base station by an order of magnitude, providing additional degrees of freedom in the channel. These additional degrees of freedom can be used to design more simple and scalable signal processing algorithms and help focusing energy into small regions of space and thus reducing interference.

Massive MIMO relies to a great extent on the exploitation of channel reciprocity in TDD systems to obtain CSIT. It is not feasible to operate massive MIMO in a FDD system with a finite rate feedback channel, because by the time the channel from all the transmit antennas has been estimated at the user and fed back to the base station, the

channel will have changed too much (the estimation+feedback time is longer than the coherence time of the channel).

Most of the calibration methods proposed for massive MIMO rely on the assumption that the calibration matrix is diagonal. However, we have seen in the previous subsection that this is not necessarily the case. On the other hand, some of those imperfections might be neglected at the expense of adding more antennas to the system. There is however—to the best of the authors knowledge—no experimental work to validate this.

There are already some platforms for experimentation with massive MIMO available [113, 114], but none of them allows for real-time bi-directional communication. This is however necessary to validate the feasibility of channel reciprocity.

Therefore we are planning to extend the OpenAirInterface testbed to massive MIMO. The platform will feature a 64 element antenna array from its partner IABG and a rack of 16 ExpressMIMO2 cards, each able to control 4 RF chains (resulting in 64 independently controllable chains). The testbed will be connected to the OpenAirInterface real-time LTE software modem. This will allow us to study the problematic of channel reciprocity but also other challenges related to massive MIMO.

### 7.2.3  Receivers for higher order MIMO

Chapters 2 and 5 presented receiver architectures for a distributed MIMO system with two spatial streams and for a MU-MIMO system with one desired stream and one interfering stream. The extension of those receiver architectures to higher order MIMO is however not trivial, since the trick that is used in the calculation for the bit metrics is only applicable to one complex dimension. For higher order MIMO a combination of a linear pre-processor and the described receiver architecture can be envisioned. For a 4 layer MIMO system, a block QR factorization could be used to decompose the channel into two blocks of of 2 layers with no interference between them and then use the existing receiver architecture. We are planning to evaluate this idea and also test it on the OpenAirInterface platform.

### 7.2.4  Aggregation of heterogeneous radio access technologies

Carrier aggregation (CA) is one of the key technologies in LTE-Advanced to enable higher throughput on the physical layer. LTE-A has been specified to support the aggregation of carrier with different transmission bandwidths and different carrier frequencies. Cross-carrier scheduling and easy enabling/disabling of different carriers allows for interference mitigation and dynamic scheduling in heterogeneous networks (HetNet) composed of macro cells and small cells.

A future enhancement would be the use of CA over heterogeneous radio access technologies (h-RATs), e.g., LTE and WiFi. Almost all recent smartphones already support both technologies, but a true aggregation of the two technologies is not yet possible as it would require a tight integration at a lower level such as the medium access control (MAC) layer. The SOLDER project will study this possibility, looking at some fundamental questions such as, multi-channel link adaptation, scheduling, interference

management, and radio resource management. At the same time a proof of concept prototype based on OpenAirInterface will be developed to demonstrate and validate the soundness of these innovative concepts.

### 7.2.5 Physical layer abstraction

Throughput improvement through innovations on the physical layer are often hard to translate to throughput improvements on the network. It is therefore important to study these innovations on a system level as well under the influence of different traffic patterns, channel and interference situations, and mobility models. However in order to make those simulations feasible (in terms of execution time and simplicity) physical layer abstraction techniques need to be used. However, especially for the more advanced transmission modes, such as higher order MIMO, cooperative multi-point transmission, etc. reliable abstraction models are very sparse or inexistent. Especially when it comes to more advanced MIMO receiver architectures, such as sphere decoding, iterative turbo receivers, interference cancellation receivers, etc. new abstraction models need to be developed.

# Bibliography

[1] G. J. Foschini. Layered space–time architecture for wireless communication in a fading environment when using multiple antennas. *Bell Labs Systems Technical Journal*, 1:41–59, 1996.

[2] G. D. Golden, C. J. Foschini, R. Valenzuela, and P. W. Wolniansky. Detection algorithm and initial laboratory results using V-BLAST space-time communication architecture. *Electronics Letters*, 35(1):14–16, 1999.

[3] Florian Kaltenberger, Rizwan Ghaffar, Raymond Knopp, Hicham Anouar, and Christian Bonnet. Design and implementation of a single-frequency mesh network using OpenAirInterface. *EURASIP Journal on Communications and Networking*, 2010, 2010. Article ID 719523, 16 pages, doi:10.1155/2010/719523.

[4] F. Kaltenberger, M. Kountouris, D. Gesbert, and R. Knopp. On the trade-off between feedback and capacity in measured MU-MIMO channels. *IEEE Trans. Wireless Commun.*, 8(9):4866–4875, September 2009.

[5] Florian Kaltenberger, Haiyong Jiang, Maxime Guillaud, and Raymond Knopp. Relative channel reciprocity calibration in MIMO/TDD systems. In *Proc. ICT Future Network and Mobile Summit*, Florence, Italy, June 2010.

[6] Maxime Guillaud and Florian Kaltenberger. Towards practical channel reciprocity exploitation: Relative calibration in the presence of frequency offset. In *WCNC 2013, IEEE Wireless Communications and Networking Conference*, Shanghai, CHINA, April 2013.

[7] Boris Kouassi, Bassem Zayen, Raymond Knopp, Florian Kaltenberger, Dirk TM Slock, Irfan Ghauri, Francesco Negro, and Luc Deneire. Design and implementation of spatial interweave LTE-TDD cognitive radio communication on an experimental platform. *IEEE Wireless Communications Magazine: Next Generation Cognitive Cellular Networks: Spectrum Sharing and Trading*, 20(2):60–67, April 2013.

[8] 3GPP. Network-assisted interference cancellation and suppression for LTE (release 12). Technical Report 36.866-V1.0.0, 3GPP, December 2013.

[9] Sebastian Wagner and Florian Kaltenberger. Interference-aware receiver design for MU-MIMO in LTE: Real-time performance measurements. *Intel Technology Journal (special issue on 4G communications)*, 18(1):154–171, 2014.

[10] Imran Latif, Florian Kaltenberger, and Raymond Knopp. Link abstraction for multi-user MIMO in LTE using interference-aware receiver. In *WCNC 2012, IEEE Wireless Communications and Networking Conference*, Paris, FRANCE, April 2012.

[11] Imran Latif, Florian Kaltenberger, Raymond Knopp, and Joan Olmos. Link abstraction for variable bandwidth with incremental redundancy HARQ in LTE. In *WIMEE 2013, 9th International Workshop on Wireless Network Measurements, In conjunction with 11th Intl. Symposium on Modeling and Optimization in Mobile, Ad Hoc, and Wireless Networks (WiOpt 2013)*, Tsukuba, JAPAN, May 2013.

[12] Imran Latif, Florian Kaltenberger, Navid Nikaein, and Raymond Knopp. Large scale system evaluations using PHY abstraction for LTE with OpenAirInterface. In *EMUTOOLS 2013, 1st Workshop on Emulation Tools, Methodology and Techniques, March 5, 2013, Cannes, France / Collocated with SIMUTools 2013, 6th International ICST Conference on Simulation Tools and Techniques*, Cannes, FRANCE, March 2013.

[13] Florian Kaltenberger, Imran Latif, and Raymond Knopp. On scalability, robustness and accuracy of physical layer abstraction for large-scale system-level evaluations of LTE networks. In *in Proc. Asilomar Conference on Signals, Systems, and Computers*, Pacific Grove, CA, November 2013. invited.

[14] Hicham Anouar, Christian Bonnet, Daniel Câmara, Fethi Filali, and Raymond Knopp. An overview of OpenAirInterface wireless network emulation methodology. *ACM SIGMETRICS Performance Evaluation Review*, 36(2):90–94, September 2008.

[15] Alexander Tyrrell and Gunther Auer. Biologically inspired intercellular slot synchronization. *EURASIP Journal on Wireless Communications and Networking*, 2009, 2009. Article ID 854087, 12 pages, doi:10.1155/2009/854087.

[16] M. Rupp, S. Caban, and C. Mehlführer. Challenges in building MIMO testbeds. In *Proc. of the 13th European Signal Processing Conference (EUSIPCO 2007)*, Poznan, Poland, September 2007.

[17] José. A. Garcia-Naya, M. González-López, and L. Castedo. An overview of MIMO testbed technology. In *Proc. 4th International Symposium on Image/Video Communications over fixed and mobile networks*, Bilbao, Spain, 2008.

[18] Ettus Research, 2009.

[19] GNU radio—the GNU software radio, 2009.

[20] Rice University. WARP project: Wireless open-access research platform, 2009.

[21] K. Mandke, S.-H. Choi, G. Kim, R. Grant, R. C. Daniels, W. Kim, S. M. Nettles, and R. W. Heath, Jr. Early results on hydra: A flexible mac/phy multihop testbed. In *Proceedings of the 65th IEEE Vehicular Technology Conference*, pages 1896–1900, April 2007.

[22] S. Gupta, C. Hunter, P. Murphy, and A. Sabharwal. WARPnet: Clean slate research on deployed wireless networks. In *Proc. 2009 ACM Mobihoc Conference*, 2009.

[23] T. Korakis, M. Knox, E. Erkip, and S. Panwar. Cooperative network implementation using open-source platforms. *Communications Magazine, IEEE*, 47(2):134–141, February 2009.

[24] S.M. Mishra, D. Cabric, C. Chang, D. Willkomm, B. van Schewick, S. Wolisz, and B.W. Brodersen. A real time cognitive radio testbed for physical and link layer experiments. In *New Frontiers in Dynamic Spectrum Access Networks (DySPAN)*, pages 562–567, November 2005.

[25] C. Chang, J. Wawrzynek, and R.W. Brodersen. Bee2: a high-end reconfigurable computing system. *Design & Test of Computers, IEEE*, 22(2):114–125, March-April 2005.

[26] Fraunhofer Institute for Telecommunications (Heinrich-Hertz-Institut). Berlin LTE-Advanced Testbed, 2009.

[27] R. Irmer, H.-P. Mayer, A. Weber, V. Braun, M. Schmidt, M. Ohm, N. Ahr, A. Zoch, C. Jandura, P. Marsch, and G. Fettweis. Multisite field trial for lte and advanced concepts. *Communications Magazine, IEEE*, 47(2):92–98, February 2009.

[28] Gaisler Research. Leon3 processor, 2009.

[29] Najam-ul-Islam Muhammad, R. Rasheed, R. Pacalet, R. Knopp, and K. Khalfallah. Flexible baseband architectures for future wireless systems. In *Proc. 11th EUROMICRO Conference on Digital System Design Architectures, Methods and Tools DSD '08*, pages 39–46, 2008.

[30] Raymond Knopp. Detailed report on broadband prototype implementation and updated system specifications. Project Deliverable SP4.D11, CHORIST, July 2009.

[31] M. Realp, A.I. Perez-Neira, and R. Knopp. Delay bounds for resource allocation in wideband wireless systems. In *Proc. IEEE International Conference on Communications (ICC '06)*, volume 10, pages 4385–4390, June 2006.

[32] R. Ghaffar and R. Knopp. Interference suppression for next generation wireless systems. In *Proc. IEEE Vehicular Technology Conference VTC-Spring*, Barcelona, Spain, April 2009.

[33] Rizwan Ghaffar and Raymond Knopp. Dual-antenna BICM reception with applications to MIMO broadcast and single frequency cellular system. In *Proc. IEEE Intl. Symposium on Personal, Indoor and Mobile Radio Communications (PIMRC)*, Cannes, France, September 2008.

[34] Rizwan Ghaffar and Raymond Knopp. A MIMO broadcast strategy and interference cancellation in single frequency cellular system. In *Proc. 1st COST2100 Workshop on MIMO and Cooperative Communications*, Trondheim, Norway, June 2008.

[35] Florian Kaltenberger, Rizwan Ghaffar, and Raymond Knopp. Low-complexity distributed MIMO receiver and its implementation on the OpenAirInterface platform. In *Proc. IEEE Int. Symp. on Pers., Indoor and Mobile Radio Comm. (PIMRC)*, Tokyo, Japan, September 2009.

[36] E. Dahlman, H. Ekstrom, A. Furuskar, Y. Jading, J. Karlsson, M. Lundevall, and S. Parkvall. The 3G long-term evolution - radio interface concepts and performance evaluation. In *Proc. IEEE 63rd Vehicular Technology Conference VTC-Spring*, volume 1, pages 137–141, May 2006.

[37] I. Medvedev, B.A. Bjerke, R. Walton, J. Ketchum, M. Wallace, and S. Howard. A comparison of MIMO receiver structures for 802.11n WLAN - performance and complexity. In *Porc. IEEE 17th International Symposium on Personal, Indoor and Mobile Radio Communications*, September 2006.

[38] H.V. Poor and S. Verdu. Probability of error in MMSE multiuser detection. *IEEE Trans. Inf. Theory*, 43(3):858–871, May 1997.

[39] G. Caire, G. Taricco, and E. Biglieri. Bit-interleaved coded modulation. *IEEE Trans. Inf. Theory*, 44(3):927–946, May 1998.

[40] J. Buck and E. Buck. Synchronous fireflies. *Scientific American*, 234(5):74–85, May 1976.

[41] O. Simeone, U. Spagnolini, Y. Bar-Ness, and S. Strogatz. Distributed synchronization in wireless networks. *IEEE Signal Process. Mag.*, 25(5):81–97, September 2008.

[42] Alexander Tyrrell, Gunther Auer, and Christian Bettstetter. Fireflies as role models for synchronization in ad hoc networks. In *Proc. Bio inspired models of network, information and computing systems (BIONETICS '06)*, Cavalese, Italy, 2006.

[43] Yao-Win Hong and A. Scaglione. A scalable synchronization protocol for large scale sensor networks and its applications. *IEEE J. Sel. Areas Commun.*, 23(5):1085–1099, May 2005.

[44] A. S. Hu and S. D. Servetto. On the scalability of cooperative time synchronization in pulse-connected networks. *IEEE Trans. Inf. Theory*, 52(6):2725–2748, June 2006.

[45] R. Ghaffar and R. Knopp. Spatial interference cancellation and pairwise error probability analysis. In *Proc. IEEE International Conference on Communications (ICC)*, Dresden, Germany, June 2009.

[46] G. J. Foschini and M. J. Gans. On limits of wireless communication in a fading environment when using multiple antennas. *Wireless Personal Communications*, 6(3):311–335, March 1998.

[47] E. Telatar. Capacity of multi-antenna Gaussian channels. *European Transactions on Telecommunications*, 10:585–595, 1999.

[48] D. Gesbert, M. Shafi, Da-Shan Shiu, P. J. Smith, and A. Naguib. From theory to practice: an overview of MIMO space-time coded wireless systems. *IEEE J. Sel. Areas Commun.*, 21(3):281–302, 2003.

[49] D. Gesbert, F. Tosato, C. van Rensburg, and F. Kaltenberger. *UMTS Long Term Evolution: From Theory to Practice*, chapter Multiple Antenna techniques in LTE. Wiley and Sons, 2009.

[50] Jeffrey G. Andrews, Arunabha Ghosh, and Rias Muhamed. *Fundamentals of WiMAX: Understanding Broadband Wireless Networking*, chapter Multiple-Antenna Techniques. Prentice Hall PTR, March 2007.

[51] G. Caire and S. Shamai (Shitz). On the achievable throughput of a multiantenna Gaussian broadcast channel. *IEEE Trans. Inf. Theory*, 49(7):1691–1706, July 2003.

[52] H. Weingarten, Y. Steinberg, and S. Shamai (Shitz). The capacity region of the Gaussian multiple-input multiple-output broadcast channel. *IEEE Trans. Inf. Theory*, 52(9):3936–3964, September 2006.

[53] C. B. Peel, B. M. Hochwald, and A. L. Swindlehurst. A vector-perturbation technique for near-capacity multiantenna multiuser communication—part I: channel inversion and regularization. *IEEE Trans. Commun.*, 53(1):195–202, January 2005.

[54] D. Gesbert, M. Kountouris, R. W. Heath, Jr., C. B. Chae, and T. Sälzer. From single user to multiuser communications: Shifting the MIMO paradigm. *IEEE Signal Process. Mag.*, 24(5):36–46, September 2007.

[55] D.J. Love, R.W. Heath, V.K.N. Lau, D. Gesbert, B.D. Rao, and M. Andrews. An overview of limited feedback in wireless communication systems. *Selected Areas in Communications, IEEE Journal on*, 26(8):1341–1365, October 2008.

[56] N. Jindal. MIMO broadcast channels with finite-rate feedback. *IEEE Trans. Inf. Theory*, 52(11):5045–5060, 2006.

[57] N. Jindal and A. Goldsmith. Dirty-paper coding versus TDMA for MIMO broadcast channels. *IEEE Trans. Inf. Theory*, 51(5):1783–1794, May 2005.

[58] T.Y. Al-Naffouri, M. Sharif, and B. Hassibi. How much does transmit correlation affect the sum-rate scaling of MIMO Gaussian broadcast channels? *IEEE Trans. Commun.*, 57(2):562–572, February 2009.

[59] F. Kaltenberger, M. Kountouris, L. S. Cardoso, R. Knopp, and D. Gesbert. Capacity of linear multi-user MIMO precoding schemes with measured channel data. In *Proc. IEEE Intl. Workshop on Signal Processing Advances in Wireless Communications (SPAWC)*, Recife, Brazil, July 2008.

[60] F. Kaltenberger, L. Bernadó, and T. Zemen. On the characterization of measured multi-user MIMO channels. In *Workshop on Smart Antennas (WSA 2009)*, Berlin, Germany, February 2009.

[61] P. Viswanath and D. Tse. Sum capacity of the vector Gaussian broadcast channel and uplink-downlink duality. *IEEE Trans. Inf. Theory*, 49(8):1912–1921, August 2003.

[62] Kaibin Huang, Robert W. Heath, Jr., and Jeffrey G. Andrews. Limited feedback beamforming over temporally-correlated channels. *IEEE Trans. Signal Process.*, 57(5):1959–1975, May 2009.

[63] R. de Lacerda, L. S. Cardoso, R. Knopp, M. Debbah, and D. Gesbert. EMOS platform: real-time capacity estimation of MIMO channels in the UMTS-TDD band. In *Proc. International Symposium on Wireless Communication Systems (IWCS)*, Trondheim, Norway, October 2007.

[64] G. Bauch, J.B. Anderson, C. Guthy, M. Herdin, J. Nielsen, J. A. Nossek, P. Tejera, and W. Utschick. Multiuser MIMO channel measurements and performance in a large office environment. In *Proc. IEEE Wireless Comm. and Net. Conf.*, pages 1900–1905, Hong Kong, March 2007.

[65] G. W. K. Colman and T. J. Willink. Limited feedback precoding in realistic MIMO channel conditions. In *Proc. IEEE Int. Conf. on Comm. (ICC)*, pages 4363–4368, Glasgow, Scotland, June 2007.

[66] Quentin H. Spencer, Jon W. Wallace, Chrisian B. Peel, Thomas Svantesson, A. Lee Swindelhurst, Harry Lee, and Ajay Gumalla. *MIMO System Technology for Wireless Communications*, chapter Performance of Multi-User Spatial Multiplexing with Measured Channel Data. CRC Press, March 2006.

[67] Adam L. Anderson, James R. Zeidler, and Michael A. Jensen. Stable transmission in the time-varying MIMO broadcast channel. *EURASIP Journal on Advances in Signal Processing*, 2008.

[68] Nicolai Czink, Bernd Bandemer, G. Vazquez Vilar, Louay Jalloul, and Arogyaswami Paulraj. Can multi-user MIMO measurements be done using a single channel sounder? Technical Report TD(08) 621, COST 2100, Lille, France, November 2008.

[69] J. Koivunen, P. Almers, V.-M. Kolmonen, J. Salmi, A. Richter, F. Tufvesson, P. Suvikunnas, A. F. Molisch, and P. Vainikainen. Dynamic multi-link indoor MIMO measurements at 5.3 GHz. In *Proc. 2nd European Conference on Antennas and Propagation (EuCAP 2007)*, Edinburgh, UK, November 2007.

[70] Wei Yu and J. M. Cioffi. Sum capacity of Gaussian vector broadcast channels. *IEEE Trans. Inf. Theory*, 50(9):1875–1892, September 2004.

[71] N. Jindal, Wonjong Rhee, S. Vishwanath, S. Jafar, and A. Goldsmith. Sum power iterative water-filling for multi-antenna Gaussian broadcast channels. *IEEE Trans. Inf. Theory*, 51(4):1570–1580, April 2005.

[72] Arogyaswami Paulraj, Dhananjay Gore, and Rohit Nabar. *Introduction to Space-Time Wireless Communications*. Cambridge University Press, 2003.

[73] R. Knopp and P. A. Humblet. Information capacity and power control in single-cell multiuser communications. In *Proc. IEEE Int. Conf. on Comm. (ICC)*, volume 1, pages 331–335, Seattle, CA, June 1995.

[74] J. H. Conway, R. H. Hardin, and N. J. A. Sloane. Packing lines, planes, etc.: Packings in Grassmannian space. *Experimental Mathematics*, 5:139–159, 1996.

[75] D. J. Love, R. W. Heath, Jr., and T. Strohmer. Grassmannian beamforming for multiple-input multiple-output wireless systems. *IEEE Trans. Inf. Theory*, 49(10):2735–2747, 2003.

[76] D. J. Love. Grassmannian subspace packing, July 2004.

[77] Philips. System-level simulation results for channel vector quantisation feedback for MU-MIMO. Technical Report R1-063028, 3GPP TSG RAN WG1, November 2006.

[78] F. Kaltenberger, L. Bernadó, and T. Zemen. Characterization of measured multi-user MIMO channels using the spectral divergence measure. Technical Report TD(08) 640, COST 2100, Lille, France, November 2008.

[79] F. Kaltenberger, M. Kountouris, D. Gesbert, and R. Knopp. Correlation and capacity of measured multi-user MIMO channels. In *Proc. IEEE Intl. Symposium on Personal, Indoor and Mobile Radio Communications (PIMRC)*, Cannes, France, September 2008.

[80] F. Kaltenberger, M. Kountouris, D. Gesbert, and R. Knopp. Performance of multi-user MIMO precoding with limited feedback over measured channels. In *Proc. IEEE Global Communications Conference (IEEE GLOBECOM 2008)*, New Orleans, USA, November 2008.

[81] Glenn S. Smith. A direct derivation of a single-antenna reciprocity relation for the time domain. *IEEE Transactions on Antennas and Propagation*, 52(6):1568–1577, June 2004.

[82] André Bourdoux, Boris Côme, and Nadia Khaled. Non-reciprocal transceivers in OFDM/SDMA systems: Impact and mitigation. In *Proc. IEEE Radio and Wireless Conference (RAWCON)*, pages 183 – 186, Boston, MA, USA, August 2003.

[83] Maxime Guillaud, Dirk T.M. Slock, and Raymond Knopp. A practical method for wireless channel reciprocity exploitation through relative calibration. In *Proc. Intl. Symposium on Signal Processing and its Applications (ISSPA '05)*, Sydney, Australia, August 2005.

[84] S. Kay. A fast and accurate single frequency estimator. *IEEE Trans. Acoust., Speech, Signal Process.*, 37(12):1987–1990, December 1989.

[85] Sabine Van Huffel. *Analysis of the Total Least Squares problem and its use in parameter estimation*. PhD thesis, Katholieke Universiteit Leuven, Leuven, Belgium, 1987.

[86] Ivan Markovsky and Sabine Van Huffel. Overview of total least-squares methods. *Signal Processing*, 87:2283–2302, 2007.

[87] Nicola Mastronardi, Philippe Lemmering, and Sabine van Huffel. Fast structured total least squares algorithm for solving the basic deconvolution problem. *SIAM Journal on Matix Analysis and Applications*, 22, 2000.

[88] Bassem Zayen, Boris Kouassi, Raymond Knopp, Florian Kaltenberger, Dirk Slock, Irfan Ghauri, and Luc Deneire. Software implementation of spatial interweave cognitive radio communication using OpenAirInterface platform. In *ISWCS 2012, 9th International Symposium on Wireless Communication Systems*, Paris, FRANCE, August 2012.

[89] 3GPP. Physical channels and modulation. Technical Specification 36.211-V8.6.0, 3GPP, September 2009.

[90] S. Sesia, I. Toufik, and M. Baker, editors. *UMTS Long Term Evolution: From Theory to Practice*. Wiley and Sons, 2009.

[91] Jonathan Duplicy, Biljana Badic, RajaRajan Balraj, Rizwan Ghaffar, Peter Horvath, Florian Kaltenberger, Raymond Knopp, Istvan Kovacs, Hung Nguyen, Deepaknath Tandur, and Guillaume Vivier. MU-MIMO in LTE systems. *EURASIP Journal on Wireless Communications and Networking*, 2011.

[92] Rizwan Ghaffar and Raymond Knopp. Interference-aware receiver structure for Multi-User MIMO and LTE. *EURASIP Journal on Wireless Communications and Networking 2011*, 2011.

[93] J. H. Bae, S. Kim, J. Lee, and I. Kang. Advanced downlink mu-MIMO receiver for 3GPP LTE-A. In *IEEE International Conference on Communications (ICC)*, pages 7004–7008, Ottowa, Canada, June 2012.

[94] Z. Bai, S. Iwelski, G. Bruck, P. Jung, B. Badic, T. Scholand, and R. Balraj. Receiver performance-complexity tradeoff in LTE mu-MIMO transmission. In *Ultra Modern Telecommunications and Control Systems and Workshops (ICUMT)*, pages 1–7, 2011.

[95] Eurecom. The openairinterface website, 2013.

[96] S. Wagner, R. Couillet, M. Debbah, and D. T. Slock. Large system analysis of linear precoding in correlated MISO broadcast channels under limited feedback. *IEEE Trans. Inf. Theory*, 58(7):4509–4537, 2012.

[97] Biljana BADIC, Andrea F. CATTONI, Michael DIEUDONNE, Jonathan DU-PLICY, Peter FAZEKAS, Florian KALTENBERGER, István Z. KOVÁCS, and Guillaume VIVIER. Advances in Carrier Aggregation and Multi-User MIMO for LTE-Advanced: Outcomes from SAMURAI project. White paper, 2012.

[98] A.F Cattoni, H.T Nguyen, Jonathan Duplicy, Deepaknath Tandur, Bilijana Badic, R Balraj, Florian Kaltenberger, Imran Latif, Ankit Bhamri, G Vivier, I.Z Kovacsk, and P Horvat. Multi-user MIMO and carrier aggregation in 4G systems: the SAMURAI approach. In *WCNC 2012, IEEE Wireless Communications and Networking Conference*, Paris, FRANCE, April 2012.

[99] Nortel Networks. OFDM Exponential Effective SIR Mapping Validation, EESM Simulation Results. Technical Report R1-040089, 3GPP, January 2004.

[100] Ricardo B. Santos, Walter C. Freitas Jr., Elvis M. G. Stancanelli, and Francisco Rodrigo P. Cavalcanti. Link-to-System Level Interface Solutions in Multistate Channels for 3GPP LTE Wireless System. In *XVV Simposio Brasileiro de Telecomunicacoes*, Recife, Brasil, September 2007.

[101] K. Brueninghaus, D. Astely, T. Salzer, S. Visuri, A. Alexiou, S. Karger, and G. A. Seraji. Link Performance Models for System Level Simulations of Broadband Radio Access Systems. In *16th Annual IEEE International Symposium on Persoanl, Indoor and Mobile Radio Communications Germany*, pages 2306–2311, 2005.

[102] Lei Wan, Shiauhe Tsai, and M. Almgren. A Fading-Insensitive Performance Metric for a Unified Link Quality Model. In *Wireless Communications and Networking Conference, 2006. WCNC 2006. IEEE*, volume 4, pages 2110 –2114, April 2006.

[103] M Döttling. Assessment of Advanced Beamforming and MIMO Technologies. Project Deliverable IST-WINNER (2003-507581), European Commission, 2005.

[104] Roshni Srinivasan, Jeff Zhuang, Louay Jalloul, Robert Novak, and Jeongho Park. IEEE 802.16m Evaluation Methodology Document (EMD). Technical Report IEEE 802.16m-08 004r5, IEEE, 2009.

[105] J. Colom Ikuno, C. Mehlführer, and M. Rupp. A novel link error prediction model for OFDM systems with HARQ. In *IEEE International conference on Communications 2011 (ICC)*, Kyoto, Japan, June 2011.

[106] Liang Cheng Jiang and Fengyi Jiang. A comprehensive and practical model for HARQ in LTE system. In *Wireless Communications and Networking Conference (WCNC), 2013 IEEE*, pages 901–905, 2013.

[107] R. Visoz, A.O. Berthet, and M. Lalam. Semi-analytical performance prediction methods for iterative mmse-ic multiuser mimo joint decoding. *Communications, IEEE Transactions on*, 58(9):2576–2589, 2010.

[108] S.M. Lopez, F. Diehm, R. Visoz, and Baozhu Ning. Measurement and prediction of turbo-SIC receiver performance for LTE. In *Vehicular Technology Conference (VTC Fall), 2012 IEEE*, pages 1–5, 2012.

[109] Sung-Hyun Moon, Kyoung-Jae Lee, Jihoon Kim, and Inkyu Lee. Link performance estimation techniques for MIMO-OFDM systems with maximum likelihood receiver. *Wireless Communications, IEEE Transactions on*, 11(5):1808–1816, 2012.

[110] Imran Latif. *Scalable System Level Evaluations for LTE Using PHY Abstraction*. PhD thesis, EURECOM, Sophia-Antipolis, France, 2013.

[111] Raymond Knopp. Some lessons learned from OpenAirInterface. EuWin Emerging Topic Workshop on Experimental Research for the Future Internet, July 2013.

[112] Mirsad Cirkic, Florian Kaltenberger, Erik G. Larsson, and Raymond Knopp. MIMO-TDD reciprocity and hardware imbalances, 2014. in preparation.

[113] Clayton Shepard, Hang Yu, Narendra Anand, Erran Li, Thomas Marzetta, Richard Yang, and Lin Zhong. Argos: Practical many-antenna base stations. In *Proceedings of the 18th Annual International Conference on Mobile Computing and Networking*, Mobicom '12, pages 53–64, New York, NY, USA, 2012. ACM.

[114] H. Suzuki, R. Kendall, K. Anderson, A. Grancea, D. Humphrey, J. Pathikulangara, K. Bengston, J.Matthews, and C. Russell. Highly spectrally efficient ngara rural wireless broadband access demonstrator. In *Proc. of IEEE International Symposium on Communications and Information Technologies (ISCIT)*, October 2012.

# List of Acronyms

| | |
|---|---|
| 3GPP | 3rd Generation Partnership |
| CA | Carrier Aggregation |
| CH | Cluster Head |
| CPU | Central Processing Unit |
| CSIT | Channel State Information Transmitter |
| DAB | Digital Audio Broadcast |
| EMOS | EURECOM MIMO OpenAir Sounder |
| eNB | Evolved Node B |
| EPC | Evolved Packet Core |
| FDD | Frequency Division Duplex |
| HARQ | Hybrid Automated Repeat Request |
| HSS | Home Subscriber Server |
| IA | Interference Aware |
| IR | Incremental Redundancy |
| IU | Interference Unaware |
| LOS | Line-of-sight |
| LTE | Long-term Evolution |
| MAC | Medium Access Control |
| MAP | Maximum A-Posteriori |
| MIMO | Multiple-Input Multiple-Output |
| MME | Mobility Management Entity |
| MMSE | Minimum Mean Squared Error |
| MR | Mesh Router |
| MU | Multi-user |
| NA | Network Aided |
| NAICS | Network Aided Interference Cancellation and Suppression |
| OFDM | Orthogonal Frequency Division Multiplexing |
| OFDMA | Orthogonal Frequency Division Multiple Access |
| PC | Personal Computer |
| PCI | Peripheral Component Interconnect |
| PGW | Packet Data Network Gateway |
| PHY | Physical |
| QAM | Quadrature Amplitude Modulation |

| | |
|---|---|
| RF | Radio Frequency |
| SDR | Software Defined Radio |
| SGW | Serving Gateway |
| SIMD | Single Instruction Multiple Data |
| TDD | Time Division Duplex |
| TD-SCDMA | Time-division Single Carrier Multiple Access |
| UE | User Equipment |
| WiMAX | Worldwide Interoperability for Microwave Access |

# Part II

# Extended Curriculum Vitae

# Florian Kaltenberger

*Extended Curriculum Vitæ*

## Affiliation

**Assistant Professor**, *Eurecom*, Campus SophiaTech, 450 Route des Chappes, 06410 Biot FRANCE.

## Education

2002–2007  **Dr. techn. in Technical Mathematics**, *Vienna University of Technology*, Austria.

Equivalent to Ph.D. degree; Subject: Low-Complexity Real-Time Signal Processing for Wireless Communications; Supervisor: Prof. Christoph W. Ueberhuber; Graduation with distinction.

1997–2002  **Dipl.-Ing. in Technical Mathematics**, *Vienna University of Technology*, Austria.

Equivalent to M.Sc. degree; Subject: Abstract Algorithms for Multidimensional Discrete Fourier Transforms; Supervisor: Prof. Christoph W. Ueberhuber; Graduation with distinction.

1996–1997  **Compulsory Military Service**, *Wr. Neustadt*, Austria.

1988–1996  **Bundesgymnasium**, *Berndorf*, Austria.

Grammar school with special emphasis on mathematics, physics and biology.

## Work Experience

Since 2011  **Assistant Professor**, *Eurecom*, Sophia Antipolis, France.

Experimental wireless communications, channel measurements, and channel modeling using the Eurecom real-time open-source *OpenAirInterface.org* platform.

2007–2010  **Research Engineer**, *Eurecom*, Sophia Antipolis, France.

LTE MODEM design and implementation on the Eurecom real-time open-source *OpenAirInterface.org* platform.

2003–2007  **Junior Researcher**, *Austrian Research Centers GmbH - ARC*, Vienna, Austria.

Development and implementation of smart antennas and MIMO algorithms on the *ARC SmartSim* real-time development platform. Research in MIMO algorithms and wireless channel modeling.

2002–2003  **Research Assistant**, *Vienna University of Technology*, Austria.

Research in massively parallel implementations of signal processing algorithms.

2001–2003  **Teaching Assistant**, *Vienna University of Technology*, Austria.

Tutor for course "Introduction to programming for technical mathematicians".

Summer 2001  **Trainee**, *British Telecom*, Ipswich, UK.

Implementation of a mobile video conferencing application using a head-tracker.

Summer 2000  **Trainee**, *Advanced Computer Vision GmbH*, Vienna, Austria.

Development and implementation of algorithms for optical tracking of users in a closed environment (optical headtracking).

| Summers 1996–1999 | **Trainee**, *Berndorf Band GmbH & Co KG*, Berndorf, Austria. |
| | Successful development of databases to optimise quality assurance through better error recognition. |

## Acquired Research Grants

| 2013–2016 | **Exploiting Channel Reciprocity in Massive MIMO**, *Ph.D. grant awarded by the Laboratoire d'excellence UCN@SOPHIA*, Total funding 73 k€. |
| 2013–2016 | **SOLDER—Spectrum OverLay through aggregation of heterogeneous DispERsed Bands**, *Collaborative research project (FP7-ICT STREP) funded by the European Commission*, Funding total/own institution: 2.3 m€/ 382 k€, Project leader for Eurecom and work-package leader. |
| | Development of a cognitive radio system exploting heterogenious radio access technologies and proof-of-concept using the Eurecom OpenAirInterface.org platform. |
| 2010–2012 | **SAMURAI—Spectrum Aggregation and Multi-User MIMO: Real-World Impact**, *Collaborative research project (FP7-ICT STREP) funded by the European Commission*, Funding total/own institution: 3 m€/ 525 k€, Project leader for Eurecom and work-package leader. |
| | Design, development and implementation of a multi-user MIMO demonstration on the Eurecom OpenAirInterface.org platform. |
| 2009–2011 | **PUCCO—Personal Unsynchronized Cooperative Communications**, *Collaborative Research Project funded by the WWTF (Vienna, Austria)*, Funding total/own institution: 417 k€/ 76 k€, Project leader for Eurecom and work package leader. |
| | Design, development and implementation of a cooperative communication scheme on the Eurecom OpenAirInterface.org platform. |
| 2005–2007 | **Future Mobile Communications—Math and MIMO**, *Collaborative Research Project funded by the WWTF (Vienna, Austria)*, Funding total/own institution: 410 k€/ 100 k€, Project leader for Austrian Research Centers and work package leader. |
| | Development of a new mathematical model for wave propagation in time-variant MIMO channels to allow their efficient simulation in real-time hardware emulators. |

## Industrial Projects

| 2013 | **At-sea broadband wireless communications using IEEE 802.11n**, *Contract with Kietta (French SME)*. |
| | Planning, execution and analysis of a measurement campaign of the performance of IEEE 802.11n equipment for broadband wireless communications between boats |
| 2009–2010 | **LTE field trial and measurement campaign**, *Contract with French Space Agency (CNES)*. |
| | Development of an LTE (3GPP Rel. 8) MODEM and realization of a measurement campaign in rural areas. |
| 2007–2008 | **PACAM—Propagation, Algorithms and Capacity of MIMO systems**, *Contract with French network operator SFR*. |
| | Development of a multi-user MIMO channel sounder based on OpenAirInterface, measurement campaign and analysis. |

## Other projects and Networks

| 2013–2015 | **4G in Vitro**, *A virtual environment to optimize 4G LTE networks*. |
| | Physical layer abstraction for LTE and LTE-Advanced |

2012–2015 **NEWCOM#**, *FP7-ICT Network of Excellence in Wireless Communications.*
Setup, maintainance, and promotion of the Eurecom OpenAirInterface as part of the European Laboratory of Wireless Communicstions for the Future Internet (EuWin).

2011–2015 **Cooperative Radio Communications for Green Smart Environments**, *COST Action IC 10-04.*

2010-2012 **SACRA - Spectrum and energy efficiency through multi-band cognitive radio**, *Collaborative research project (FP7-ICT-STREP).*
Development and demonstration of carrier aggregation between licensed and unlicensed bands.

2009–2012 **PROTON—Programmable Telematics On-Board Radio**, *DeuFraKo collaborative research project with BMW and others.*
Development of a software radio MODEM for car-to-car and car-to-infrastructure communication.

2008–2010 **SENDORA—SEnsor Network for Dynamic and cOgnitive Radio Access**, *Collaborative reseach project (FP7-ICT STREP).*
Development of a collaborative relaying strategy for mesh networks.

2007–2010 **NEWCOM++**, *FP7-ICT Network of Excellence in Wireless Communications.*
Active Participation in WPR1 *Radio Channel Modeling* and WPR2 *Feedback and Resolution of the Channel State.*

2007–2010 **Pervasive Mobile & Ambient Wireless Communications**, *COST Action 2100.*
Active Participation in WG2 *Radio Channel Measurements and Modeling.*

2006–2009 **CHORIST—Integrating Communications for enHanced envirOnmental RISk management and citizens safeTy**, *Collaborative research project (FP6-IST IP).*
Design and Implementation of a of a distributed MIMO receiver to enable a single-frequency Mesh Network using OpenAirInterface.

## Organization of summer/winter schools

May 2013 **First Newcom# school on "Interference Management for Tomorrows' Wireless Networks"**, *Eurecom, Sophia-Antipolis (France).*
Local organizer.

## Teaching Activities

2011- **Radio Engineering**, *Master-level course at Eurecom.*
This course treats the subject of modern radio engineering and includes typical RF architectures and their characterizations, modeling, prediction and simulation of radio-wave propagation, cellular planning, systems-level aspects of modern radio network design. Three practical lab sessions using typical RF equipment (such as OpenAirInterface) and measurement tools are offered.

Nov. 2013 **Physical layer abstraction for LTE**, *Lecture at the Newcom# summer winter school "Beyond 4G Networks in Cities: from Theory to Experimentation and Back".*

July 2013 **Introduction to OpenAirInterface and its Usage in ITS Applications**, *Half-day course at the Franco-German Summer School on Smart Mobility.*

May 2013 **OpenAirInterface Overview and Lab Session**, *Half-day course at the NEWCOM# Summer School on Interference Management for Tomorrow's Wireless Networks.*

| Feb. 2012 | **LTE PHY evaluation and abstraction using OpenAirInterface**, *Half-day course at the ACROPOLIS Winter School on Experimental Methods in Wireless Communications.* |
| July 2011 | **OpenAirInterface Radio Network Modeling**, *Half-day course at the ACROPOLIS Winter School on Cognitive Wireless Communications.* |

## Supervision of Master students

| 2014 | **Mohamed Achraf Khsiba**, *Alcatel-Lucent (France)*, LTE Modem test-bench calibration automation. |
| 2013 | **Alami Oussama**, *Amadeus (France)*, Air Cache Modeling and Optimization. |
| 2012 | **Antonino Maniaci**, *Aria (Italy)*, WiMax: Network Analysis Planning and Optimization. |
| 2012 | **Eren Unlu**, *Eurecom (France)*, Physical Layer Aspects of OpenAir4G Platform. |
| 2012 | **Eric Fotimeli**, *Alcatel Lucent (France)*, LTE Radio Channel Modeling. |
| 2012 | **Sandip Ghangakhedkar**, *Alcatel Lucent Bell Labs (France)*, Integration of Resource Allocation Strategies for Multiple Component Carriers in OpenAirInterface. |
| 2011 | **Qi Ning**, *Eurecom (France)*, Carrier Aggregation and its Integration onto OpenairInterface. |
| 2011 | **Joe Soueidi**, *BMW (Germany)*, In-Vehicular Femtocells: Concept Analysis and Signal Propagation Study. |
| 2011 | **Ankit Bhamri**, *Eurecom (France)*, Distributed Coding and Modulation for two-hop Communication via Relays. |
| 2010 | **Torbjorn Sorby**, *Eurecom (France)*, Demonstration of Spatial Interweave Cognitive Radio. |
| 2009 | **Haiyong Jiang**, *Eurecom (France)*, Relative Channel Reciprocity Calibration in MIMO/OFDM System. |

## Supervision of Ph.D. students

| 2014- | **Tao Wang**, *Exploiting Channel Reciprocity in Massive MIMO*, University of Nice Sophia-Antipolis (France), Co-supervision with Luc Deneire. |
| 2014- | **Elena Lukashova**, *Physical Layer Abstraction for LTE-Advanced*, Telecom ParisTech (France), Co-supervison with Christian Bonnet. |
| 2014- | **George Arvanitakis**, *Spectrum Overlay through Aggregation of Heterogeneous Dispersed Bands*, Telecom ParisTech (France), Co-supervision with Raymond Knopp. |
| 2011-2014 | **Ankit Bhamri**, *Multi-user MIMO scheduling in LTE*, Aalto University (Finland), Co-supervision with Jyri Hämäläinen. |
| 2010-2013 | **Imran Latif**, *Scalable System Level Evaluations for LTE Using PHY Abstraction*, Telecom ParisTech (France), Co-supervision with Raymond Knopp. Defended 28.8.2013 with highest honors. |

## Supervision of Post-Docs

| 2012–2013 | **Sebastian Wagner**, *Implementation of an Interference Aware Receiver on the OpenAirInterface Platform.* |

| 2012–2013 | **Rehan Hasmat**, *Implementation of Carrier Aggregation on the OpenAirInterface Platform.* |
| 2011–2012 | **Sébastien Aubert**, *Implementation of an Interference Aware Receiver on the OpenAirInterface Platform.* |

## Jury membership

| Dec. 2013 | **Bazhou Ning**, *Performance Analysis of Iterative Soft Interference Cancellation Algorithms and New Link Adaptation Strategies for Coded MIMO Systems*, Ph.D. thesis, École Supérieure d'Électricité (SUPELEC). Examinor. |
| Oct. 2013 | **Boris Kouassi**, *Stratégies de Coopération dans les Réseaux Radio Cognitif*, Ph.D. thesis, University of Nice Sophia-Antipolis. Examinor. |

## Impact

**Citations: 467,    h-index: 13,    i10-index: 16**.
Source: Google scholar (Feb. 2014)

## Awards

| 2013 | **Neal Shepherd Best Propagation Award**. |
| | Oestges, Claude; Czink, Nicolai; Bandemer, Bernd; Castiglione, Paolo; Kaltenberger, Florian; Paulraj, Arogyaswami, "Experimental characterization and modeling of outdoor-to-indoor and indoor-to-indoor distributed channels," IEEE Transactions on Vehicular Technology, Vol.59, N°5, June 2010 |

## Other Activities

| Since 2005 | **Member**, *Institute of Electrical and Electronic Engineers (IEEE).* |
| | **Reviewer** for several journals and conferences, including IEEE Transactions on Wireless Communications, IEEE Transactions on Vehicular Technology, IEEE Transactions on Antennas and Propagation, IEEE Journal on Selected Topics in Signal Processing, IEEE Communications Letters, EURASIP Journal on Advances in Signal Processing, EURASIP Journal on Wireless Communications and Networking |

## Research Interests

| Signal processing | Mathematical signal processing, signal processing for wireless communications, distributed signal processing. |
| Wireless communications | MIMO, massive MIMO, physical layer abstraction, LTE-Advanced, cooperative communications. |
| Channel modeling | Characterization and modeling of time-variant, multi-user MIMO channels, real-time channel emulation. |
| Software defined radio | Real-time systems, low-complexity receiver architectures, rapid prototyping, automatic code generation. |

## Languages

German: Mother tongue    English: Fluent    French: Intermediate

# List of Publications

## Book chapters

Rizwan Ghaffar, Raymond Knopp, and Florian Kaltenberger. *Recent Trends in Multi-user MIMO Communications*, chapter Multi-user MIMO in LTE and LTE-Advanced - Receiver Structure and Precoding Design. InTech, 2013.

D. Gesbert, F. Tosato, C. van Rensburg, and F. Kaltenberger. *UMTS Long Term Evolution: From Theory to Practice*, chapter Multiple Antenna techniques in LTE. Wiley and Sons, 2009.

## Journal papers

Sebastian Wagner and Florian Kaltenberger. Interference-aware receiver design for MU-MIMO in LTE: Real-time performance measurements. *Intel Technology Journal (special issue on 4G communications)*, 18(1):154–171, 2014.

Boris Kouassi, Bassem Zayen, Raymond Knopp, Florian Kaltenberger, Dirk TM Slock, Irfan Ghauri, Francesco Negro, and Luc Deneire. Design and implementation of spatial interweave LTE-TDD cognitive radio communication on an experimental platform. *IEEE Wireless Communications Magazine: Next Generation Cognitive Cellular Networks: Spectrum Sharing and Trading*, 20(2):60–67, April 2013.

Jonathan Duplicy, Biljana Badic, RajaRajan Balraj, Rizwan Ghaffar, Peter Horvath, Florian Kaltenberger, Raymond Knopp, Istvan Kovacs, Hung Nguyen, Deepaknath Tandur, and Guillaume Vivier. MU-MIMO in LTE systems. *EURASIP Journal on Wireless Communications and Networking*, 2011.

Claude Oestges, Nicolai Czink, Bernd Bandemer, Paolo Castiglione, Florian Kaltenberger, and Arogyaswami Paulraj. Experimental characterization and modeling of outdoor-to-indoor and indoor-to-indoor distributed channels. *IEEE Trans. Veh. Technol.*, 59(5):2253–2265, June 2010. Received 2013 Neal Shepherd Best Propagation Award.

Florian Kaltenberger, Rizwan Ghaffar, Raymond Knopp, Hicham Anouar, and Christian Bonnet. Design and implementation of a single-frequency mesh network using OpenAirInterface. *EURASIP Journal on Communications and Networking*, 2010, 2010. Article ID 719523, 16 pages, doi:10.1155/2010/719523.

F. Kaltenberger, M. Kountouris, D. Gesbert, and R. Knopp. On the trade-off between feedback and capacity in measured MU-MIMO channels. *IEEE Trans. Wireless Commun.*, 8(9):4866–4875, September 2009.

T. Zemen, C.F. Mecklenbräuker, Florian Kaltenberger, and B. Fleury. Minimum-energy band-limited time-variant channel prediction with dynamic subspace selection. *IEEE Trans. Signal Process.*, 55(9):4534–4548, September 2007.

F. Kaltenberger, T. Zemen, and C. W. Ueberhuber. Low-complexity geometry-based MIMO channel simulation. *EURASIP Journal on Advances in Signal Processing*, 2007, 2007. Article ID 95281, 17 pages, doi:10.1155/2007/95281.

Charlotte Dumard, Florian Kaltenberger, and Klemens Freudenthaler. Low-cost LMMSE equalizer based on Krylov subspace methods for HSDPA. *IEEE Trans. Wireless Commun.*, 6(5):1610–1614, May 2007.

## Conference papers

Ankit Bhamri, Navid Nikaein, Florian Kaltenberger, Jyri Hämäläinen, and Raymond Knopp. Three-step iterative scheduler for QoS provisioning to users running multiple services in parallel. In *Proc. IEEE Veh. Technol. Conf. (VTC)*, Seoul, Korea, May 2014.

Ankit Bhamri, Navid Nikaein, Florian Kaltenberger, Jyri Hämäläinen, and Raymond Knopp. Pre-processor for MAC-layer scheduler to efficiently manage buffer in modern wireless networks. In *Proc. IEEE Wireless Comm. and Net. Conf.*, Istanbul, TURKEY, April 2014.

Imran Latif, Florian Kaltenberger, Navid Nikaein, and Raymond Knopp. Large scale system evaluations using PHY abstraction for LTE with OpenAirInterface. In *EMUTOOLS 2013, 1st Workshop on Emulation Tools, Methodology and Techniques, March 5, 2013, Cannes, France / Collocated with SIMUTools 2013, 6th International ICST Conference on Simulation Tools and Techniques*, Cannes, FRANCE, March 2013.

Imran Latif, Florian Kaltenberger, Raymond Knopp, and Joan Olmos. Link abstraction for variable bandwidth with incremental redundancy HARQ in LTE. In *WIMEE 2013, 9th International Workshop on Wireless Network Measurements, In conjunction with 11th Intl. Symposium on Modeling and Optimization in Mobile, Ad Hoc, and Wireless Networks (WiOpt 2013)*, Tsukuba, JAPAN, May 2013.

Florian Kaltenberger, Imran Latif, and Raymond Knopp. On scalability, robustness and accuracy of physical layer abstraction for large-scale system-level evaluations of LTE networks. In *in Proc. Asilomar Conference on Signals, Systems, and Computers*, Pacific Grove, CA, November 2013. invited.

Nathalie Haziza, Mohamed Kassab, Raymond Knopp, Jérôme Härri, Florian Kaltenberger, Philippe Agostini, Marion Berbineau, Christophe Gransart, Joëlle Besnier, Jacques Ehrlich, and Hasnaa Aniss. Multi-technology vehicular cooperative system based on software defined radio (SDR). In *NET4CARS 2013, 5th International Workshop on Communication Technologies for Vehicles*, Lille, FRANCE, May 2013.

Maxime Guillaud and Florian Kaltenberger. Towards practical channel reciprocity exploitation: Relative calibration in the presence of frequency offset. In *WCNC 2013, IEEE Wireless Communications and Networking Conference*, Shanghai, CHINA, April 2013.

Mingming Gan, Francesco Mani, Florian Kaltenberger, Claude Oestges, and Thomas Zemen. A ray tracing algorithm using the discrete prolate spheroidal subspace. In *ICC 2013, IEEE International Conference on Communications, Wireless Communications Symposium*, Budapest, HUNGARY, June 2013.

Ankit Bhamri, Florian Kaltenberger, Raymond Knopp, and Jyri Hämäläinen. Improving MU-MIMO performance in LTE-(Advanced) by efficiently exploiting feedback resources and through dynamic scheduling. In *Proc. IEEE Wireless Comm. and Net. Conf.*, Shanghai, CHINA, April 2013.

Ankit Bhamri, Jyri Hämäläinen, Florian Kaltenberger, and Raymond Knopp. Minimizing the effect of feedback delay in a multi-user system through adaptive feedback scheduling. In *Proc. IEEE Veh. Technol. Conf. (VTC)*, Las Vegas, UNITED STATES, September 2013.

Bassem Zayen, Boris Kouassi, Raymond Knopp, Florian Kaltenberger, Dirk Slock, Irfan Ghauri, and Luc Deneire. Software implementation of spatial interweave cognitive radio communication using OpenAirInterface platform. In *ISWCS 2012, 9th International Symposium on Wireless Communication Systems*, Paris, FRANCE, August 2012.

Imran Latif, Florian Kaltenberger, and Raymond Knopp. Link abstraction for multi-user MIMO in LTE using interference-aware receiver. In *WCNC 2012, IEEE Wireless Communications and Networking Conference*, Paris, FRANCE, April 2012.

A.F Cattoni, H.T Nguyen, Jonathan Duplicy, Deepaknath Tandur, Bilijana Badic, R Balraj, Florian Kaltenberger, Imran Latif, Ankit Bhamri, G Vivier, I.Z Kovacsk, and P Horvat. Multi-user MIMO and carrier aggregation in 4G systems: the SAMURAI approach. In *WCNC 2012, IEEE Wireless Communications and Networking Conference*, Paris, FRANCE, April 2012.

Fernando Sanchez, Thomas Zemen, Gerald Matz, Florian Kaltenberger, and Nicolai Czink. Cooperative Space-Time coded OFDM with timing errors and carrier frequency offsets. In *ICC 2011 Wireless Communications Symposium (ICC'11 WCS)*, Kyoto, Japan, June 2011.

Imran Latif, Florian Kaltenberger, Rizwan Ghaffar, Raymond Knopp, Dominique Nussbaum, Hervé Callewaert, and Gaël Scot. Performance of LTE in rural areas - benefits of opportunistic Multi-User MIMO. In *22nd IEEE Personal Indoor Mobile Radio Communications (PIMRC'11 - WACC)*, Toronto, Canada, September 2011.

Christian Bonnet, Riadh Ghaddab, Aawatif Hayar, Florian Kaltenberger, Raymond Knopp, Dominique Nussbaum, Navid Nikaein, Erhan Yilmaz, Daniel Camara, Bassem Zayen, Bertrand Mercier, and Lorenzo Iacobelli. OpenAirInterface.org and agile spectrum access. In *Fifth IEEE International Symposium on New Frontiers in Dynamic Spectrum Access Networks 2011(DySPAN 2011) (IEEE DySPAN 2011)*, Aachen, Germany, May 2011.

Ankit Bhamri, Florian Kaltenberger, Raymond Knopp, and Jyri Hämäläinen. Smart Hybrid-ARQ (SHARQ) for cooperative communication via distributed relays in LTE-Advanced. In *2011 IEEE 12th International Workshop on Signal Processing Advances in Wireless Communications (SPAWC 2011)*, pages 46–50, San Francisco, USA, June 2011.

Erhan Yilmaz, Raymond Knopp, Florian Kaltenberger, and David Gesbert. Low-complexity multiple-relay strategies for improving uplink coverage in 4g wireless networks. In *in Proc. Asilomar Conference on Signals, Systems, and Computers*, Pacific Grove, CA, USA, November 2010.

F. Sánchez González, B. Bandemer, G. Matz, C. Oestges, F. Kaltenberger, and N. Czink. Performance of transmission-time optimized relaying schemes in real-world channels. In *Proc. 4th European Conference on Antennas and Propagation (EuCAP)*, Barcelona, Spain, April 2010.

Florian Kaltenberger, Haiyong Jiang, Maxime Guillaud, and Raymond Knopp. Relative channel reciprocity calibration in MIMO/TDD systems. In *Proc. ICT Future Network and Mobile Summit*, Florence, Italy, June 2010.

O. Gustafsson, K. Amiri, D. Andersson, A. Blad, C. Bonnet, J.R. Cavallaro, J. Declerck, A. Dejonghe, P. Eliardsson, M. Glasse, A. Hayar, L. Hollevoet, C. Hunter, M. Joshi, F. Kaltenberger, R. Knopp, K. Le, Z. Miljanic, P. Murphy, F. Naessens, N. Nikaein, D. Nussbaum, R. Pacalet, P. Raghavan, A. Sabharwal, O. Sarode, P. Spasojevic, Yang Sun, H.M. Tullberg, T. Vander Aa, L. Van der Perre, M. Wetterwald, and M. Wu. Architectures for cognitive radio testbeds and demonstrators—an overview. In *Proc. Cognitive Radio Oriented Wireless Networks & Communications (CROWNCOM)*, Cannes, France, June 2010.

N. Czink, F. Kaltenberger, Y. Zhouz, L. Bernadó, T. Zemen, and X. Yinz. Low-complexity geometry-based modeling of diffuse scattering. In *Proc. 4th European Conference on Antennas and Propagation (EuCAP)*, Barcelona, Spain, April 2010.

Paolo Castiglione, Claude Oestges, Nicolai Czink, Bernd Bandemer, Florian Kaltenberger, and Arogyaswami Paulraj. Multi-link level simulation model of indoor peer-to-peer radio channels. In *Proc. 4th European Conference on Antennas and Propagation (EuCAP)*, Barcelona, Spain, April 2010.

Daniel Sacristán-Murga, Florian Kaltenberger, Antonio Pascual-Iserte, and Ana I. Pérez-Neira. Differential feedback in MIMO communications: Performance with delay and real channel measurements. In *Workshop on Smart Antennas (WSA 2009)*, Berlin, Germany, February 2009.

Claude Oestges, Nicolai Czink, Bernd Bandemer, Paolo Castiglione, Florian Kaltenberger, and Arogyaswami Paulraj. Experimental characterization and modeling of indoor-to-indoor distributed channels. In *Proc. IEEE Int. Symp. on Pers., Indoor and Mobile Radio Comm. (PIMRC)*, Tokyo, Japan, September 2009.

Florian Kaltenberger, Rizwan Ghaffar, and Raymond Knopp. Low-complexity distributed MIMO receiver and its implementation on the OpenAirInterface platform. In *Proc. IEEE Int. Symp. on Pers., Indoor and Mobile Radio Comm. (PIMRC)*, Tokyo, Japan, September 2009.

F. Kaltenberger, L. Bernadó, and T. Zemen. On the characterization of measured multi-user MIMO channels. In *Workshop on Smart Antennas (WSA 2009)*, Berlin, Germany, February 2009.

F. Kaltenberger, M. Kountouris, D. Gesbert, and R. Knopp. Performance of multi-user MIMO precoding with limited feedback over measured channels. In *Proc. IEEE Global Communications Conference (IEEE GLOBECOM 2008)*, New Orleans, USA, November 2008.

F. Kaltenberger, M. Kountouris, D. Gesbert, and R. Knopp. Correlation and capacity of measured multi-user MIMO channels. In *Proc. IEEE Intl. Symposium on Personal, Indoor and Mobile Radio Communications (PIMRC)*, Cannes, France, September 2008.

F. Kaltenberger, M. Kountouris, L. S. Cardoso, R. Knopp, and D. Gesbert. Capacity of linear multi-user MIMO precoding schemes with measured channel

data. In *Proc. IEEE Intl. Workshop on Signal Processing Advances in Wireless Communications (SPAWC)*, Recife, Brazil, July 2008.

Hicham Anouar, Christian Bonnet, Florian Kaltenberger, and Raymond Knopp. OpenAirMesh—an experimental platform for cooperative mesh networks. In *Proc. 1st COST2100 Workshop on MIMO and Cooperative Communications*, Trondheim, Norway, June 2008.

Christian Mehlführer, Markus Rupp, Florian Kaltenberger, and Gerhard Humer. Low-complexity MIMO channel simulation by reducing the number of paths. In *Proc. Workshop on Smart Antennas (WSA 2007)*, Vienna, Austria, February 2007.

F. Kaltenberger, T. Zemen, and C. W. Ueberhuber. Low complexity simulation of wireless channels using discrete prolate spheroidal sequences. In *Proc. MATHMOD Conference*, Vienna, Austria, February 2006.

F. Kaltenberger, T. Zemen, and C. W. Ueberhuber. Low complexity doubly selective channel simulation using multidimensional discrete prolate spheroidal sequences. In *Proc. IST Mobile and Wireless Communications Summit*, Myconos, Greece, June 2006.

F. Kaltenberger, G. Steinböck, G. Humer, and T. Zemen. Low-complexity geometry-based MIMO channel emulation. In *Proc. European Conference on Antennas and Propagation (EuCAP 2006)*, Nice, France, November 2006. invited.

Wolfgang Herzner, Florian Kaltenberger, and Rupert Schlick. Checking data flow models for correct use of physical units. In *Proc. 2006 ERCIM / DECOS Workshop on Dependable Embedded Systems*, Cavtat/Dubrovnik, Croatia, August 2006.

J. Wehinger, K. Freudenthaler, F. Kaltenberger, and J. Berkmann. Influence of SNR estimation on HARQ combining in UMTS-HSDPA. In *Proc. Global Mobile Congress (GMC)*, pages 349–354, Chongqing, China, October 2005.

G. Meindl-Pfeiffer, R. Kloibhofer, F. Kaltenberger, and G. Humer. Multi-standard development platform for MIMO software defined radio. In *Proc. EUSIPCO*, Antalya, Turkey, September 2005.

G. Meindl-Pfeiffer, R. Kloibhofer, F. Kaltenberger, and G.Humer. Development platform for MIMO software defined radio. In *Proc. Embedded World Conference*, pages 243–251, Nuernberg, Germany, February 2005.

Christian Mehlführer, Markus Rupp, Florian Kaltenberger, and Gerhard Humer. A scalable rapid prototyping system for real-time MIMO transmissions. In *Proc. IEE Conference on DSP Enabled Radio*, pages 1–5, Univ of Southampton, UK, September 2005.

F. Kaltenberger, G. Steinböck, R. Kloibhofer, R. Lieger, and G. Humer. A multi-band development platform for rapid prototyping of MIMO systems. In *Proc. ITG Workshop on Smart Antennas*, Duisburg, Germany, April 2005.

F. Kaltenberger, K. Freudenthaler, S. Paul, J. Wehinger, C.F. Mecklenbräuker, and A. Springer. Throughput enhancment by cancellation of synchronization and pilot channel for UMTS high speed downlink packet access. In *Proc. 6th*

*IEEE Workshop on Signal Processing Advances in Wireless Communications (SPAWC)*, pages 580–584, New York, USA, June 2005.

K. Freudenthaler, F. Kaltenberger, S. Paul, C.F. Mecklenbräuker, M. Huemer, and A. Springer. Cancellation of interference from synchronization and pilot channels on high speed downlink shared channel in UMTS. In *Proc. European Wireless Conference (EWC)*, pages 498–503, Nicosia, Cyprus, June 2005.

K. Freudenthaler, F. Kaltenberger, S. Geirhofer, S. Paul, J. Berkman, J. Wehinger, C.F. Mecklenbräuker, and A. Springer. Throughput analysis for a UMTS high speed downlink packet access LMMSE equalizer. In *Proc. IST Mobile and Wireless Communications Summit*, Dresden, Germany, June 2005.

Joachim Wehinger, Christoph F. Mecklenbräuker, Steffen Paul, and Florian Kaltenberger. Two-stage space-time receiver for UMTS frequency division duplex. In *ITG Workshop on Smart Antennas*, pages 231–234, Munich, Germany, March 2004.

F. Kaltenberger, G. Humer, and G. Pfeiffer. MIMO/smart antenna development platform. In *Workshop on Software Radios (WSR04)*, pages 117–121, Karlsruhe, Germany, March 2004.

Franz Franchetti, Florian Kaltenberger, and C. W. Ueberhuber. FFT kernels with FMA utilization. In *Proc. APLIMAT Conference*, pages 333–339, Bratislava, CZ, February 2003.

## Other

Biljana BADIC, Andrea F. CATTONI, Michael DIEUDONNE, Jonathan DUPLICY, Peter FAZEKAS, Florian KALTENBERGER, István Z. KOVÁCS, and Guillaume VIVIER. Advances in Carrier Aggregation and Multi-User MIMO for LTE-Advanced: Outcomes from SAMURAI project. White paper, 2012.